XA-02-AR

66-50916

WAD: R572-Q2

Contract NAS 9-5424

March 15, 1966 - June 14, 1966

THE DEVELOPMENT OF A SEGMENTED, AXIALLY CONDUCTING, PYROLYTIC GRAPHITE REACTION CONTROL ENGINE

Second Quarterly Report

prepared by

Wright Aeronautical Division
Curtiss-Wright Corporation
Wood-Ridge, New Jersey 07075

for

NASA-MANNED SPACECRAFT CENTER
HOUSTON, TEXAS

66-50916

WAD: R572-Q2

Copy _____

Contract NAS 9-5424

March 15, 1966 - June 14, 1966

THE DEVELOPMENT OF A SEGMENTED, AXIALLY CONDUCTING, PYROLYTIC GRAPHITE REACTION CONTROL ENGINE

Second Quarterly Report

prepared by

Wright Aeronautical Division
Curtiss-Wright Corporation
Wood-Ridge, New Jersey 07075

for

NASA-MANNED SPACECRAFT CENTER

HOUSTON, TEXAS

ABSTRACT

This is the second quarterly report covering the work performed under NASA contract NAS-9-5424 during the period from March 15, 1966 through June 14, 1966. The objective of this program is to demonstrate a flight type configuration of an Axially Conducting Engine (ACE) in which pyrolytic graphite (PG) wedges, restrained by an elastic structure, form the combustion chamber and nozzle of the engine.

During this quarter, fabrication of parts for the first engine build was completed and the first test series was accomplished.

Table Of Contents

ILLUSTRATIONS

ILLUSTRATIONS (CONT)

LIST OF TABLES

I. INTRODUCTION

A. Program Scope and Objective

A thirteen month program is being conducted for the preliminary development of a segmented, axially conducting, 100 pound thrust pyrolytic graphite (PG) rocket engine. The program schedule is shown in Figure 1-1. The development plan includes thermal and structural analyses, design verification tests of two rig engines, two flight configuration engine tests for final design demonstration, and an examination of engine compatibility with advanced propellants. The delivery of a flight configuration engine to NASA Manned Spacecraft Center will occur at the end of the fourteenth month.

The objective of this program is to demonstrate the feasibility of the Axially Conducting Engine (ACE) concept for reaction control engine applications. Ultimately, the engine will be capable of buried and/or exposed installation on a spacecraft and will be capable of use with the fluorine family of advanced propellants.

The design conditions for the flight type ACE engine are as follows:

Vacuum Thrust:	100 lb with 40:1 nozzle area ratio
Chamber Pressure:	100 psia
Propellant Inlet Pressure:	195 $\pm$ 5 psia
Fuel:	Monomethylhydrazine
Oxidizer:	Nitrogen Tetroxide
Oxidizer/Fuel Ratio:	1.6:1
Specific Impulse:	290 seconds when operating with 40:1 area ratio nozzle for pulse pulses of 1.0 second duration or longer.

Minimum Impulse Bit:	0.5 lb-sec
Life:	1000 seconds total time including a 500 second continuous run.
Weight:	Not specified but all efforts shall be made to attain a minimum value.

The Curtiss-Wright designation for the engine being developed under this contract is WLR-23.

B. Summary of Program Status

The first quarterly report described the progress of the program through the rig engine design (Phase I) and the test of the watchband test specimen (Phase II - Task 1). Figure 1-1 shows the program schedule and the general status of the engine at the end of the second quarter.

Prior to rig engine testing, two versions of a low fill time 16-port injector were evaluated for possible use with the WLR-23 rig engine. These were direct copies of high fill time injectors, used during pre-contract investigations, with the exception of the upstream manifolding. The manifold was reduced in size to achieve fill times consistent with contractual response requirements. The high pressure drop version of the injector appeared to be satisfactory in stability characteristics and performance and was selected for use with the rig engine.

All detail parts required for the build of the first WLR-23 rig engine were available by the end of March and assembly of the engine was initiated. While expanding the watchband on a tapered plug for installation over the wedge assembly several cracks occurred at the slot root locations. Investigations showed that the cause was substandard material. The calculated watchband installation stresses were within a few percent of the ultimate tensile strength of the billet from which the part was machined. New forgings were procured and were found to be satisfactory by metallurgical and Zyglo inspection and a second watchband of the same design was fabricated.

The first rig engine was built and a test series was initiated in mid-May to evaluate the initial engine design. During a 60 second firing it was observed that the deflection probe readings were in excess of predicted values. Subsequent analysis of this data showed that the engine inner wall temperature was running substantially hotter than the design values.

It appears that the differences in manifolding between the low fill time injector currently being used and the high fill time injector that provided empirical data for the design have caused a combustion phenomenon (as yet unrecognized) which resulted in an increased heat load to the chamber.

The higher temperatures caused overstressing of both the watchband and the wedges at the land locations. Crushing of the land material and permanent deformation of the watchband occurred. The test series was terminated since the land crushing caused leakage in the engine.

A program was then undertaken with the copper chamber to determine the effect on chamber wall temperature of increasing the spray cooling flow rate. This program is now in process and to date indicates that an increase in spray cooling flow to a value of approximately 0.06 lb per second is required to achieve satisfactory temperature levels with the existing injector. This requires some adjustment in the overall design point of the fixed injector configuration to preclude the possibility of running into a zone of instability that exists at an injector O/F ratio of 2.2 - 2.4. This effort is continuing into the third quarter.

The second series of tests on the ACE rig engine will be run when a suitable spray cooling configuration is achieved. The wedge assembly has been completed and the installation of the watchband is being held pending final outcome of the copper engine tests as some adjustment of the pinch fit may be required. It is estimated that the start of the second series of rig engine tests can be initiated early in July.

PROGRAM SCHEDULE

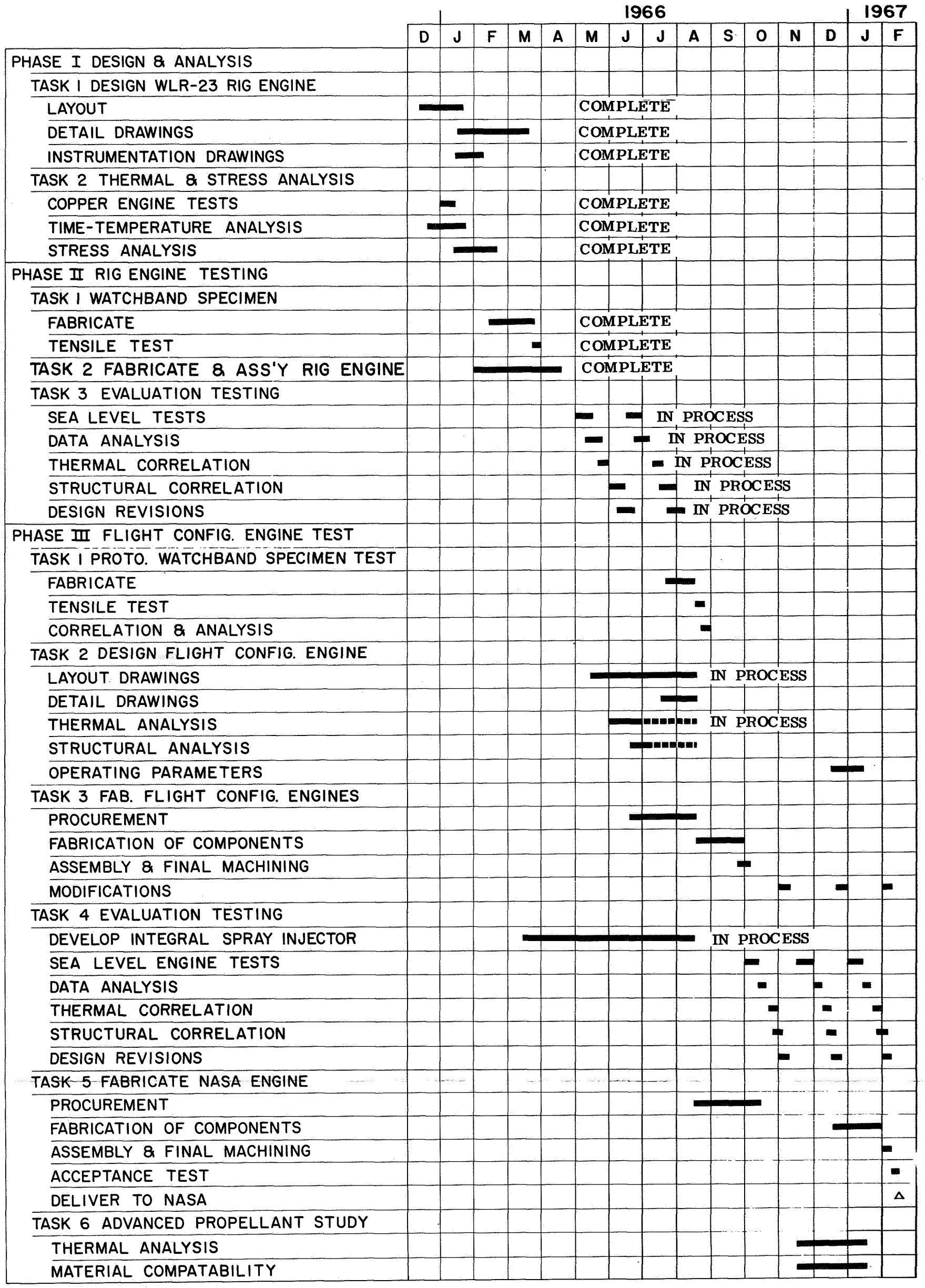

Figure 1-1

II. ENGINE TESTING

A. Injector Development

Two versions of a low fill time injector were designed and fabricated for possible use with the WLR-23 rig engine. One version (ES156903N1) incorporated orifices sized to produce pressure drops of 40 psi for the oxidizer and 78 psi for the fuel. This injector is identical to the high fill time injector (ES156732) used during the initial copper engine test runs 23-1 and 23-2 except for reduced inlet manifold volume. A variation of the low fill time design (ES156903N2) reduces the fuel orifice pressure drop to meet the target feed pressure requirements. Both injectors were evaluated to determine which would be used for the ACE rig engine test series.

ES156903N2 Test Series - The low ΔP version was tested at design point and the results are shown in Table I and Figures 2-1 and 2-2 . The traces show that the general amplitude of the combustion chamber pressure fluctuations was approximately 10%. In addition, random peaks were observed as high as 80 psi. It was concluded after these two initial tests that this version of the injector was not suitable for use with the WLR-23 engine.

ES156903N1 Test Series - The high ΔP version of the 16-port low fill injector was initially subjected to 25 tests without spray cooling. Table II lists the pertinent run parameters with notes regarding stability and Figures 2-3 through 2-27 show chamber pressure and propellant inlet pressure traces. Runs 23-5, -7, -17, -21, -22 and -27 approximate the engine design point and are completely acceptable from the standpoint of performance and stability characteristics. Other points were run to obtain a stability map, Figure 2-28, to provide an indication of the limits of satisfactory injector operation.

A series of tests, Runs 23-30 through 23-45, were then made with spray cooling to obtain similar information. Table II lists the run parameters and Figures 2-29 through 2-44 show traces recorded during the tests. Runs 23-30, -34, -38 and - 43 approximate the design point requirements and again demonstrated satisfactory stability performance. As the basic

injector O/F and flow rates (as they affect delta P) were varied, varying degrees of stability were achieved as indicated by the traces. A stability map for the spray cooled runs is shown in Figure 2-45 .

It was concluded that the high delta P injector (ES156903N1) provided adequate stability and performance for use in the WLR-23 rig engine test series.

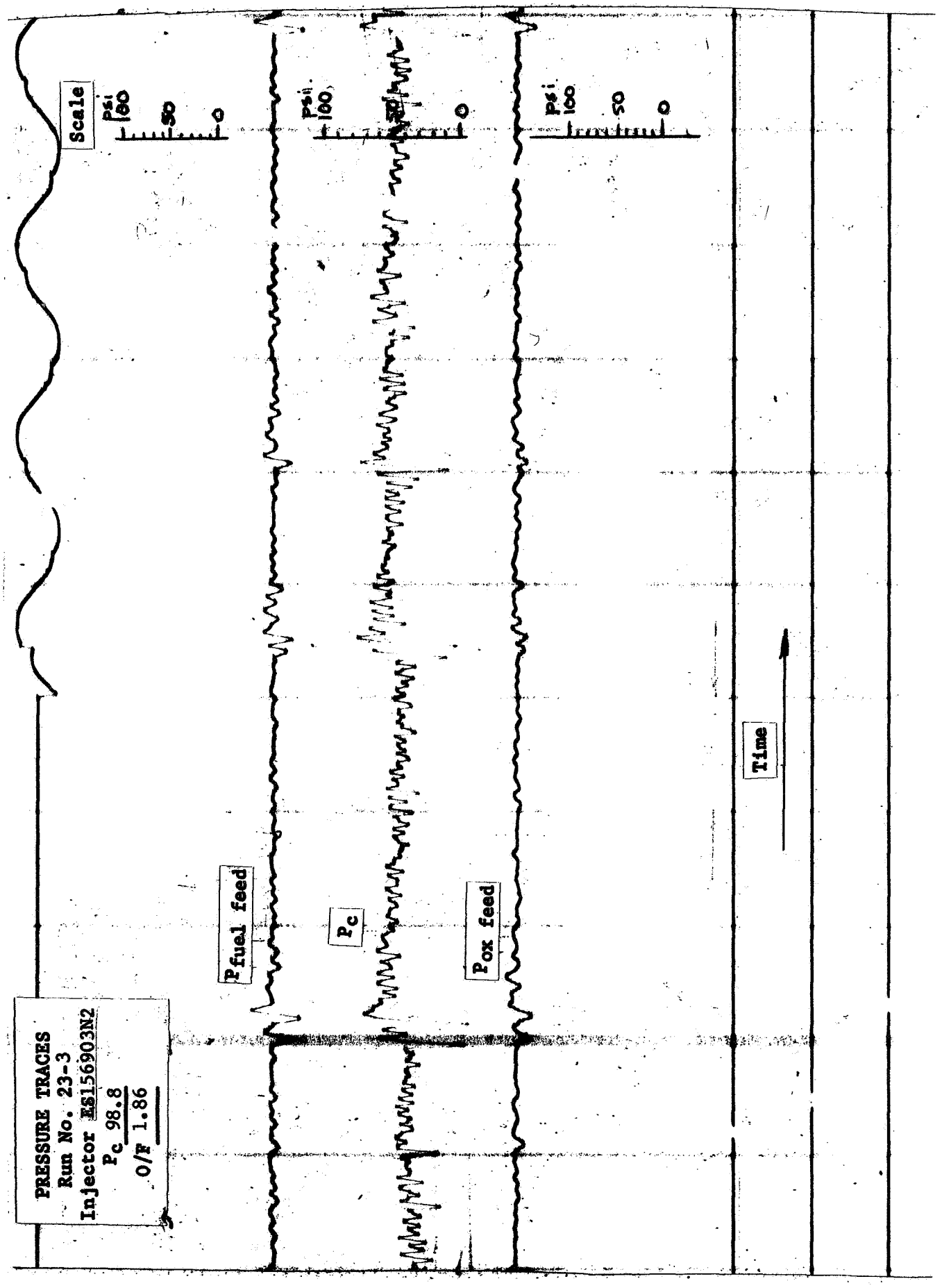
PRESSURE TRACES
Run No. 23-3
Injector ES156903N2
Pc 98.8
O/F 1.86
Scale
Psi
100
50
0
Pfuel feed
Pc
Pox feed
Time
10 ms

Figure 2-1

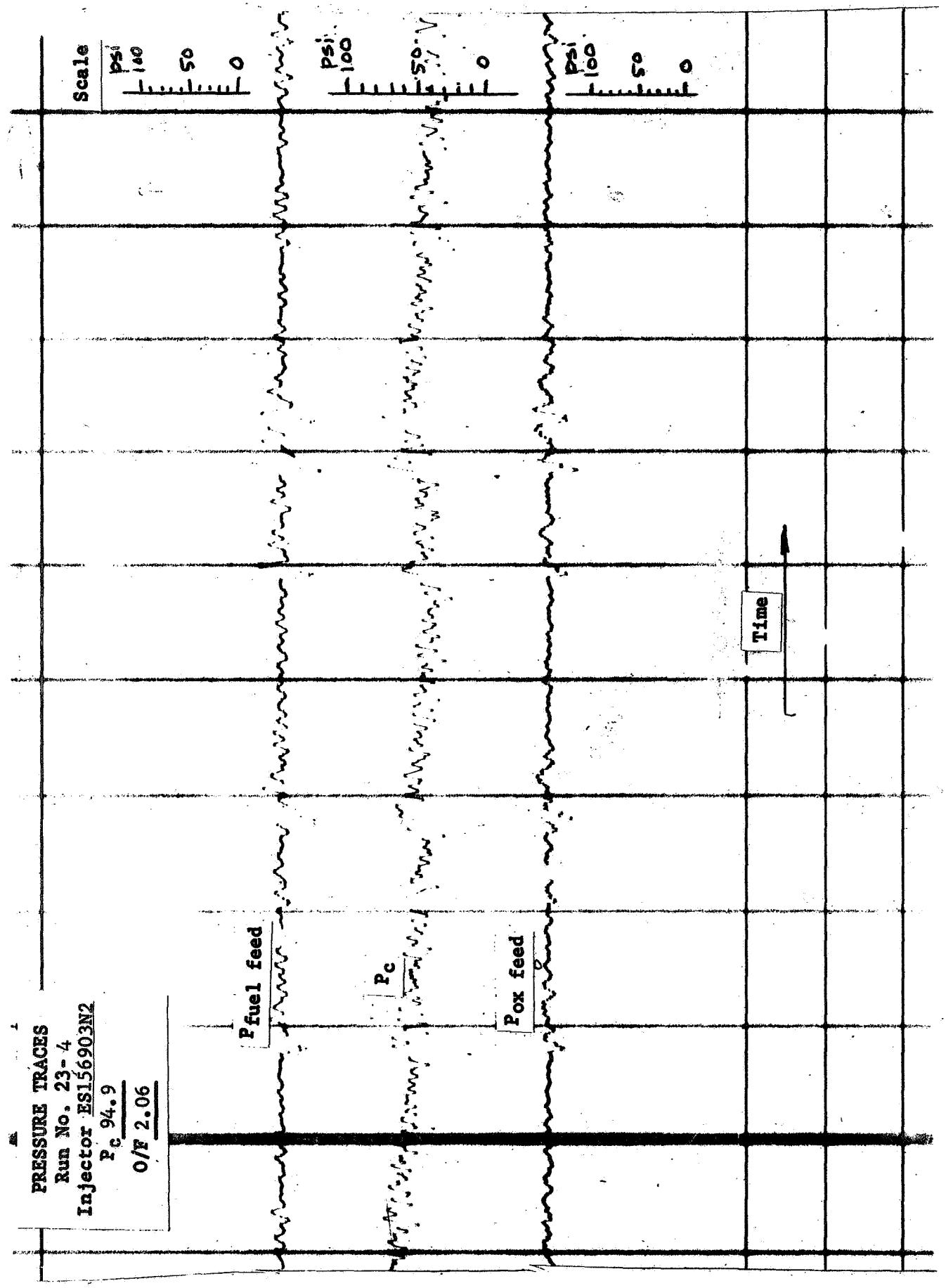

20-395

Figure 2-2

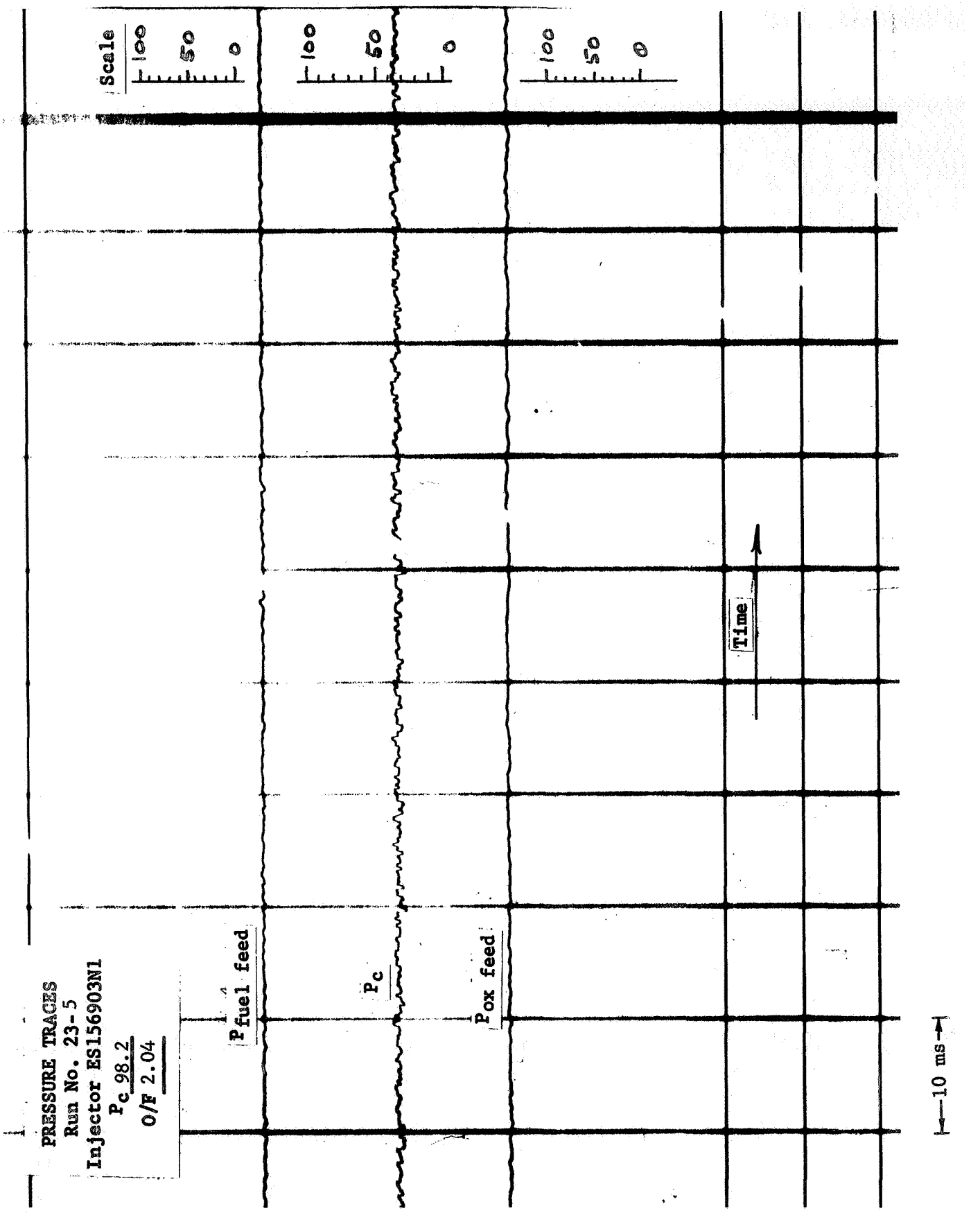
PRESSURE TRACES
Run No. 23-5
Injector ES156903N1
P_c 98.2
O/F 2.04
$P_{fuel\ feed}$
P_c
$P_{ox\ feed}$
Time
10 ms
Scale
100
50
0
100
50
0
100
50
0

Figure 2-3

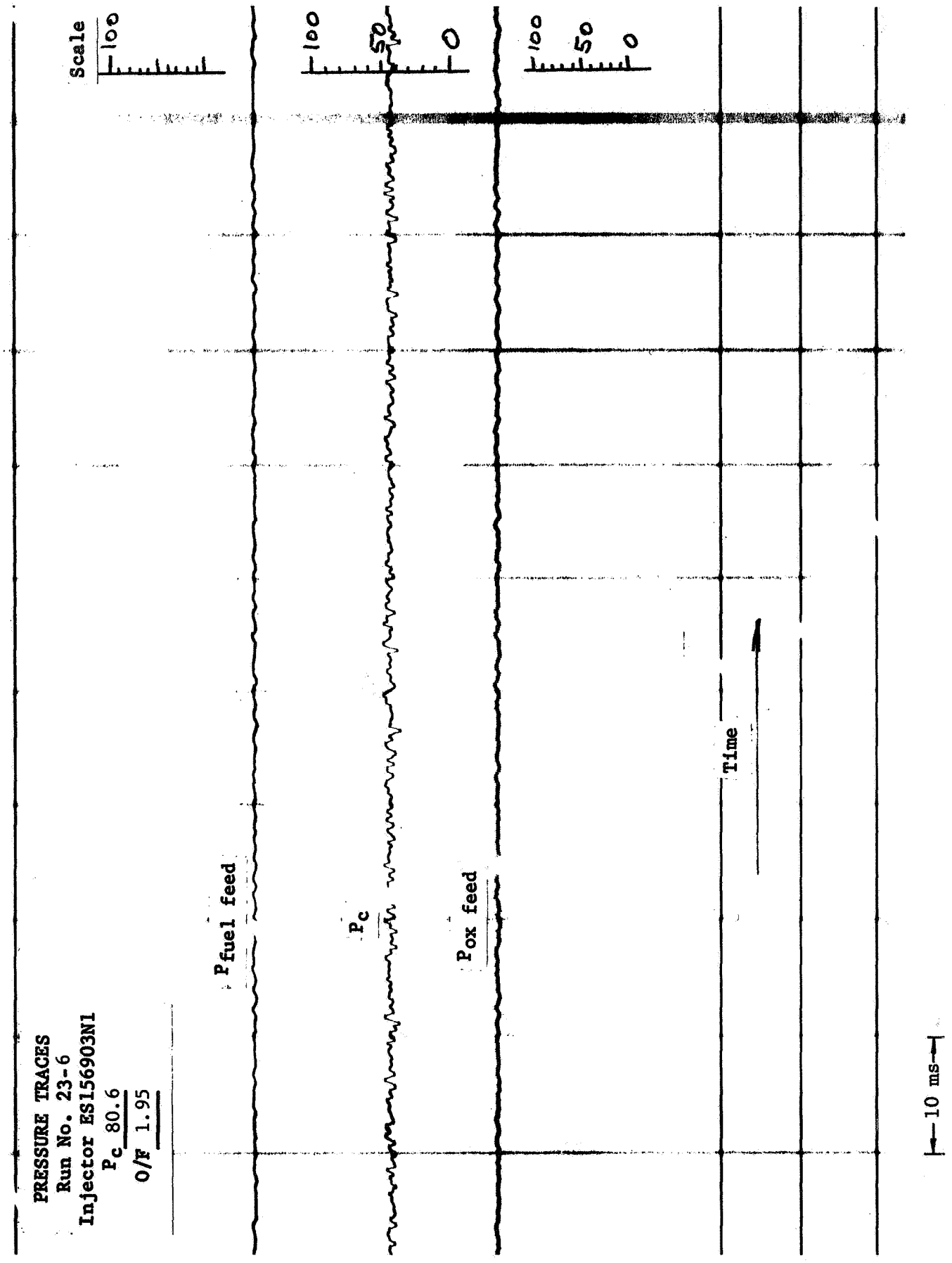

20-370

Figure 2-4

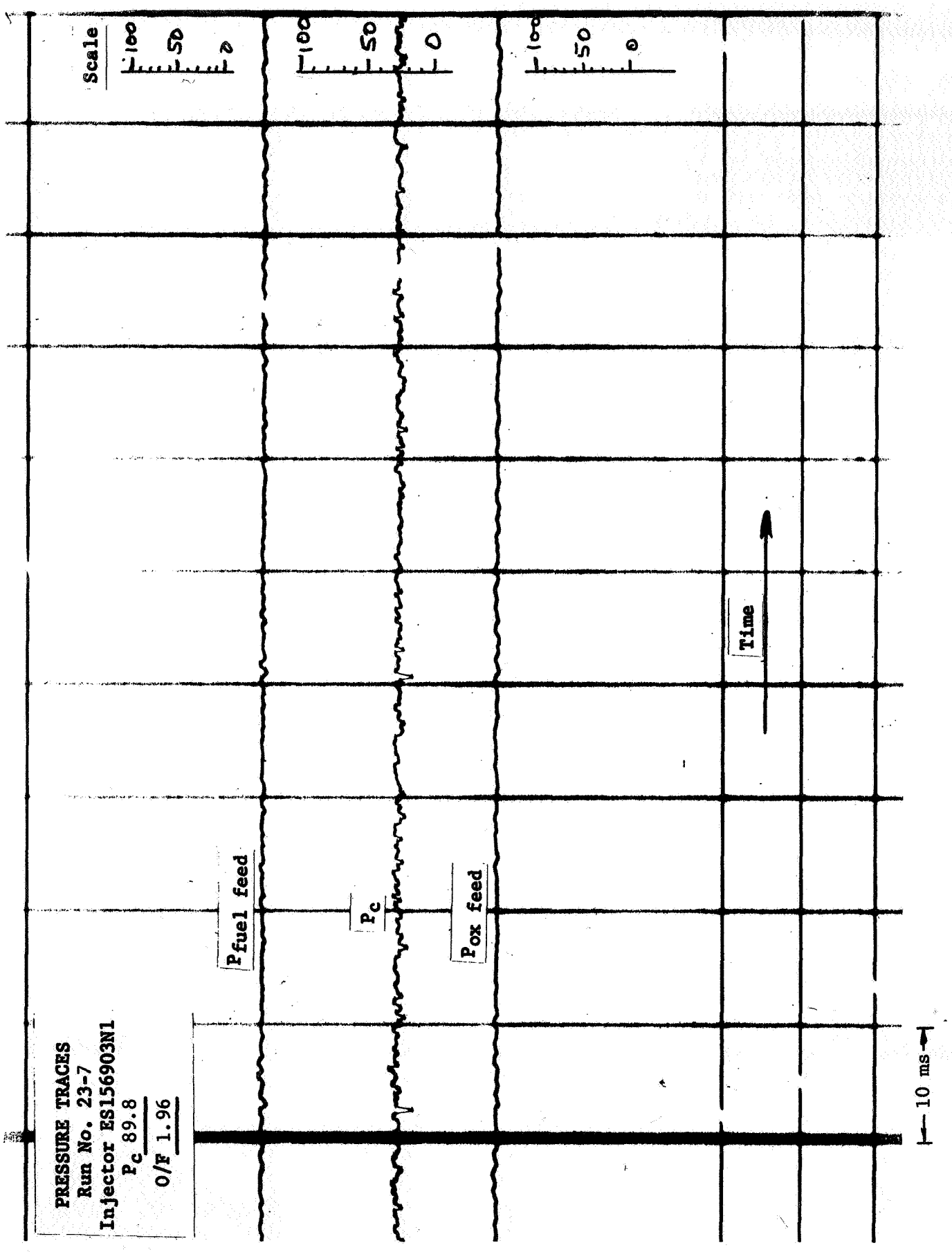

20-375

Figure 2-5

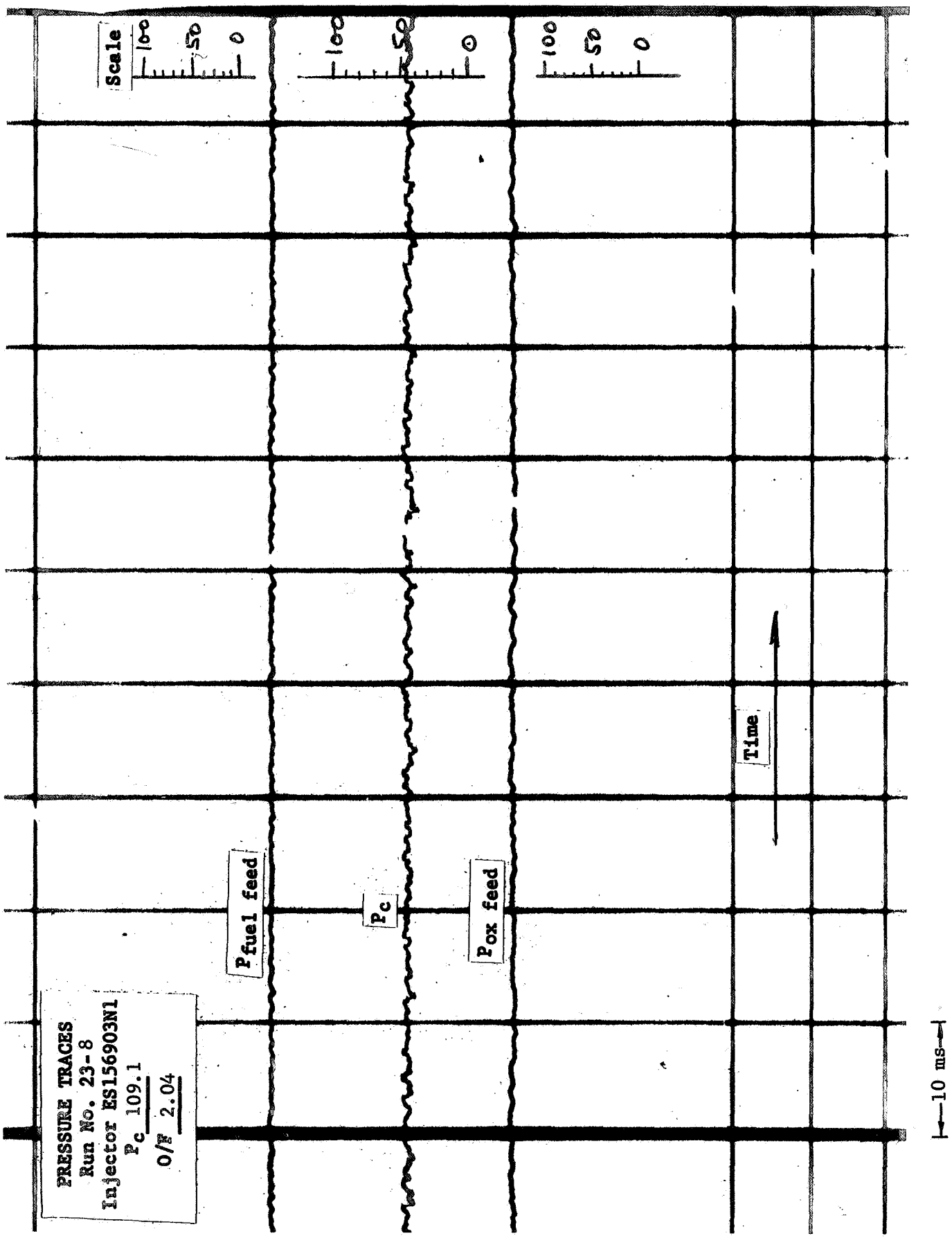

20-380

Figure 2-6

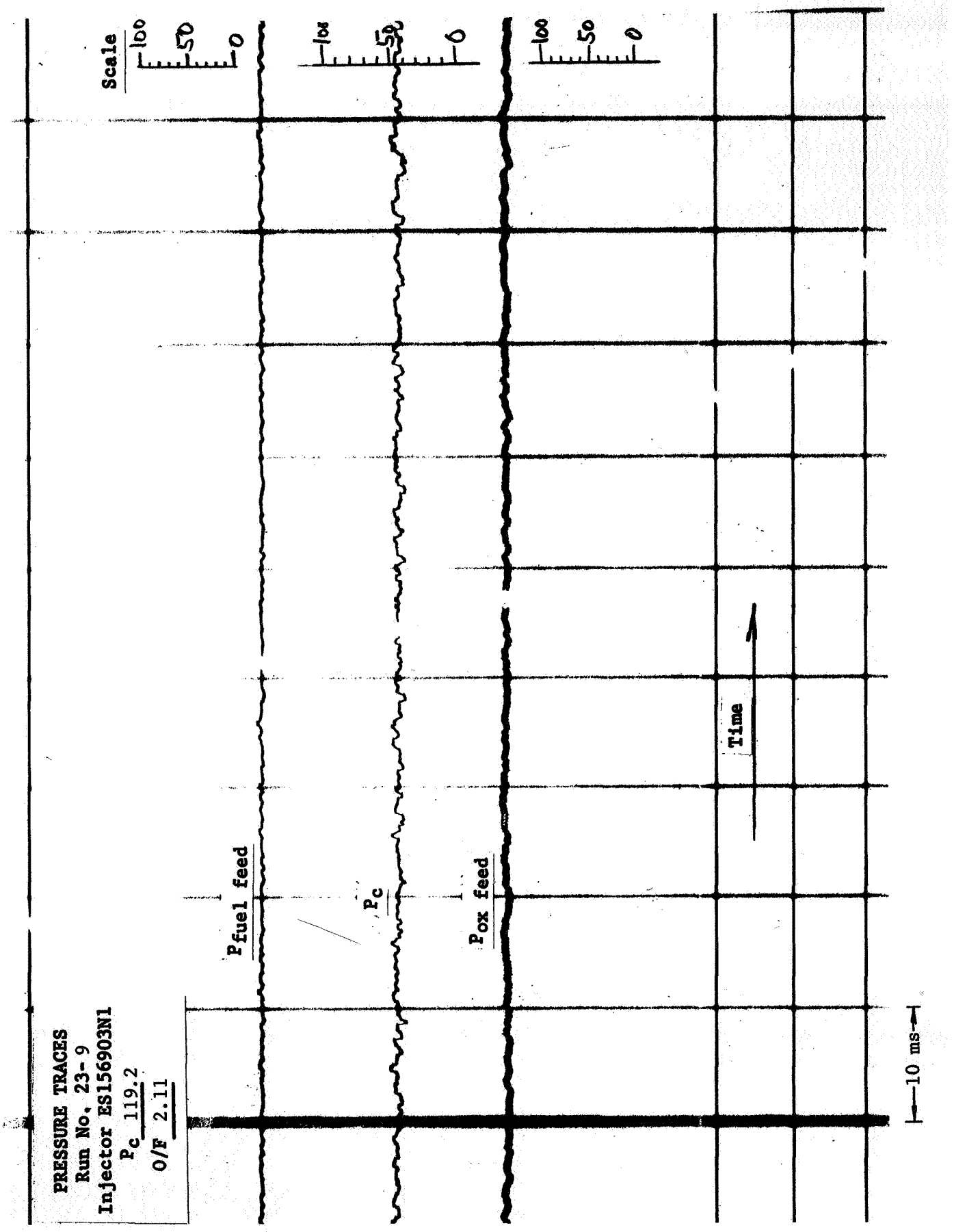
Scale
100
50
0
100
50
0
100
50
0
Pfuel feed
Pc
Pox feed
Time
10 ms
PRESSURE TRACES
Run No. 23-9
Injector ES156903N1
Pc 119.2
O/F 2.11

Figure 2-7

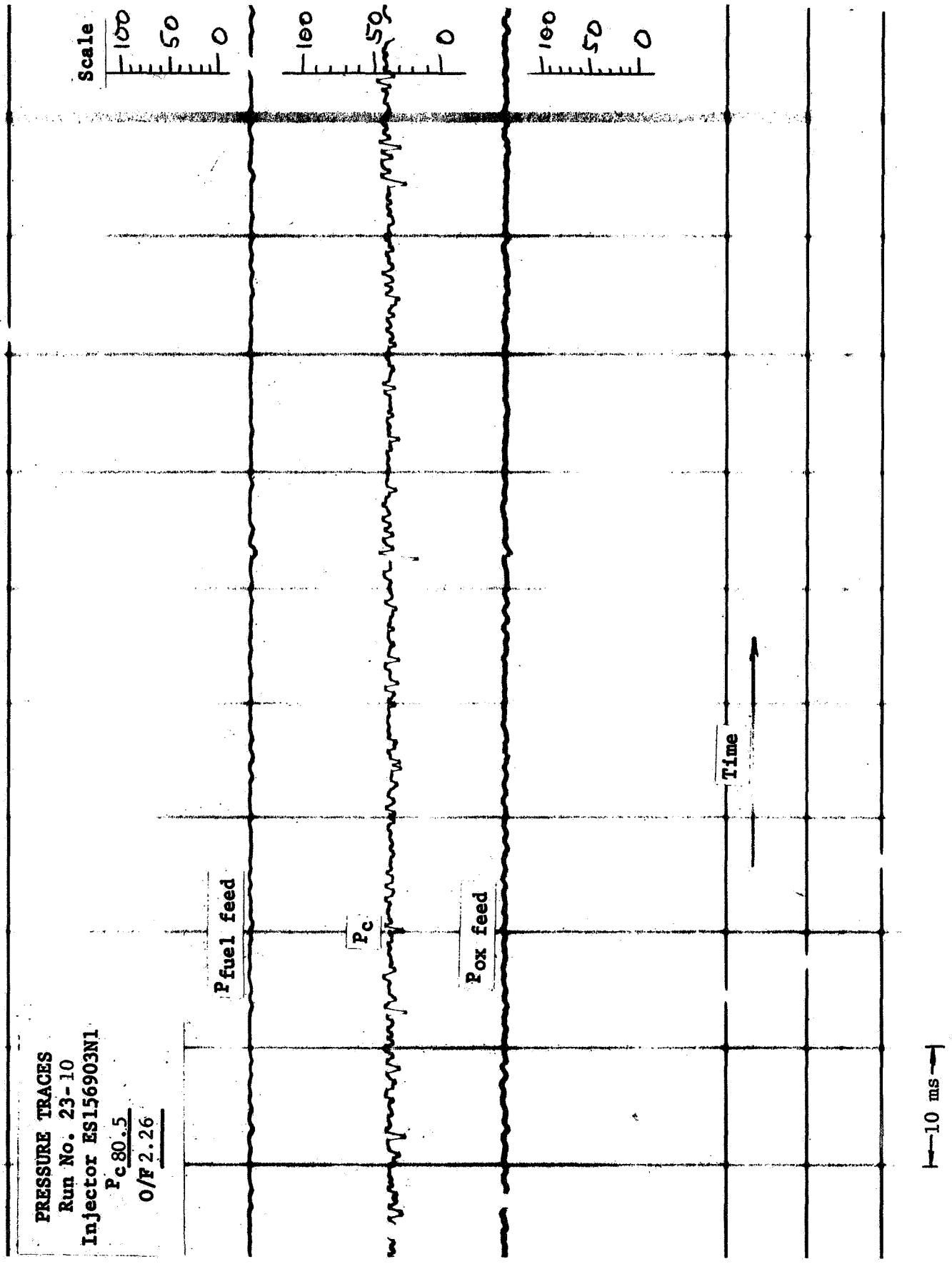
PRESSURE TRACES
Run No. 23-10
Injector ES156903N1
P_c 80.5
O/F 2.26
Scale
100
50
0
100
50
0
100
50
0
$P_{fuel\ feed}$
P_c
$P_{ox\ feed}$
Time
10 ms

Figure 2-8

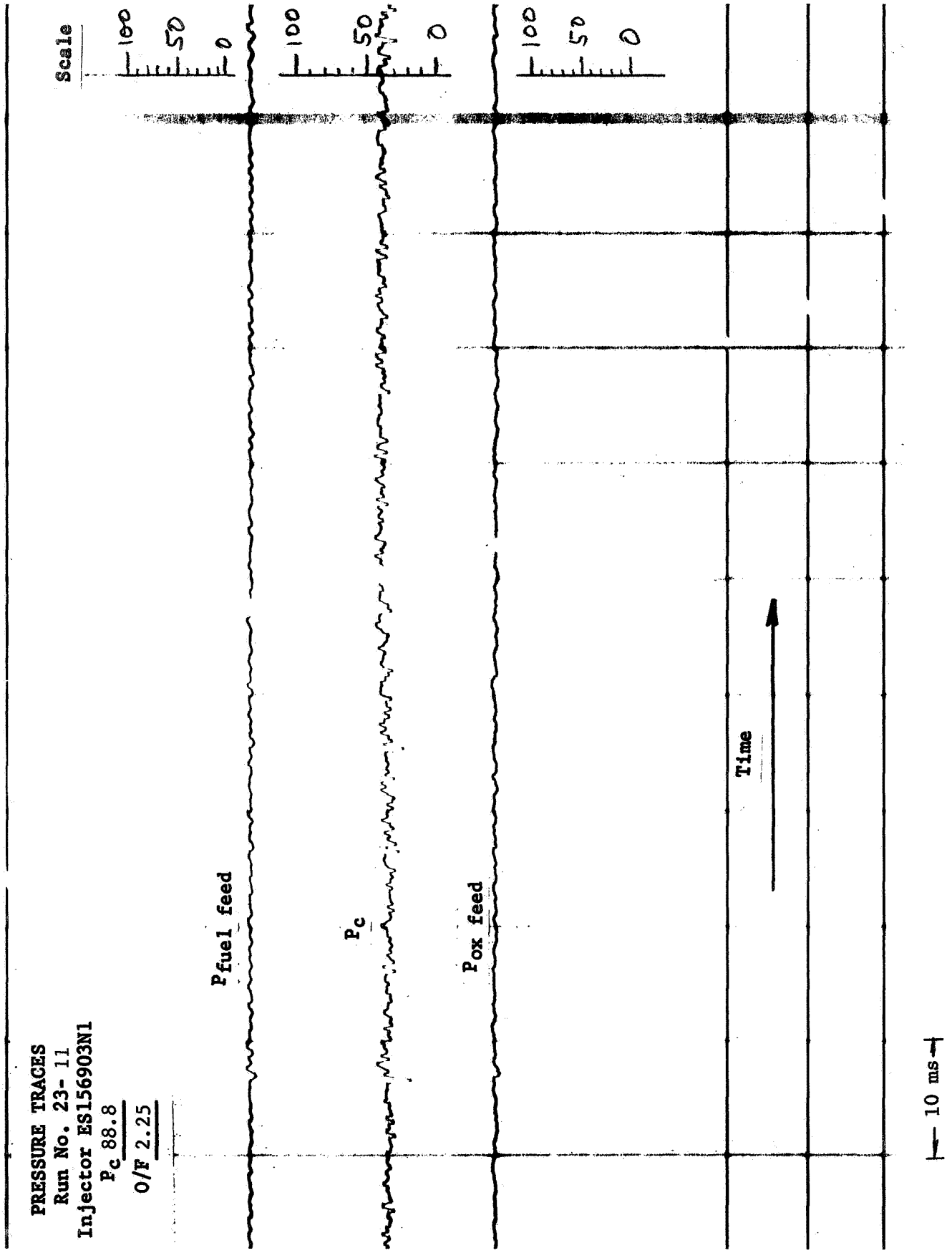
Scale
100
50
0
100
50
0
100
50
0
Pfuel feed
Pc
Pox feed
Time
10 ms
PRESSURE TRACES
Run No. 23-11
Injector ES156903N1
Pc 88.8
O/F 2.25

Figure 2-9

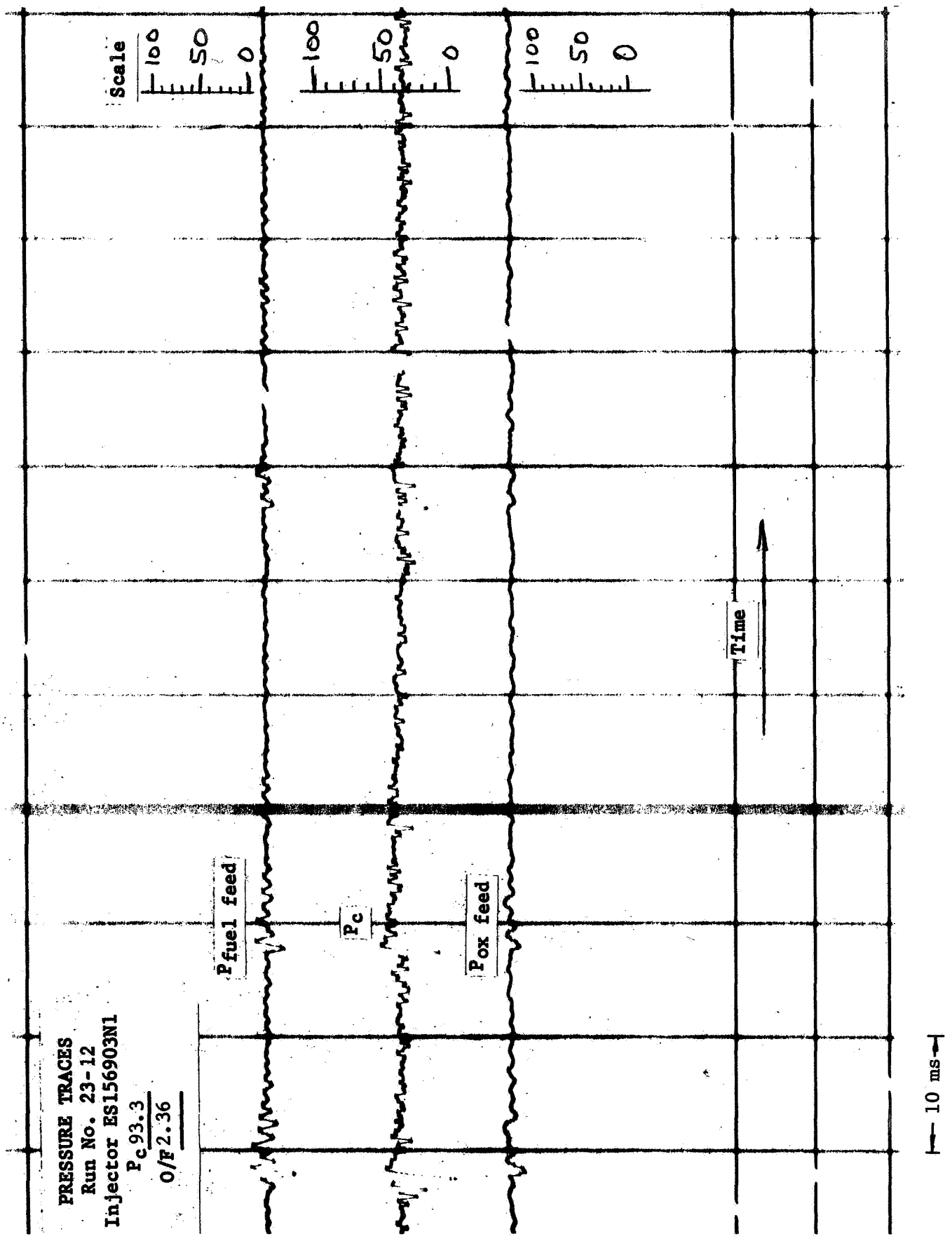
Scale
100
50
0
100
50
0
100
50
0
Time
$P_{fuel\ feed}$
P_c
$P_{ox\ feed}$
10 ms
PRESSURE TRACES
Run No. 23-12
Injector ES156903N1
P_c 93.3
O/F 2.36

Figure 2-10

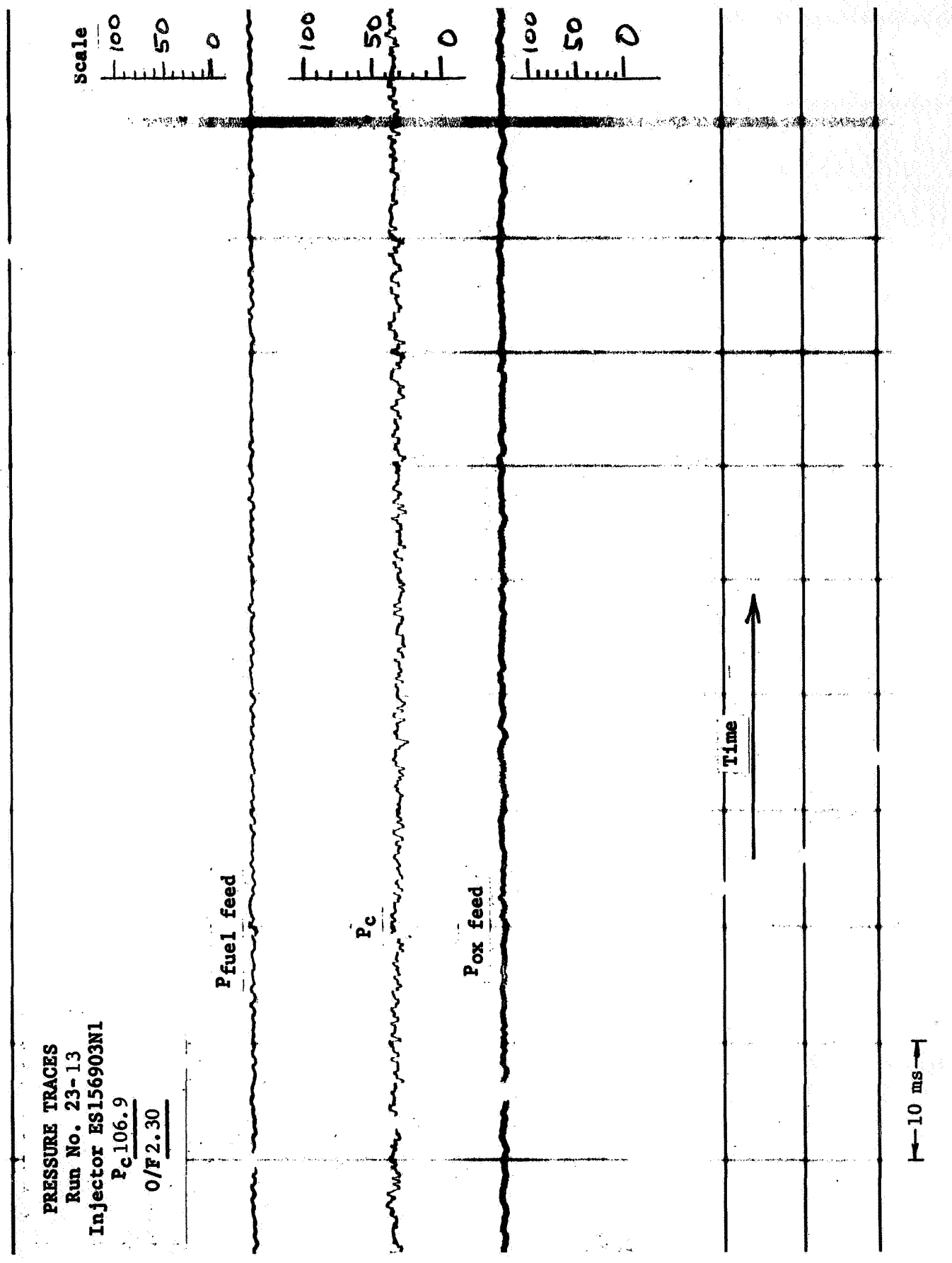
Scale
100
50
0
100
50
0
100
50
0
PRESSURE TRACES
Run No. 23-13
Injector ES156903N1
Pc 106.9
O/F 2.30
Pfuel feed
Pc
Pox feed
Time
10 ms

Figure 2-11

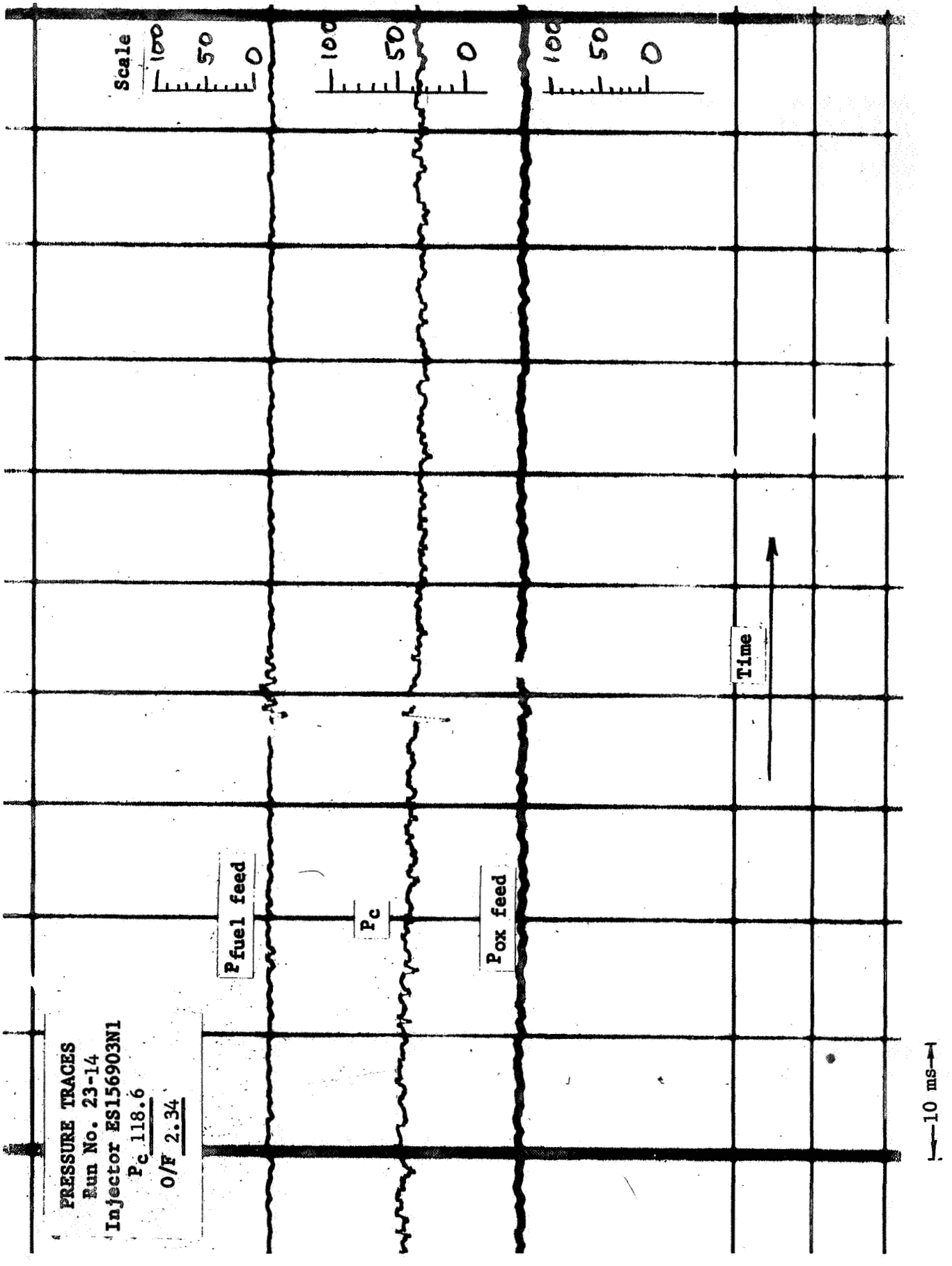

20-309

Figure 2-12

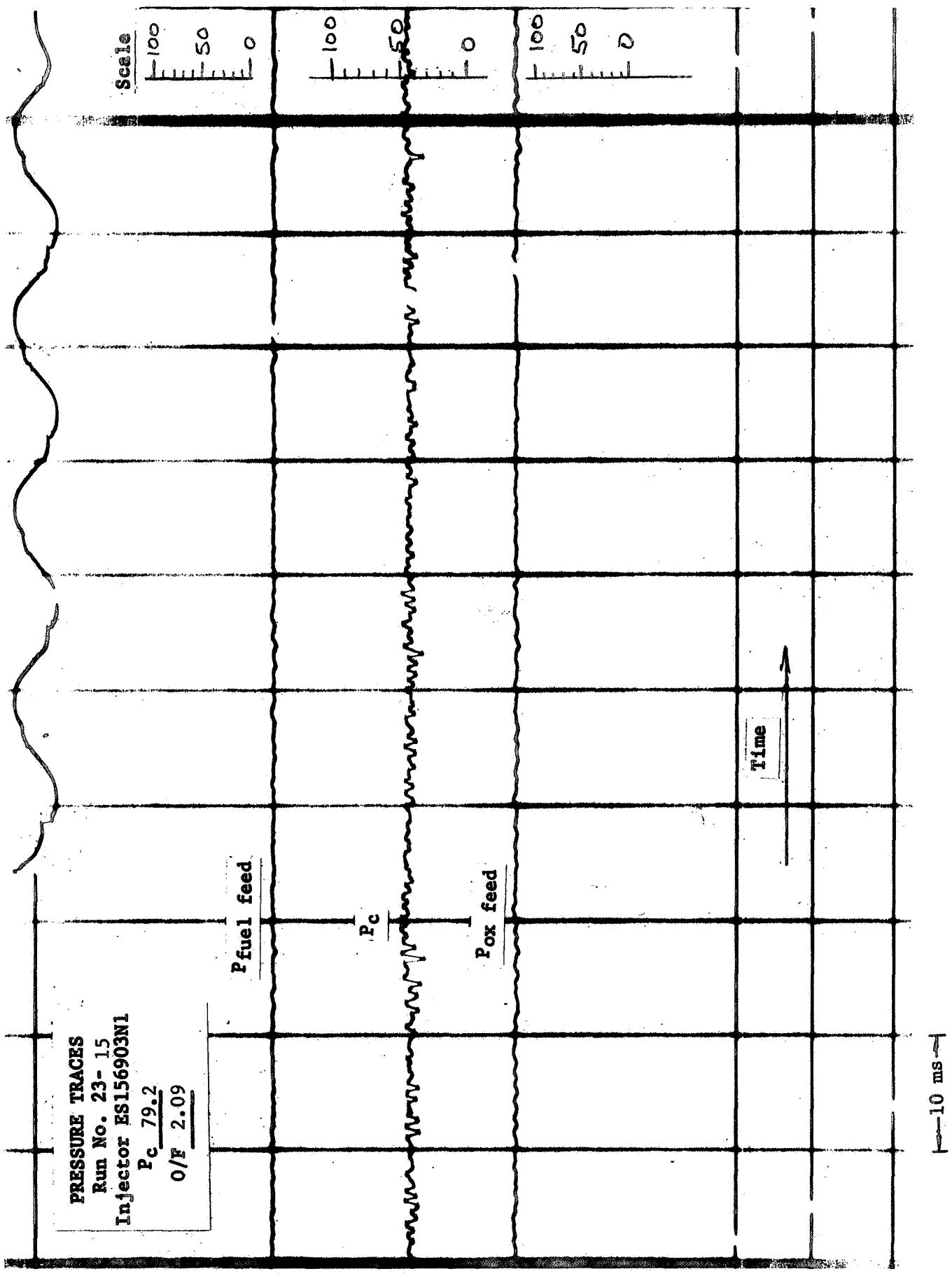

20-408

Figure 2-13

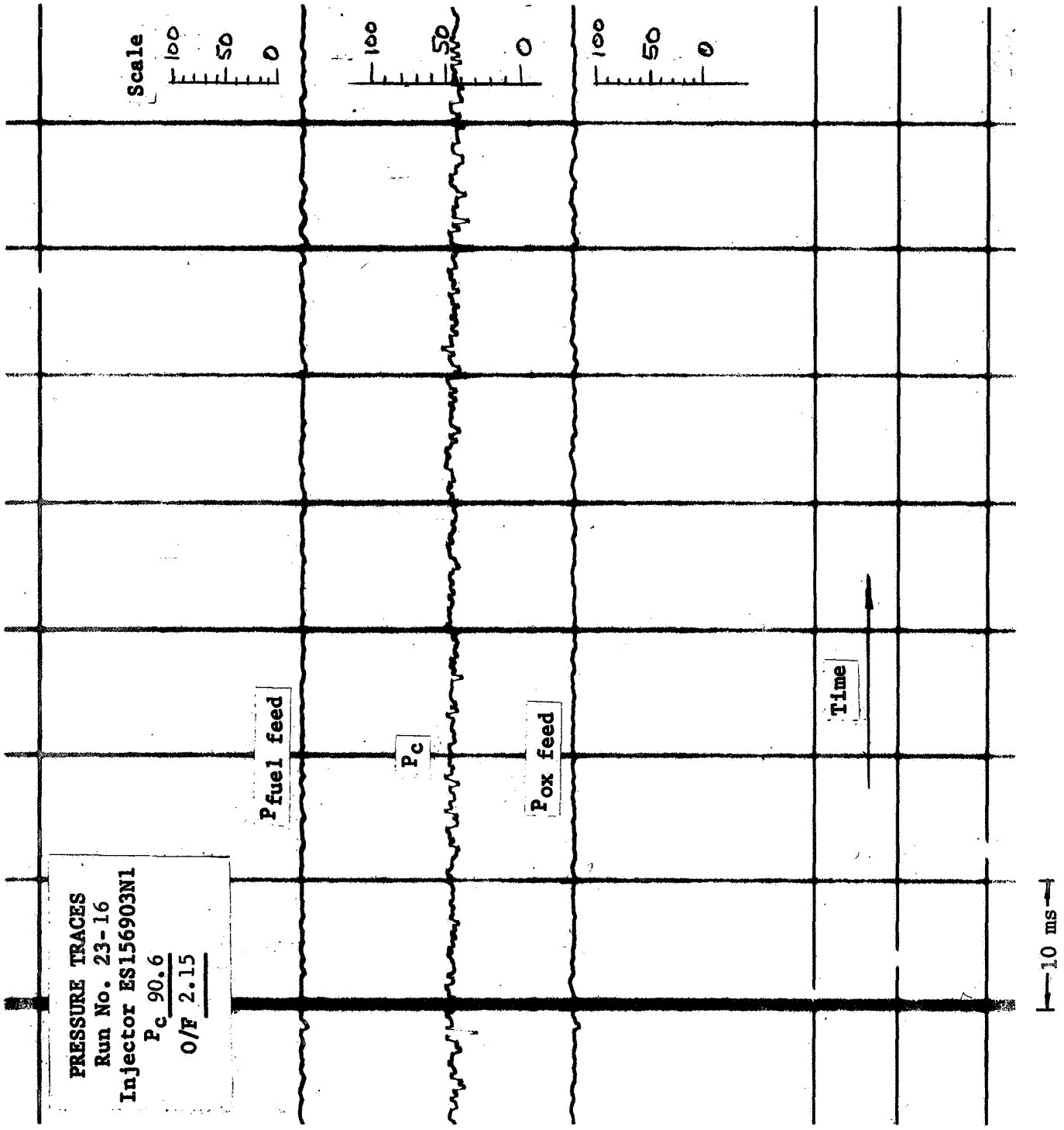
Scale
100
50
0
100
50
0
100
50
0
Pfuel feed
Pc
Pox feed
Time
10 ms
PRESSURE TRACES
Run No. 23-16
Injector ES156903N1
Pc 90.6
O/F 2.15

Figure 2-14

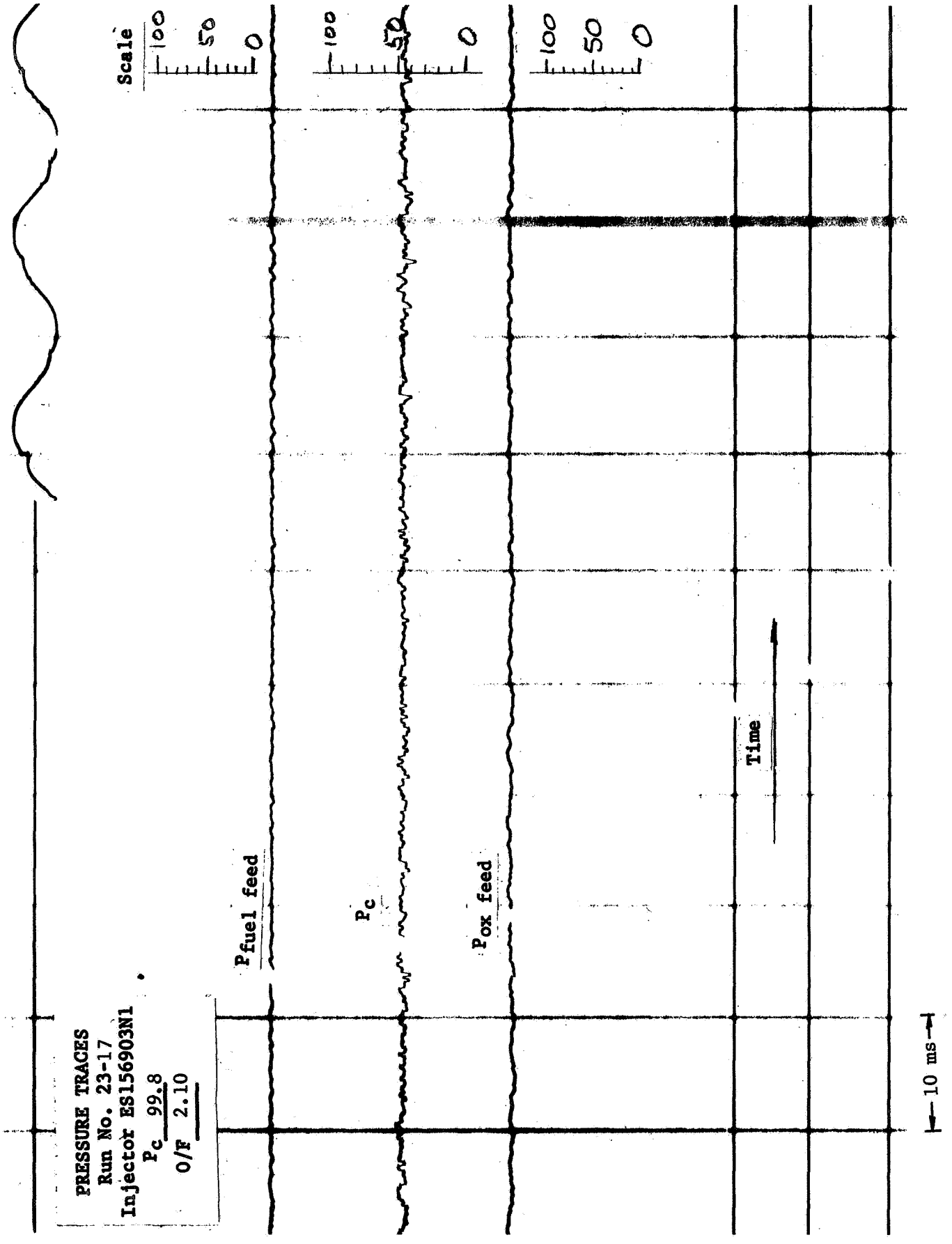

20-351

Figure 2-15

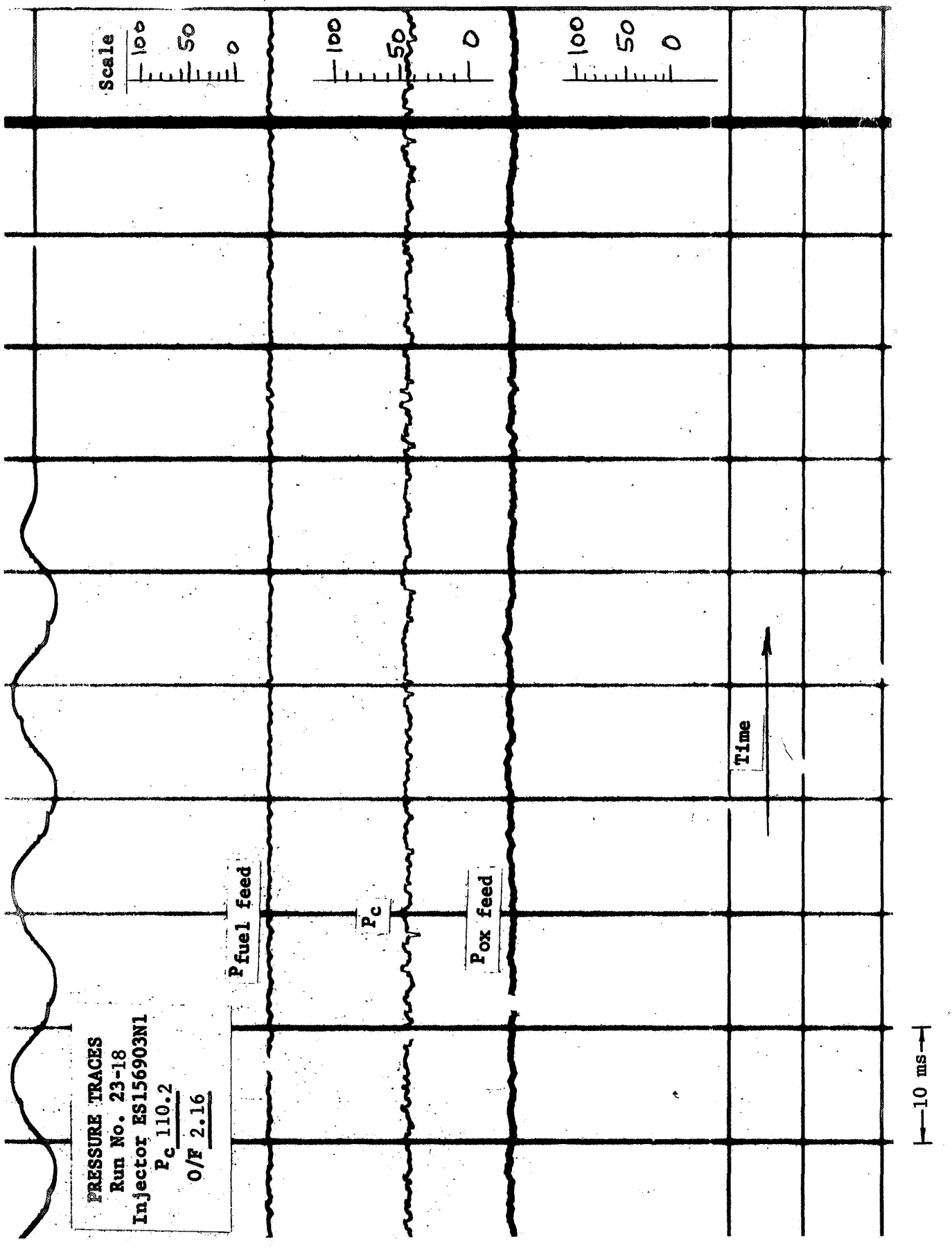
Scale
100
50
0
100
50
0
100
50
0
Time
$P_{fuel\ feed}$
P_c
$P_{ox\ feed}$
PRESSURE TRACES
Run No. 23-18
Injector ES156903N1
P_c 110.2
O/F 2.16
10 ms

Figure 2-16

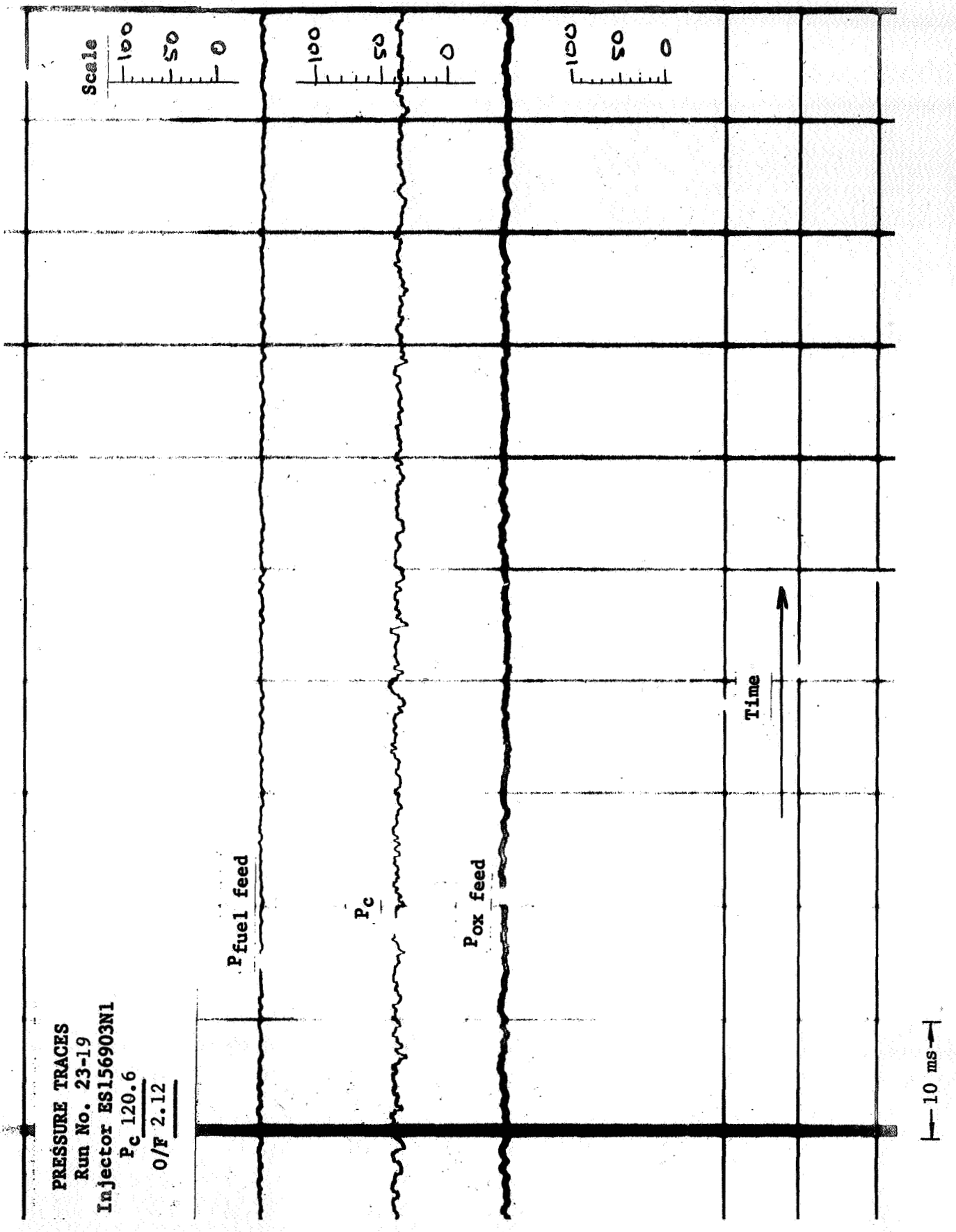
Scale
100
50
0
100
50
0
100
50
0
PRESSURE TRACES
Run No. 23-19
Injector ES156903N1
Pc 120.6
O/F 2.12
Pfuel feed
Pc
Pox feed
Time
10 ms

Figure 2-17

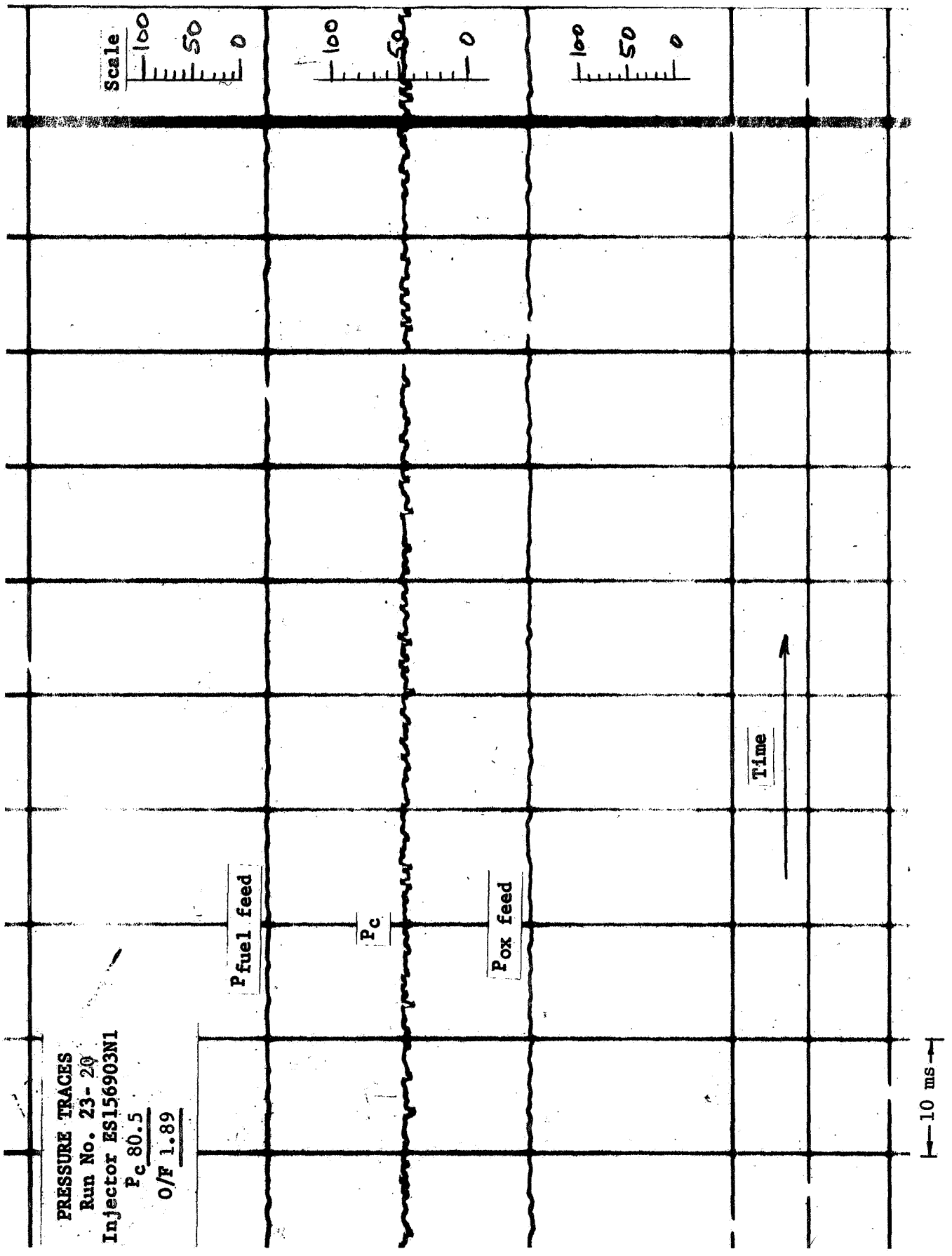

20-385

Figure 2-18

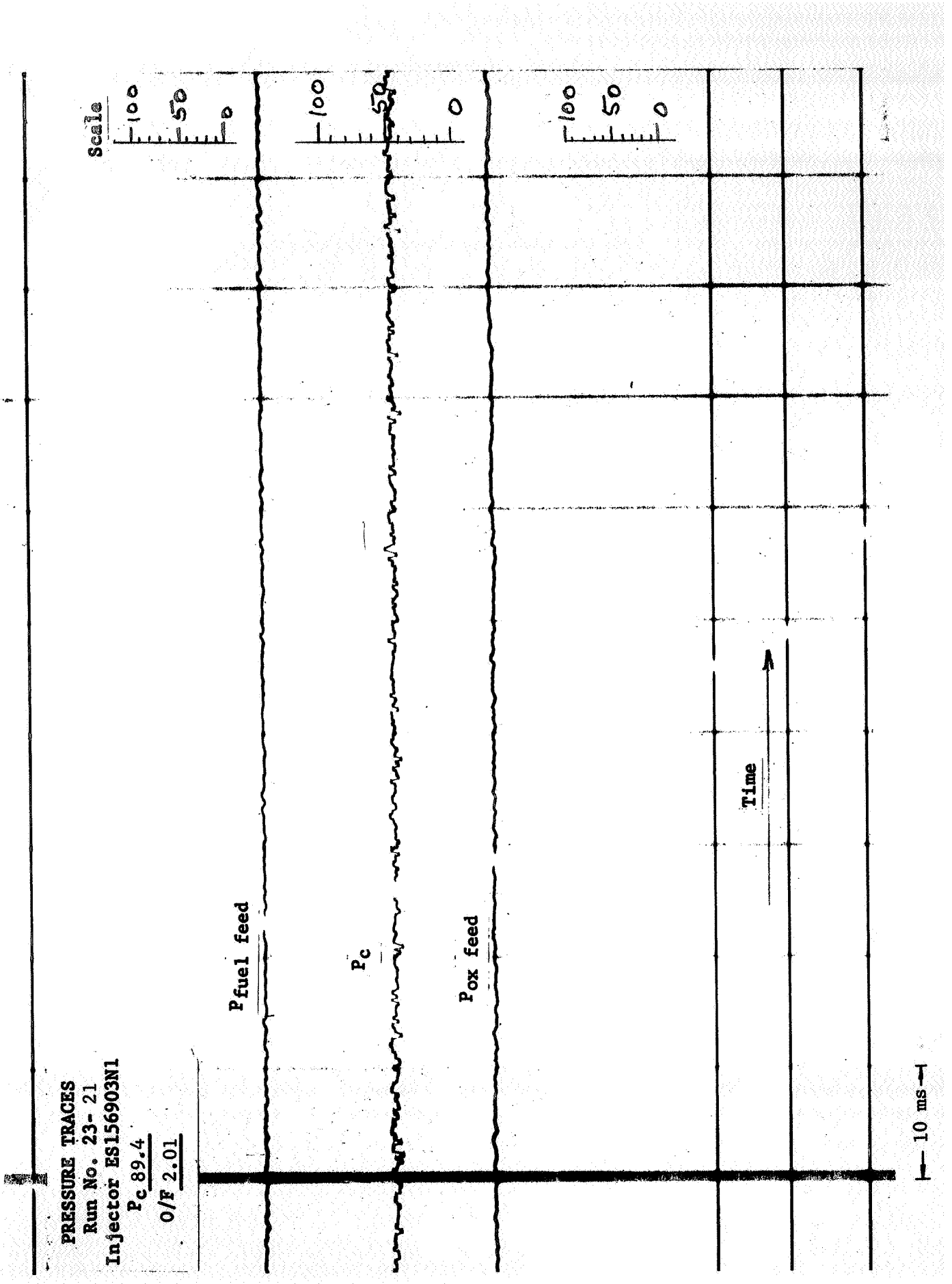
Scale
100
50
0
100
50
0
100
50
0
PRESSURE TRACES
Run No. 23-21
Injector ES156903N1
Pc 89.4
O/F 2.01
Pfuel feed
Pc
Pox feed
Time
10 ms

Figure 2-19

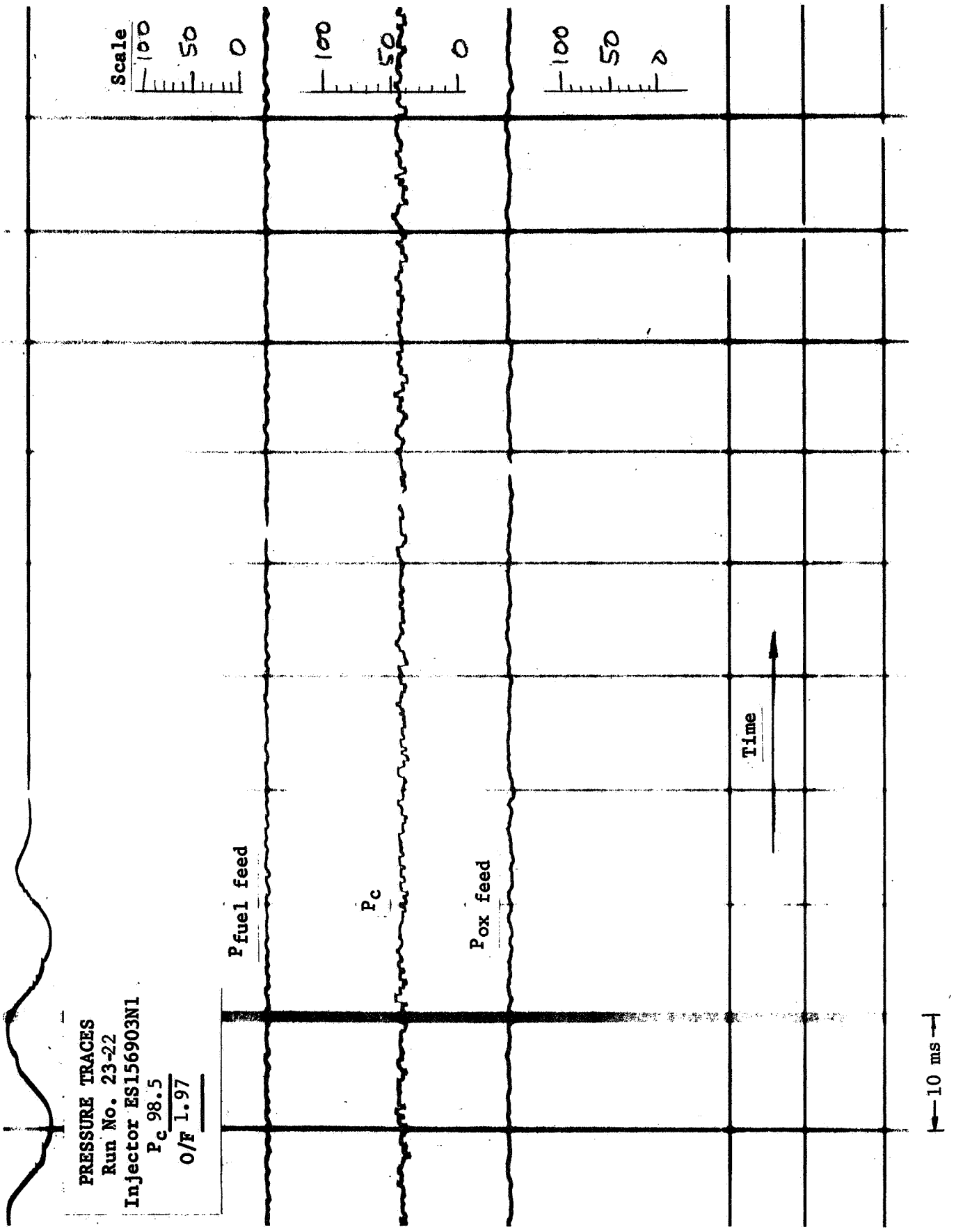

20-317

Figure 2-20

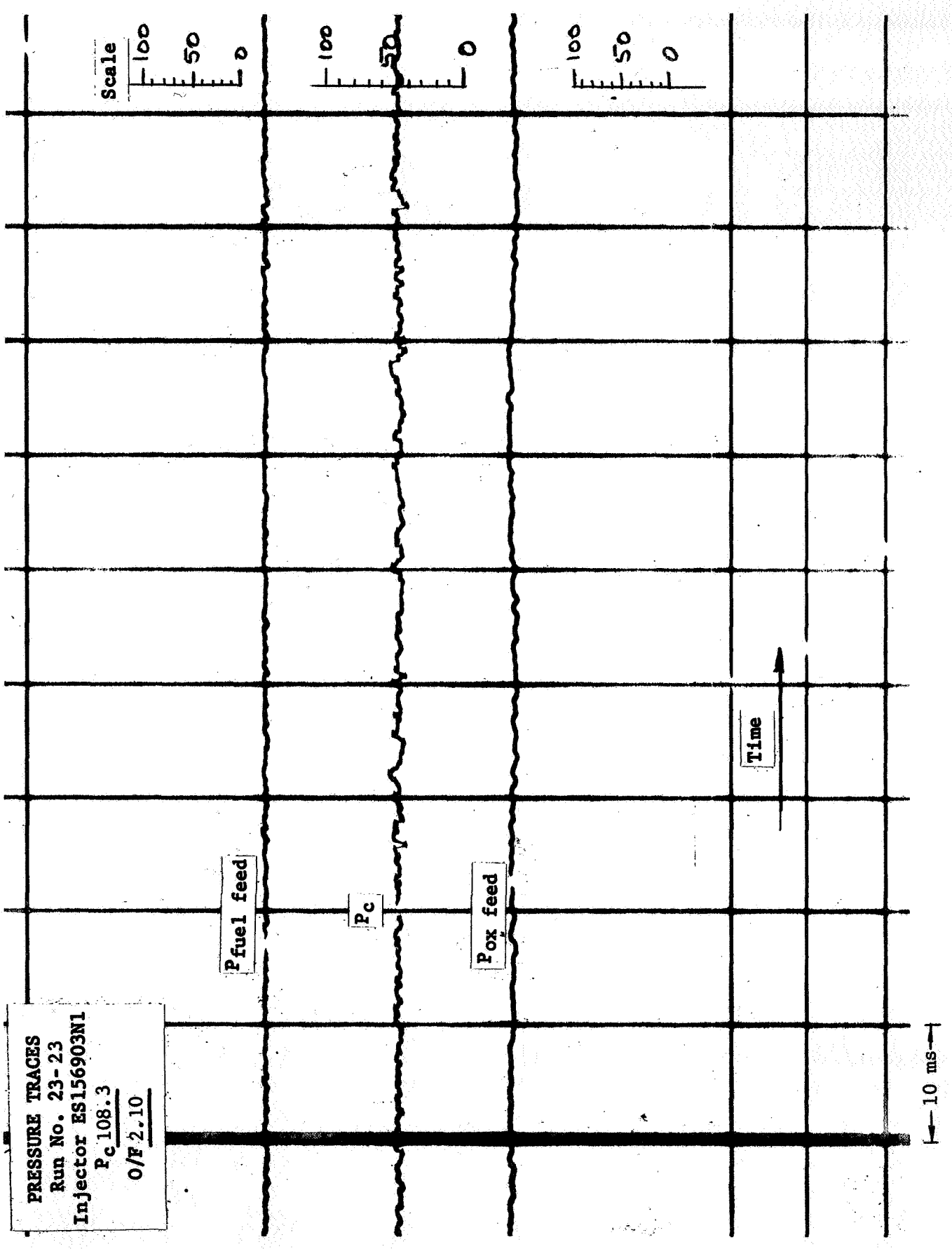

20-394

Figure 2-21

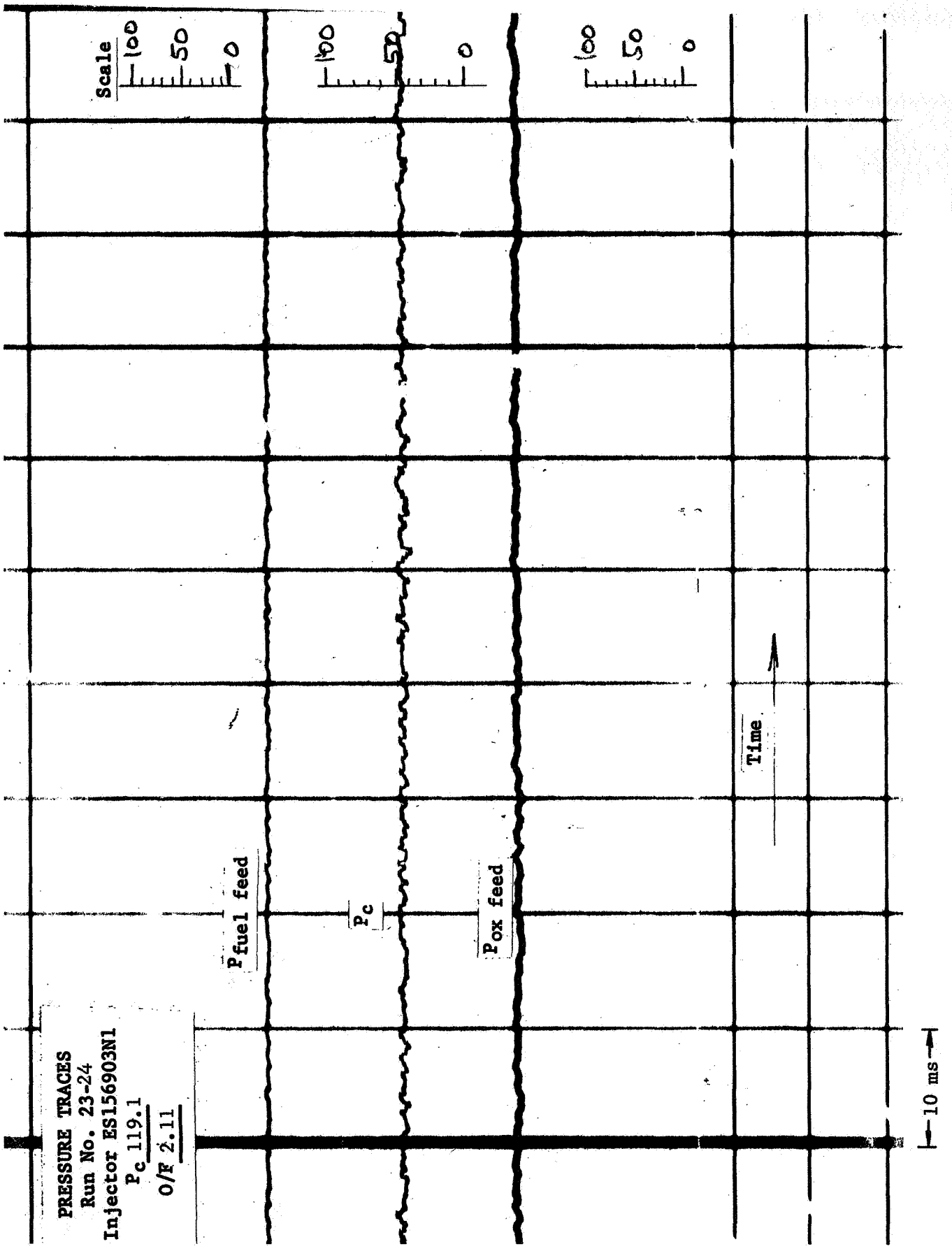

20-332

Figure 2-22

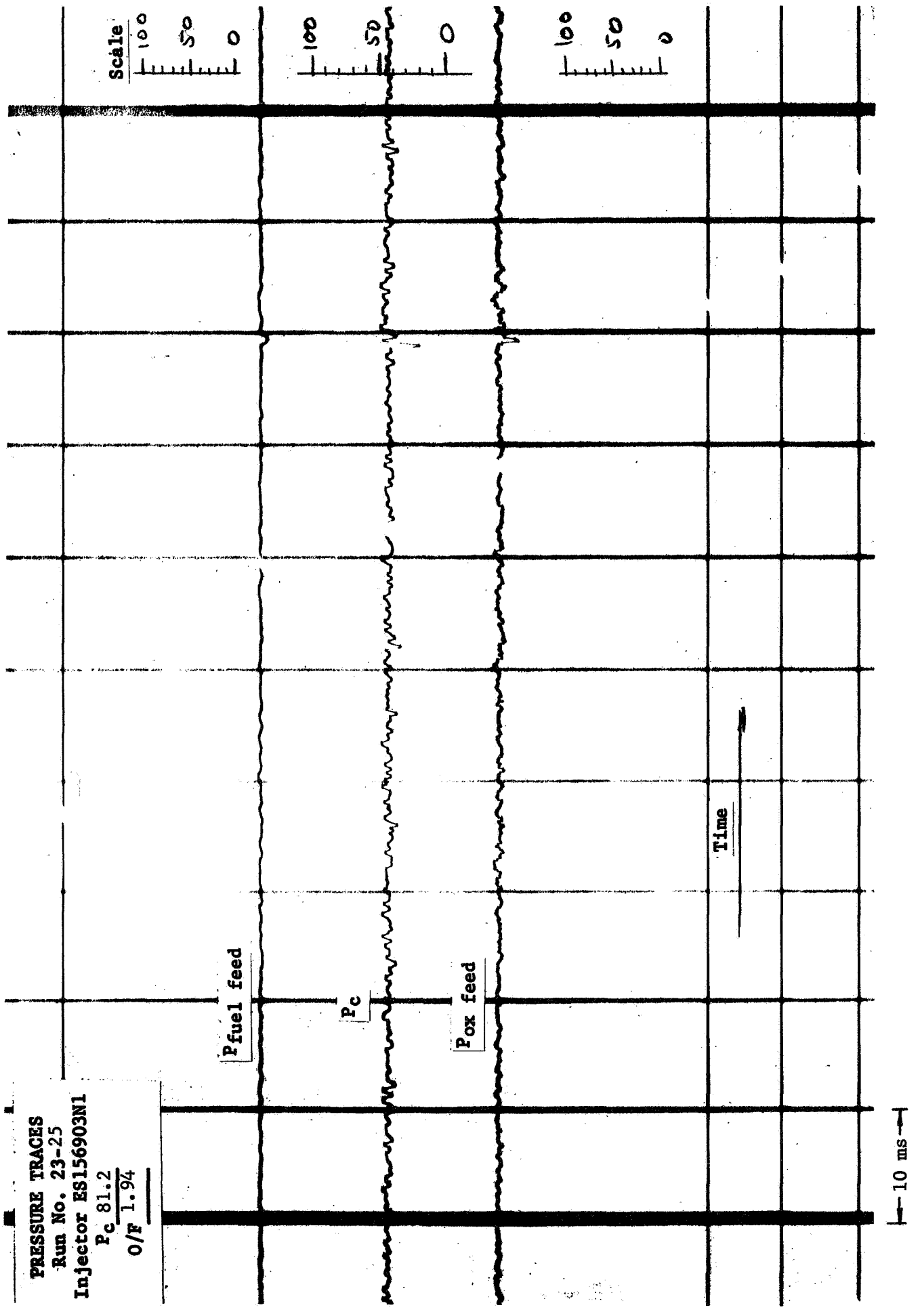

20-365

Figure 2-23

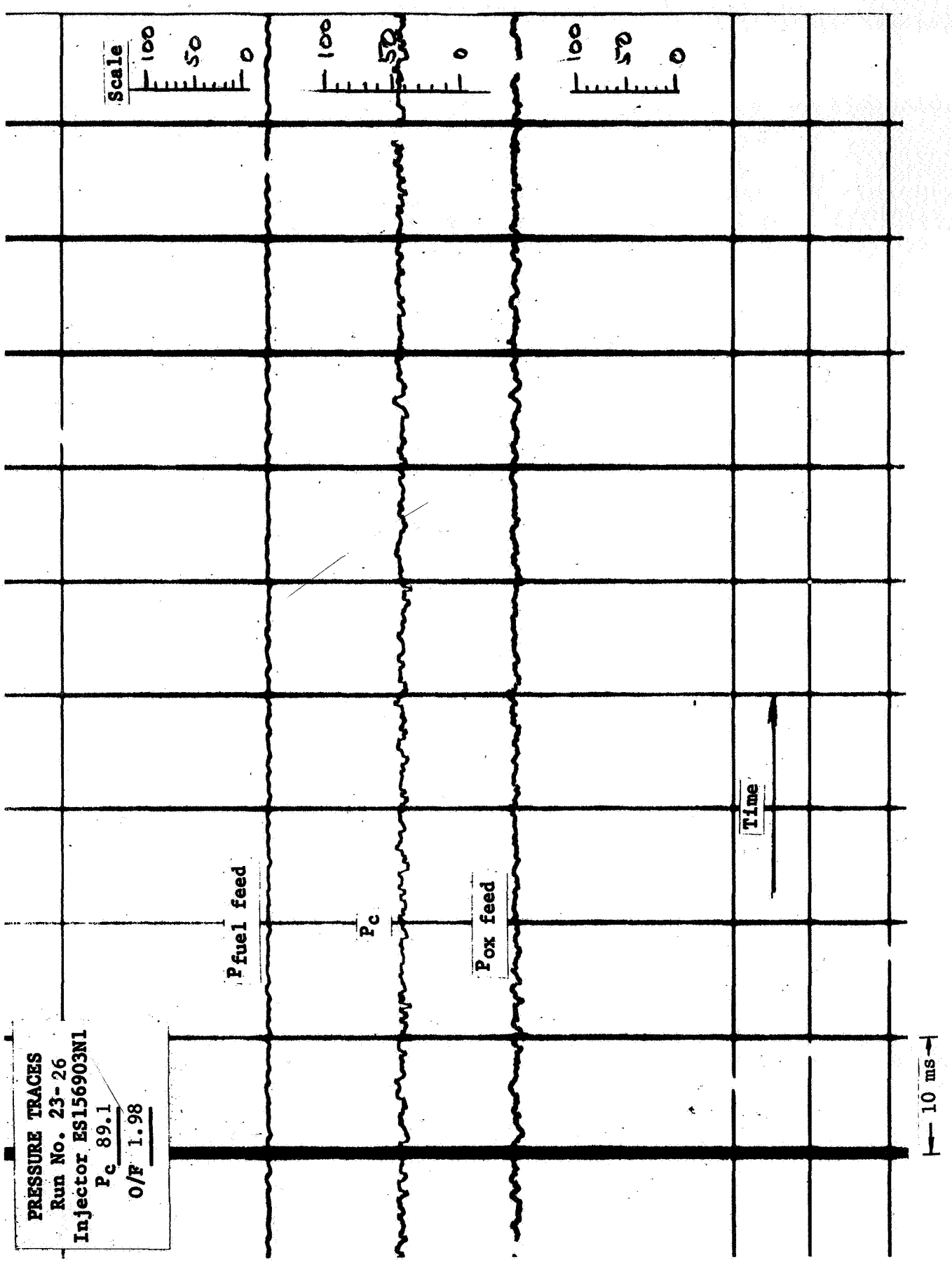
Scale
100
50
0
100
50
0
100
50
0
Pfuel feed
Pc
Pox feed
Time
10 ms
PRESSURE TRACES
Run No. 23-26
Injector ES156903N1
Pc 89.1
O/F 1.98

Figure 2-24

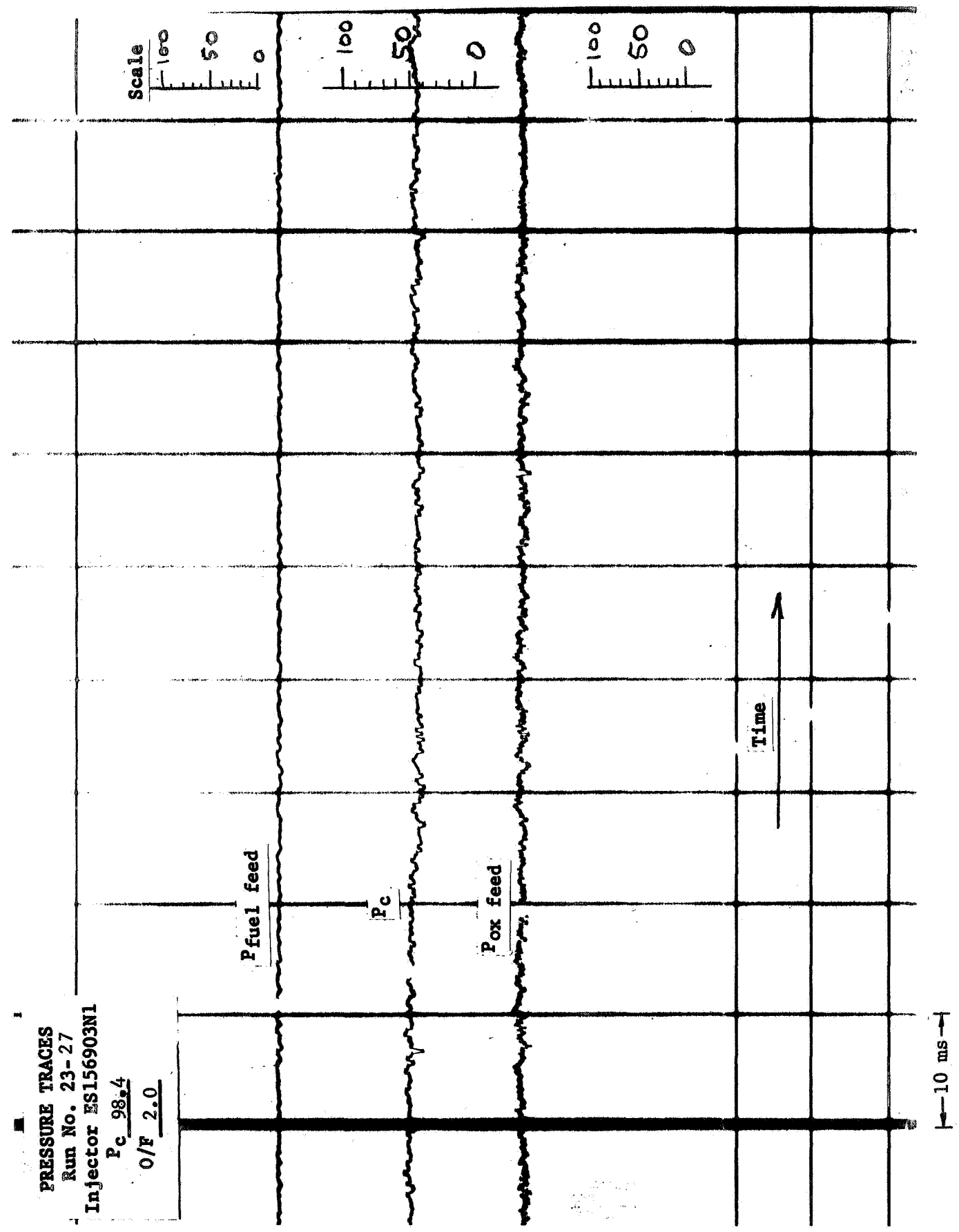

20-322

Figure 2-25

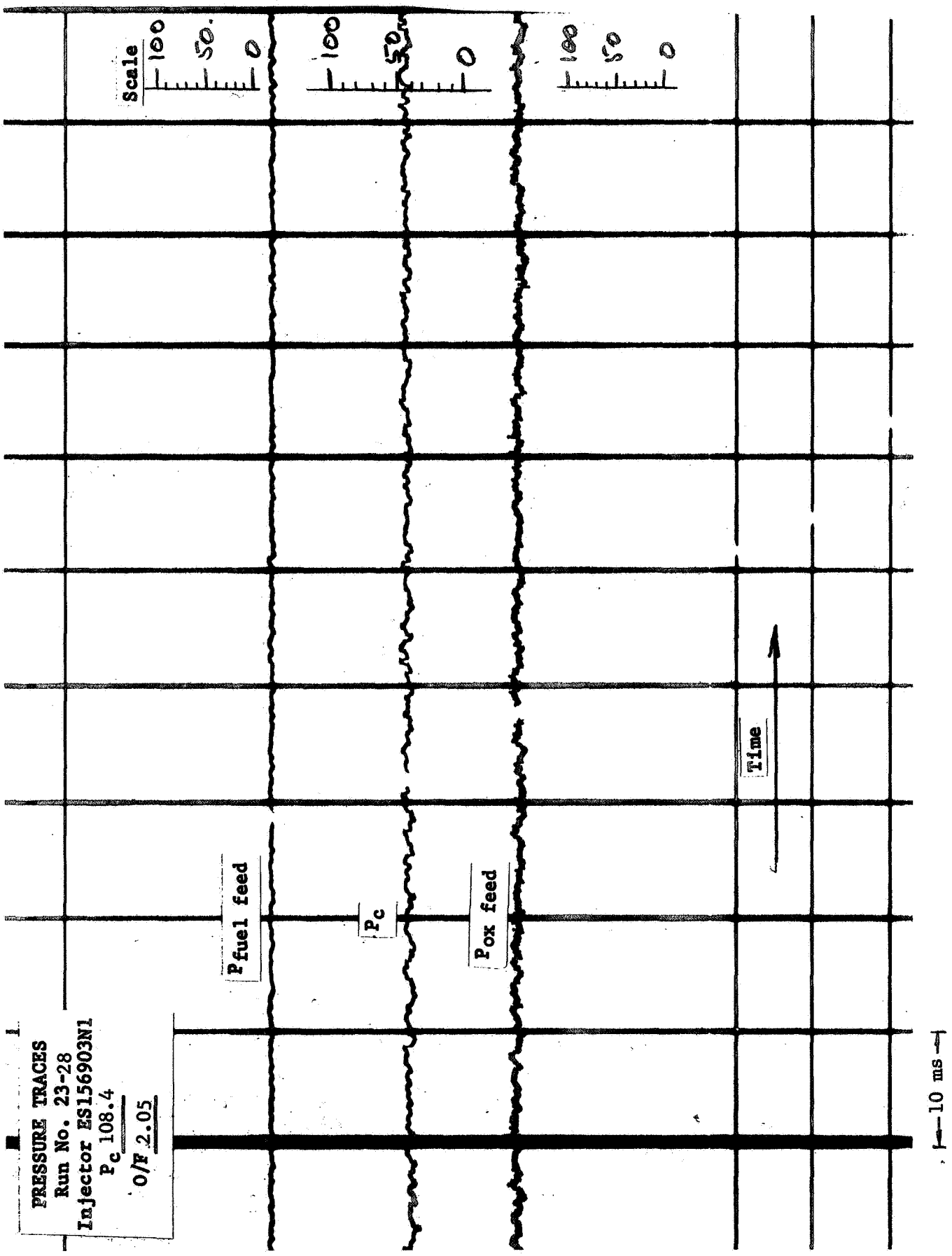
Scale
100
50
0
100
50
0
100
50
0
Pfuel feed
Pc
Pox feed
Time
10 ms
PRESSURE TRACES
Run No. 23-28
Injector ES156903N1
Pc 108.4
O/F 2.05

Figure 2-26

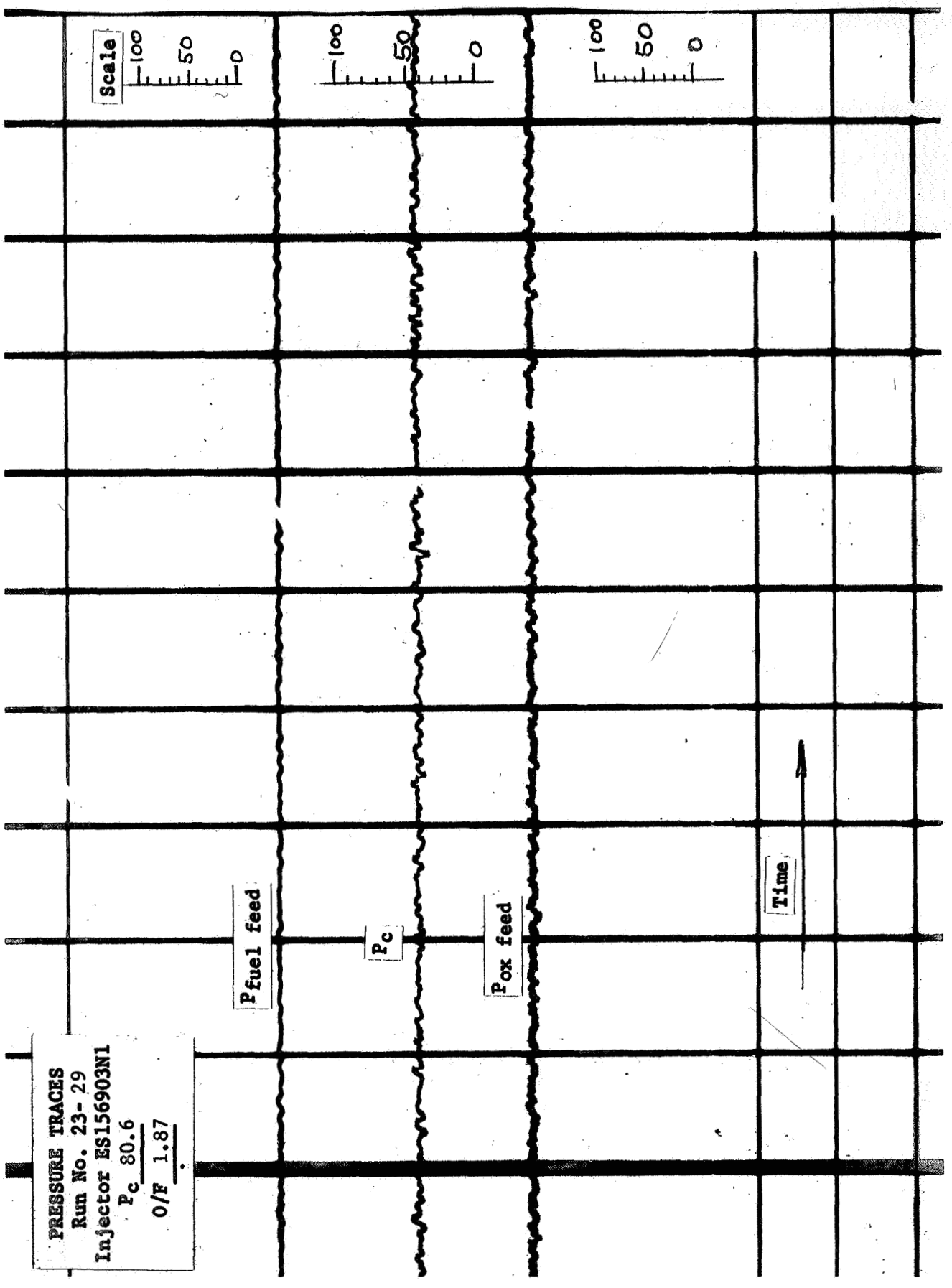

20-390

Figure 2-27

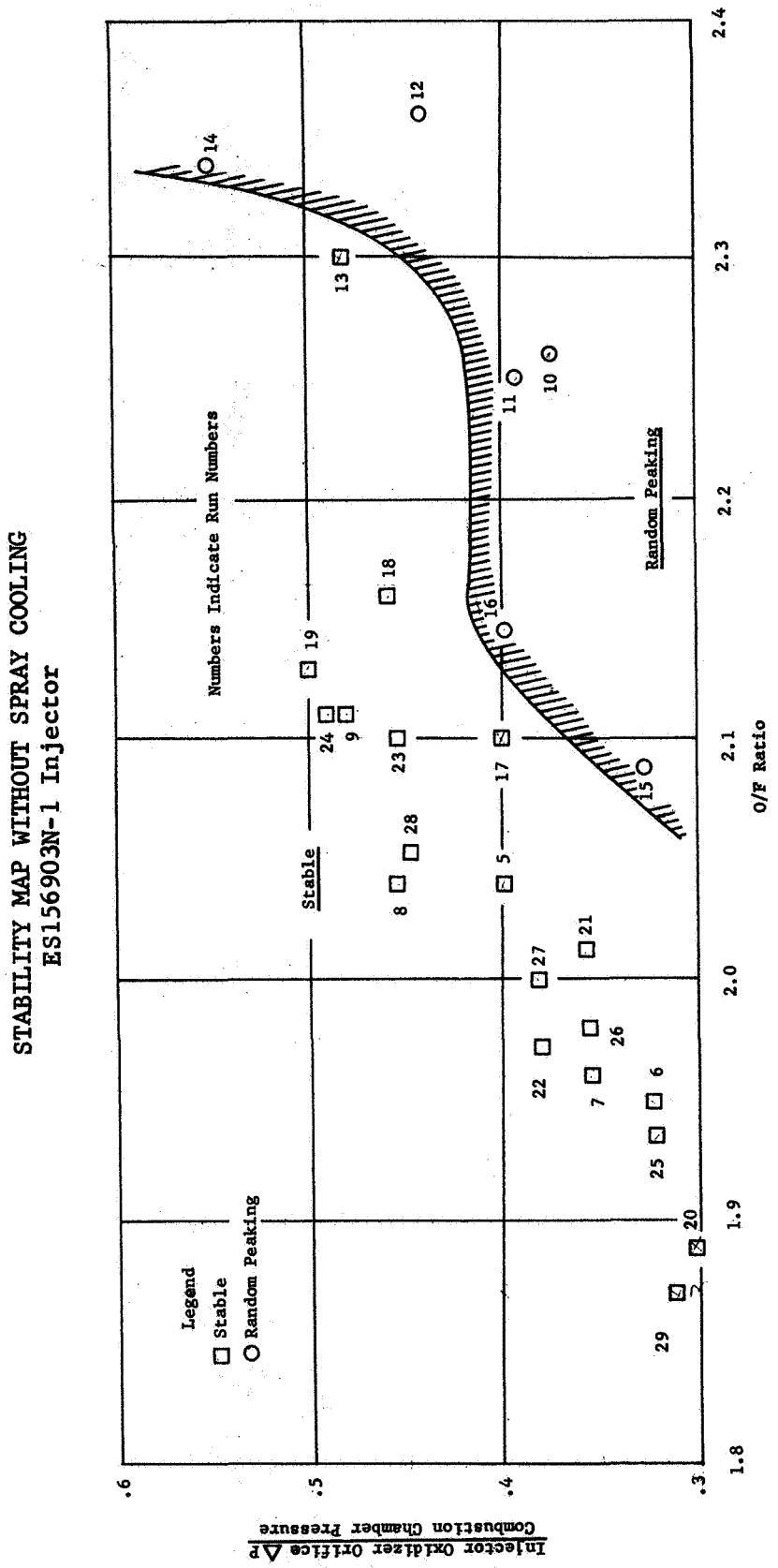
STABILITY MAP WITHOUT SPRAY COOLING
ES156903N-1 Injector
Numbers Indicate Run Numbers
Stable
Random Peaking
Legend
Stable
Random Peaking
Injector Oxidizer Orifice ΔP / Combustion Chamber Pressure
O/F Ratio
.6
.5
.4
.3
1.8
1.9
2.0
2.1
2.2
2.3
2.4

Figure 2-28

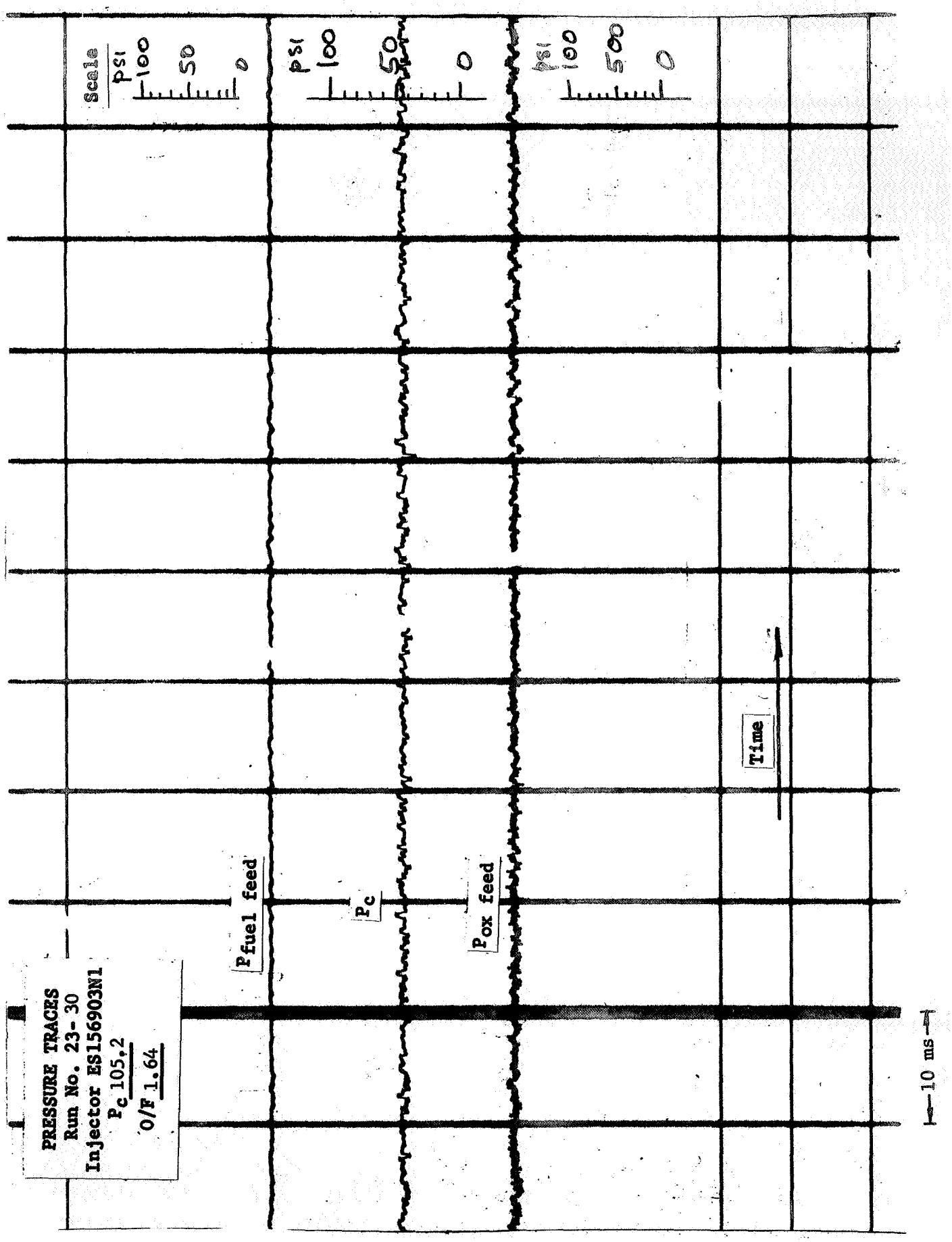
Scale
PSI
100
50
0
PSI
100
50
0
PSI
100
500
0
PRESSURE TRACES
Run No. 23-30
Injector ES156903N1
Pc 105.2
O/F 1.64
Pfuel feed
Pc
Pox feed
Time
10 ms

Figure 2-29

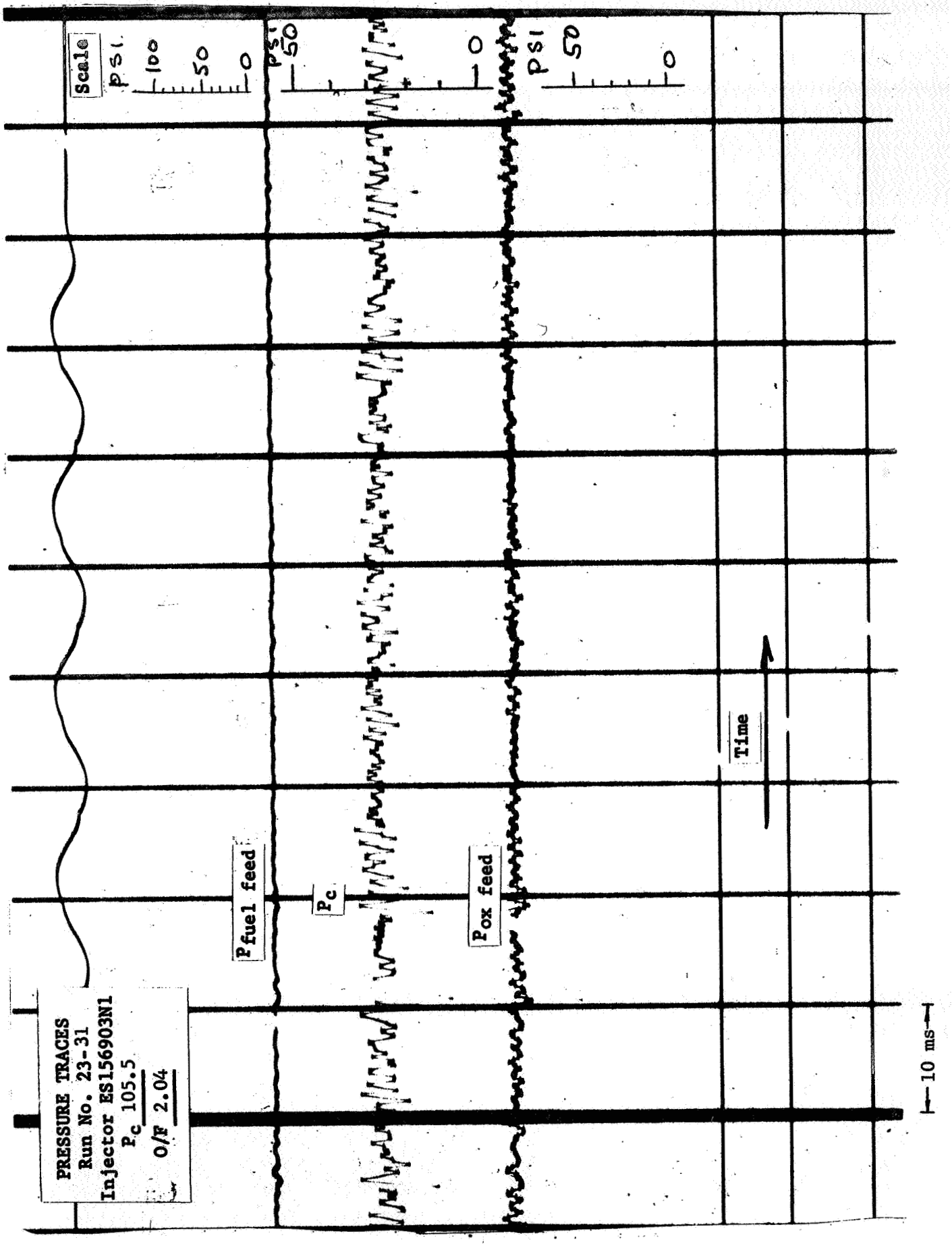

20-055

Figure 2-30

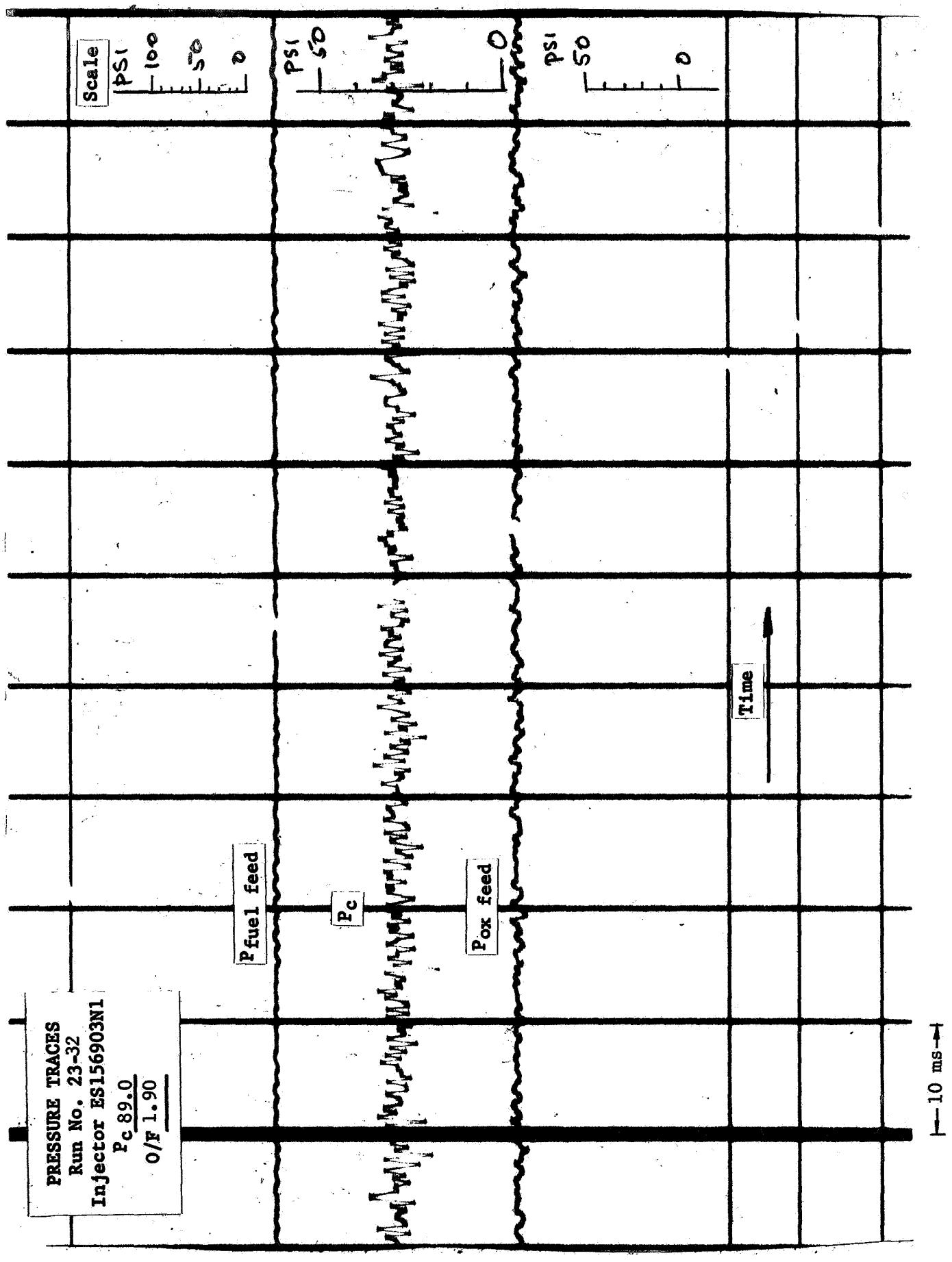

20-068

Figure 2-31

20-059

Figure 2-32

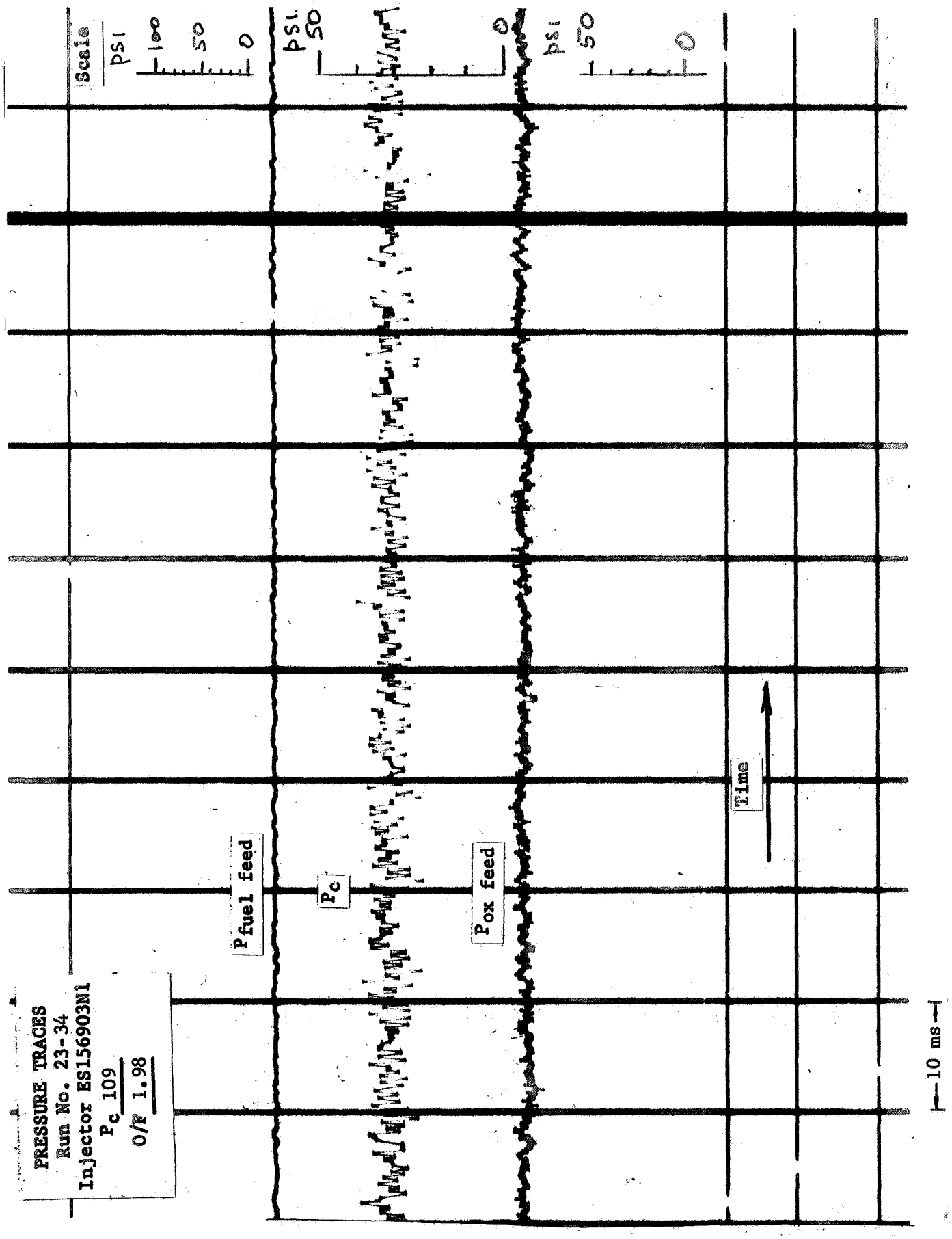

20-072

Figure 2-33

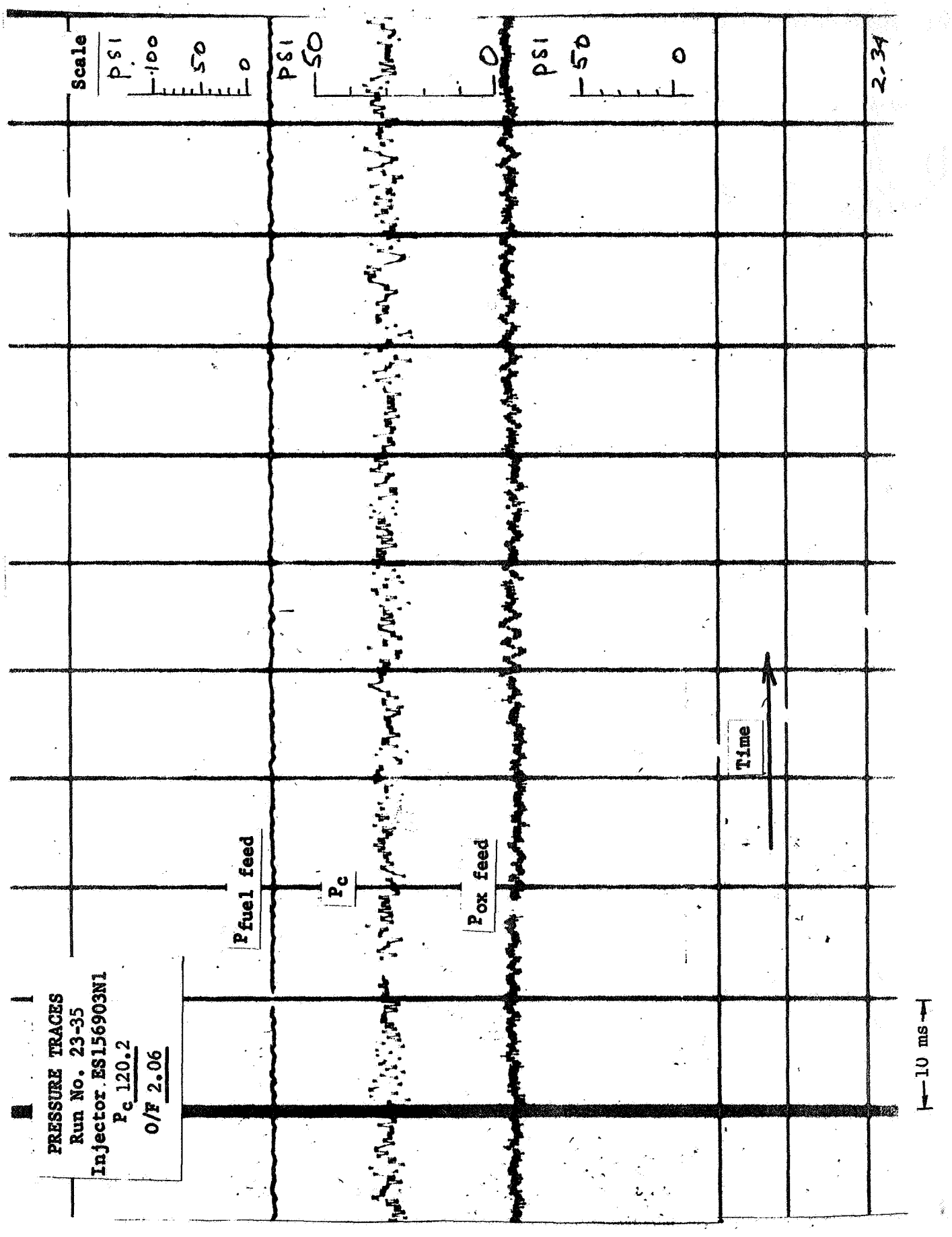

20-050

Figure 2-34

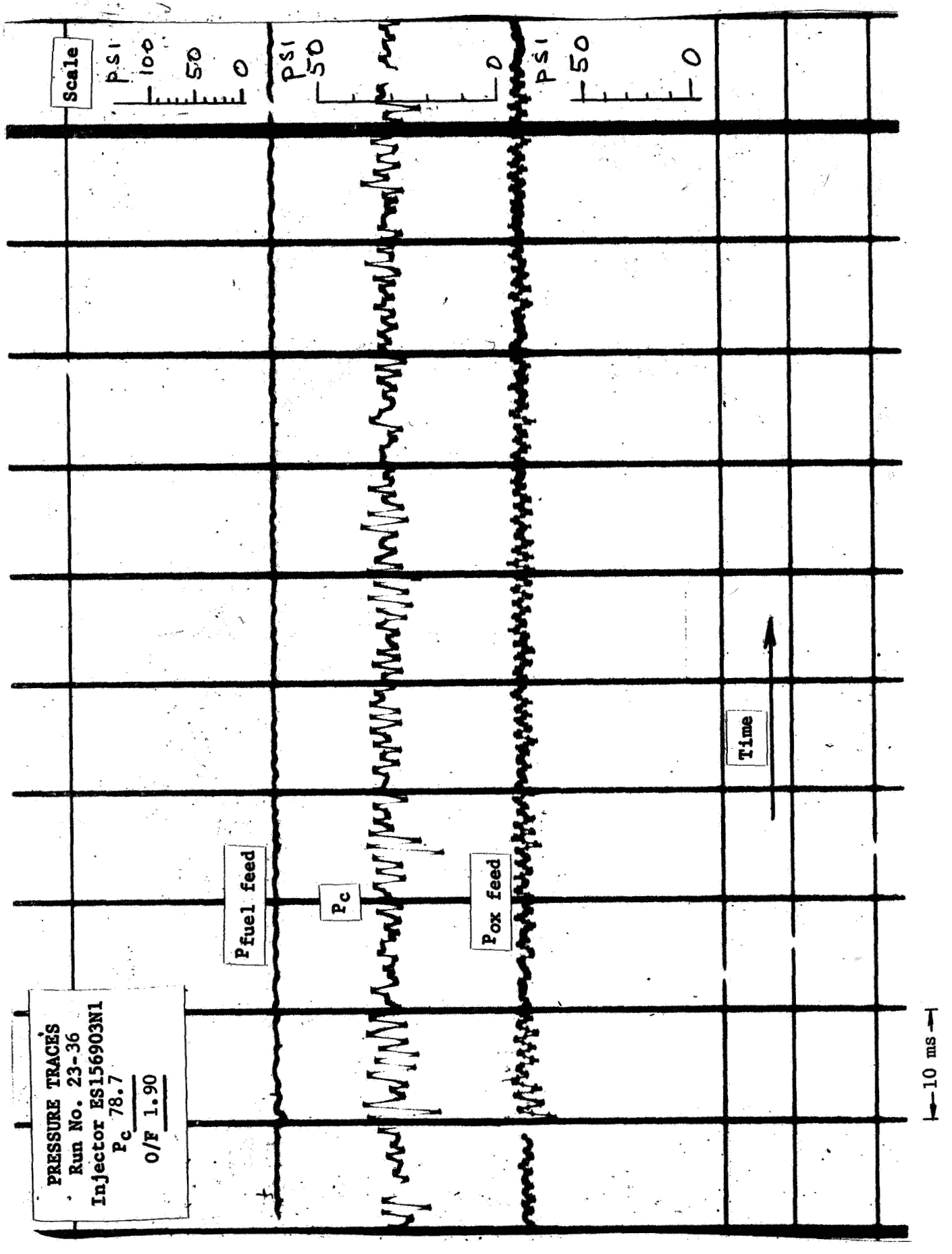

20-021

Figure 2-35

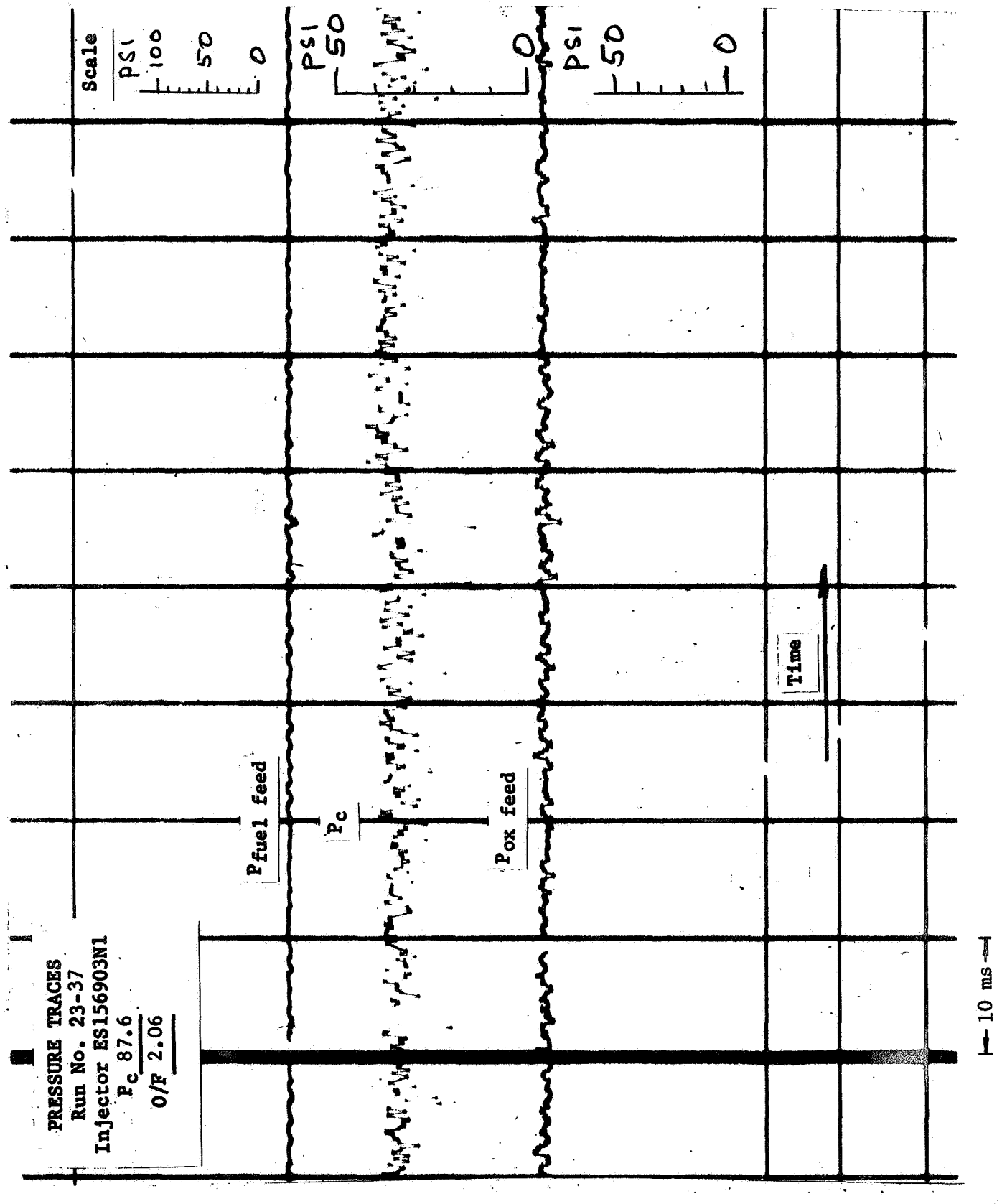
PRESSURE TRACES
Run No. 23-37
Injector ES156903N1
Pc 87.6
O/F 2.06
Scale
PSI
100
50
0
PSI
50
0
PSI
50
0
Pfuel feed
Pc
Pox feed
Time
10 ms

Figure 2-36

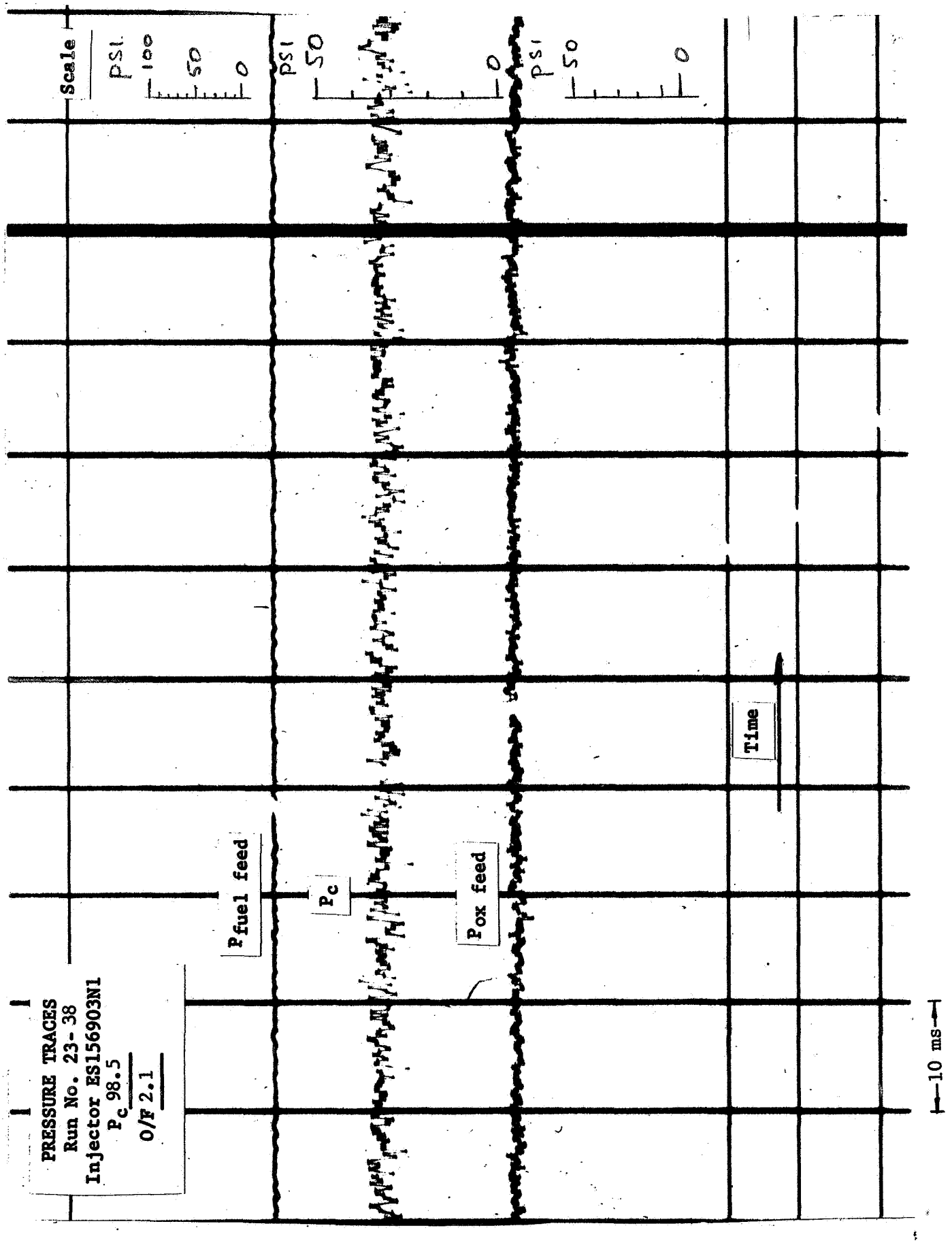

20-036

Figure 2-37

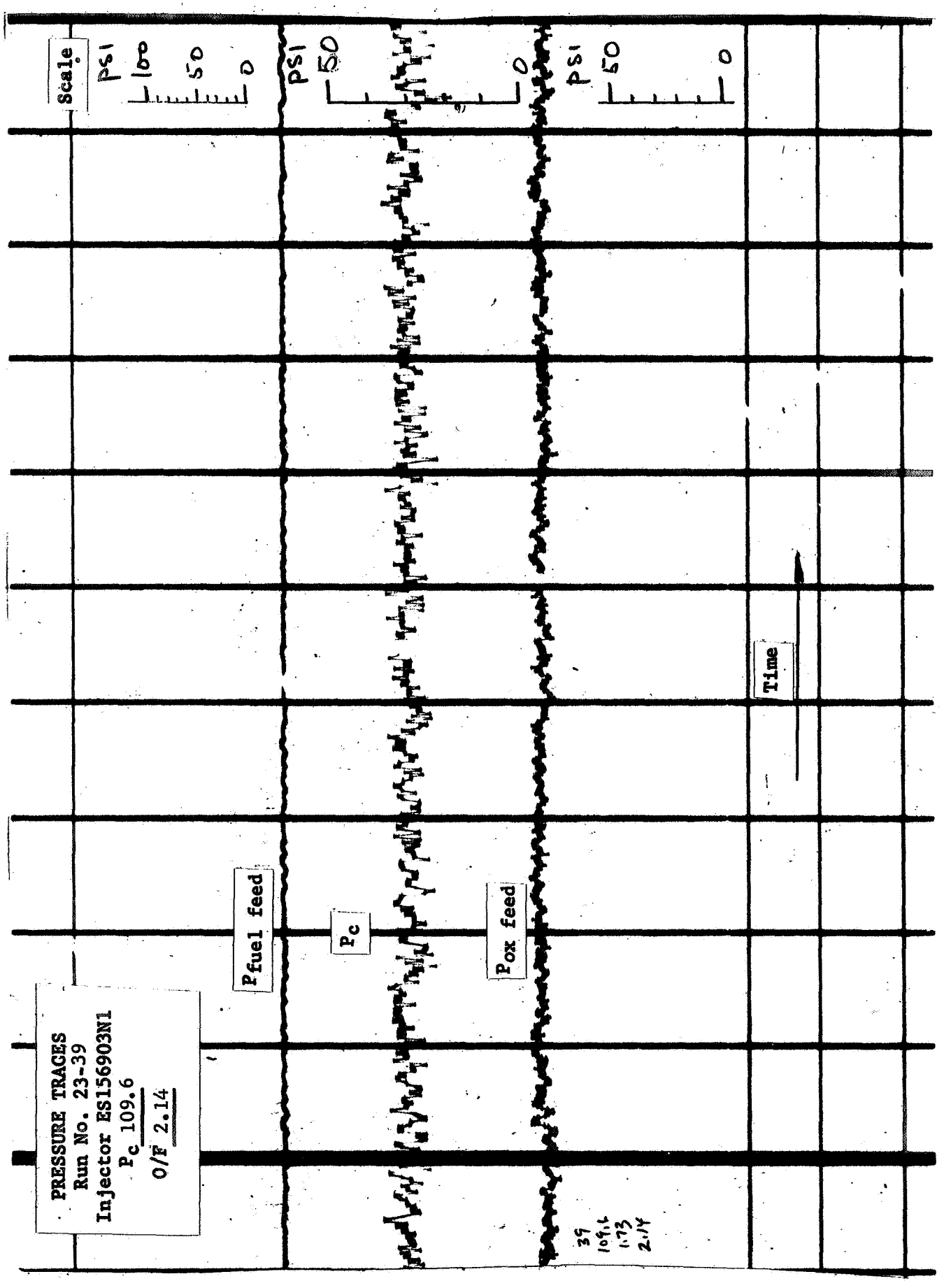
Scale
PSI
100
50
0
PSI
50
0
PSI
50
0
PRESSURE TRACES
Run No. 23-39
Injector ES156903N1
Pc 109.6
O/F 2.14
Pfuel feed
Pc
Pox feed
Time
10 ms
39
109.6
1.73
2.14

Figure 2-38

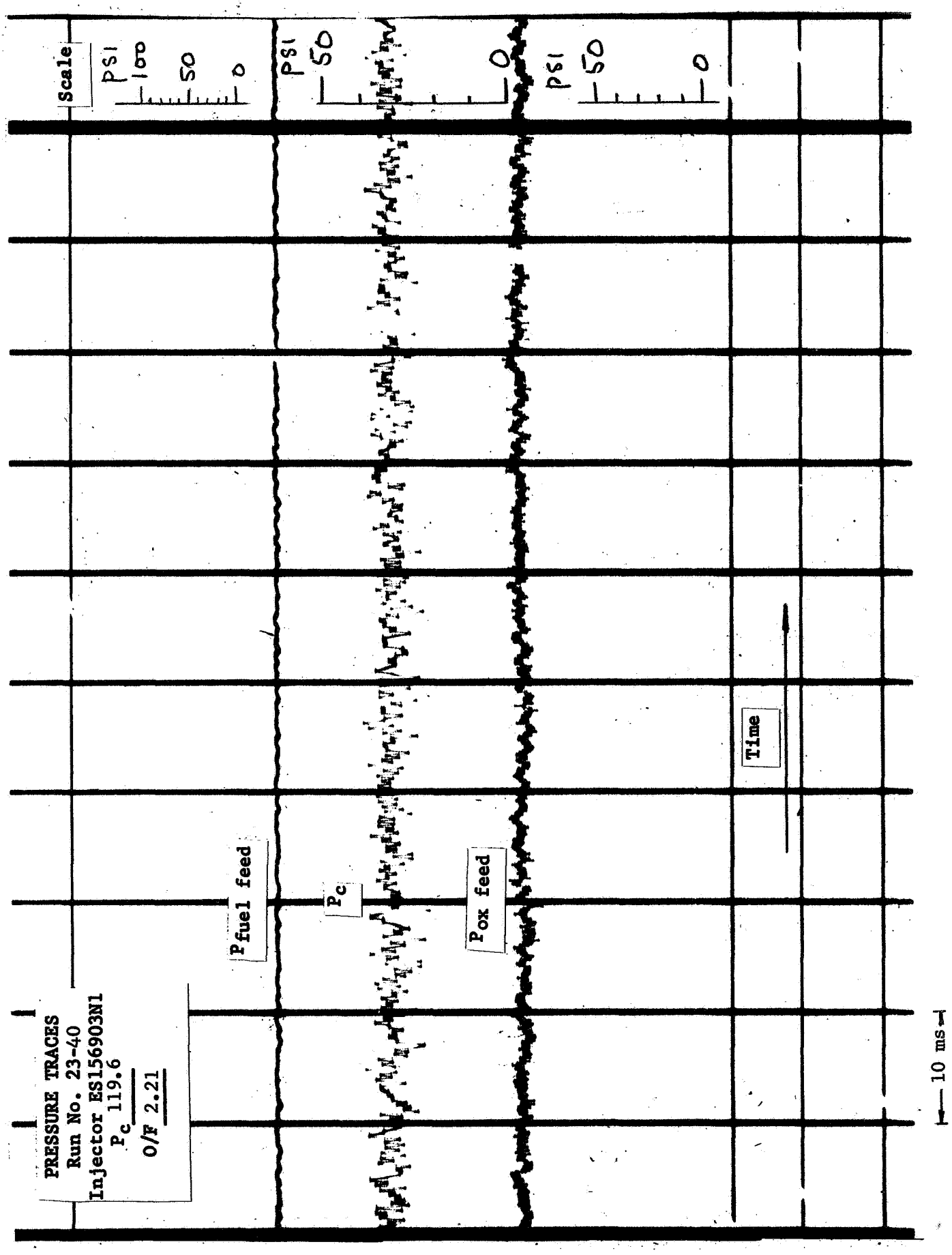

20-045

Figure 2-39

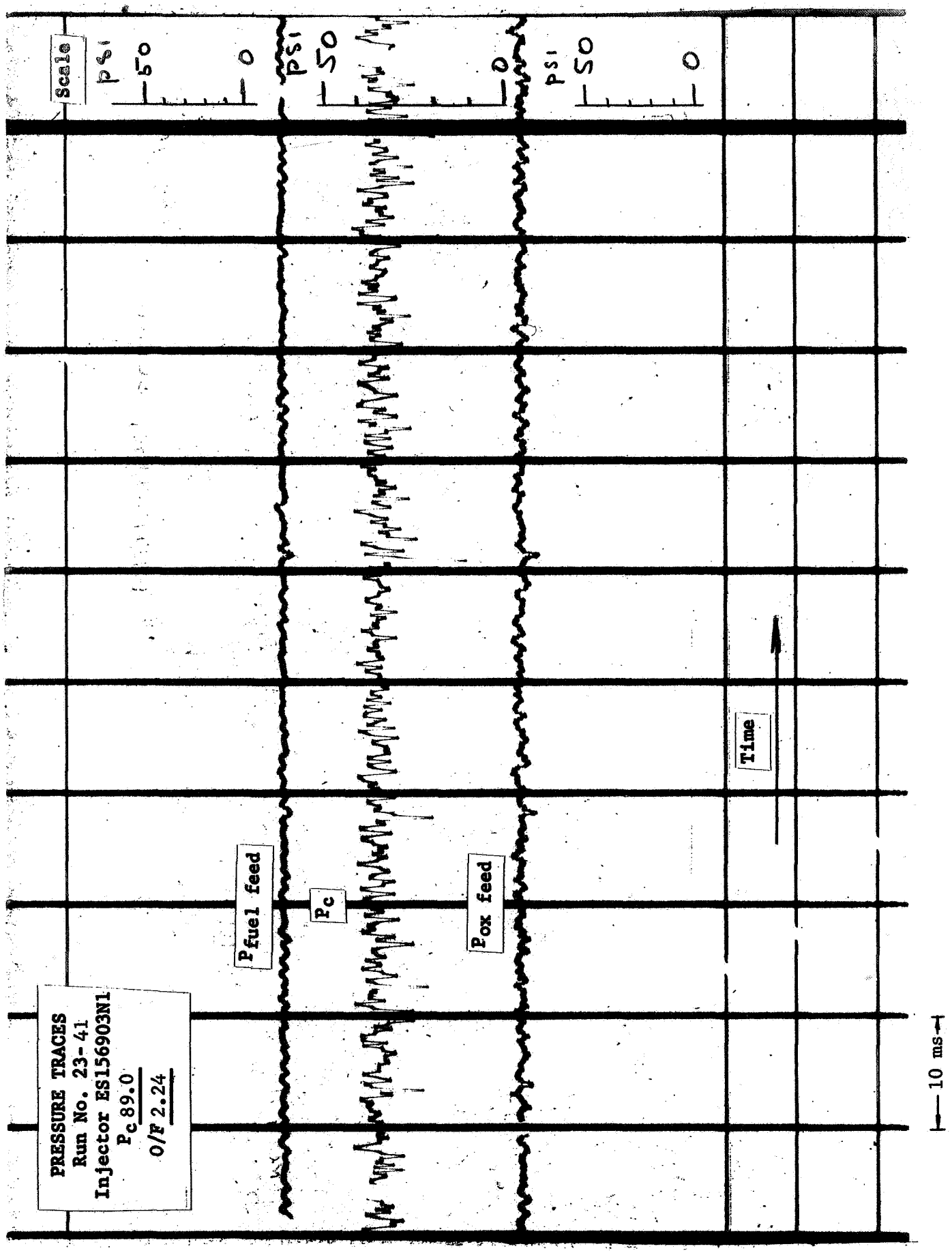
Scale
psi
50
0
psi
50
0
psi
50
0
Time
$P_{fuel\ feed}$
P_c
$P_{ox\ feed}$
PRESSURE TRACES
Run No. 23-41
Injector ES156903N1
P_c 89.0
O/F 2.24
10 ms

Figure 2-40

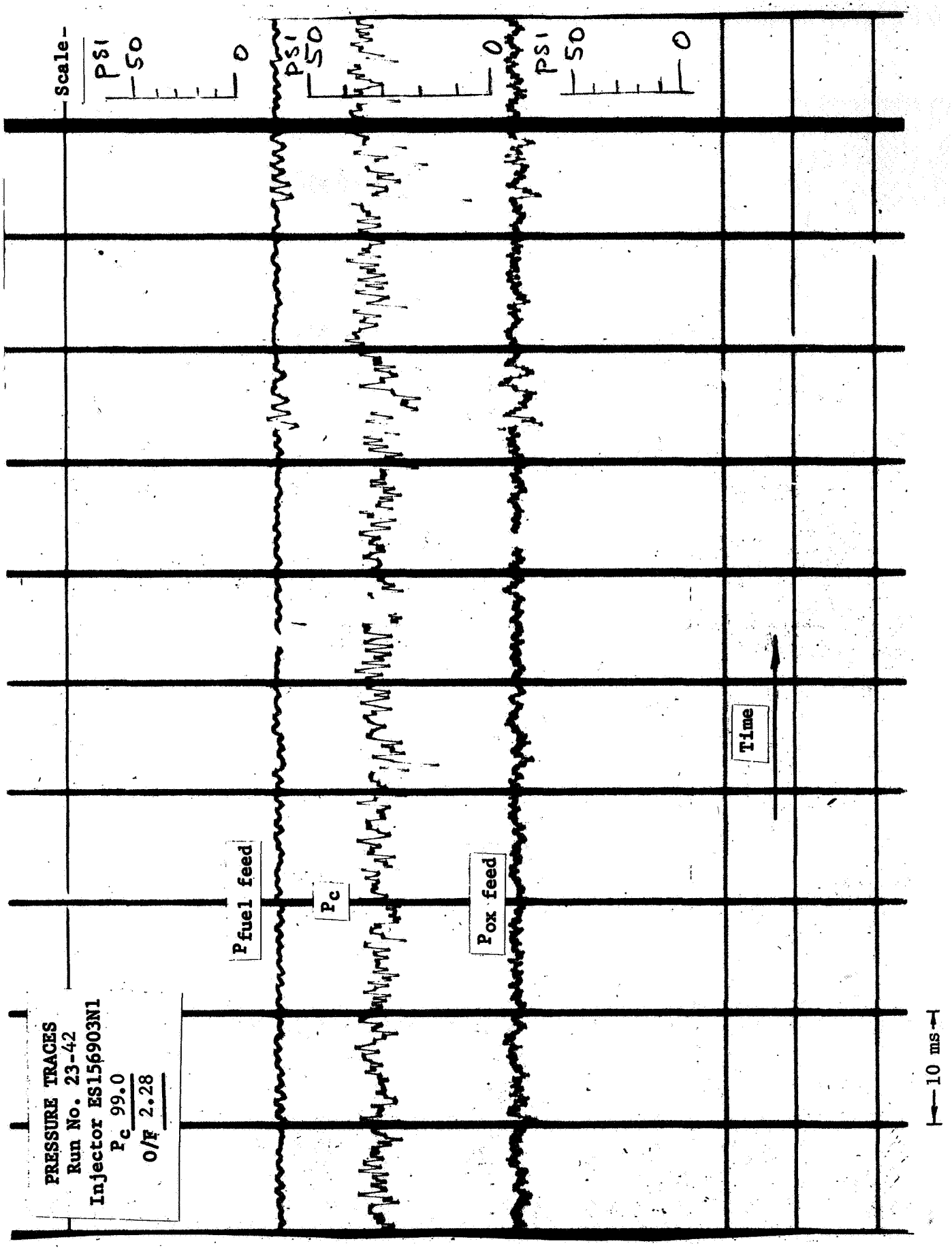

20-381

Figure 2-41

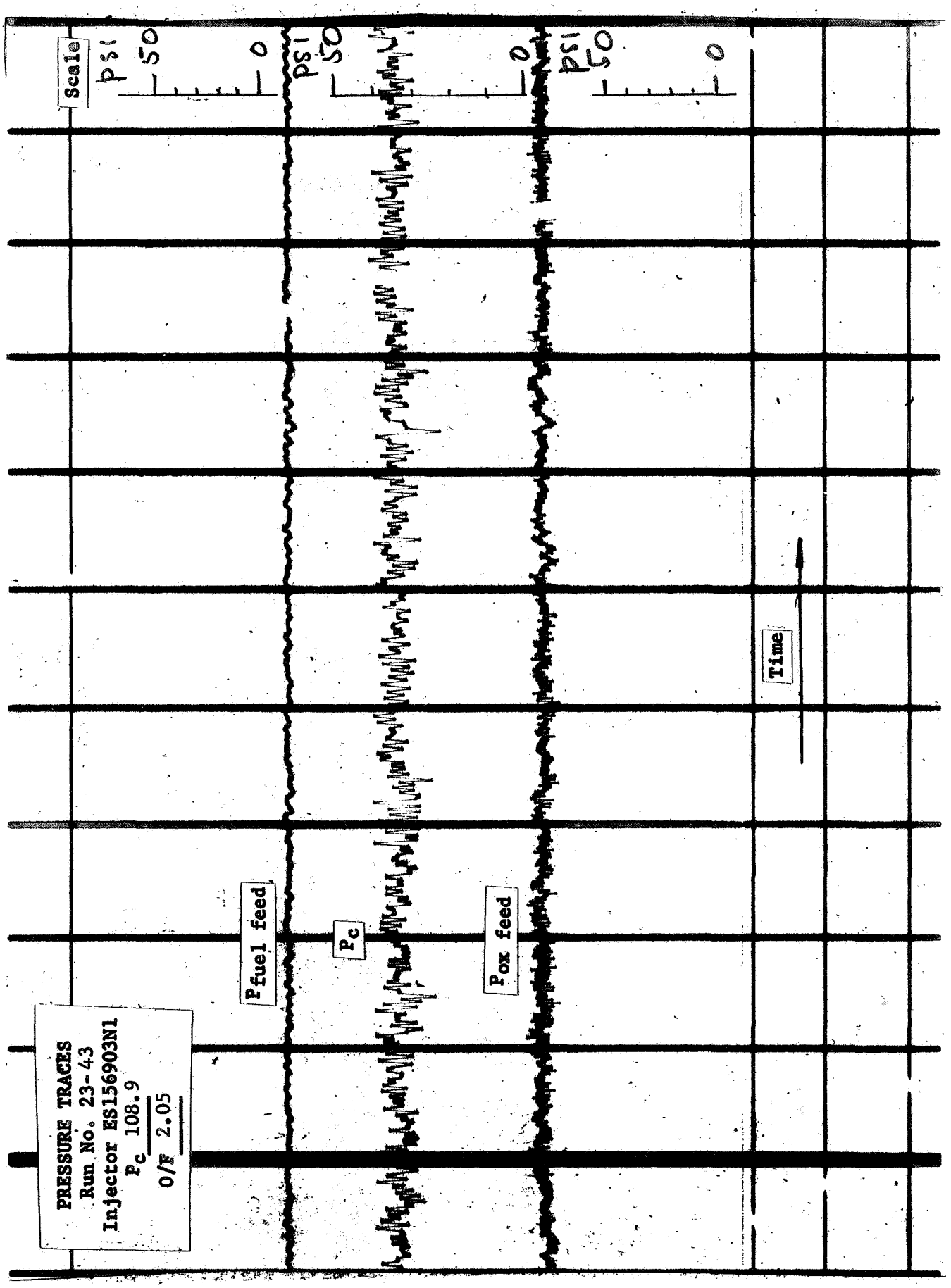

20-404

Figure 2-42

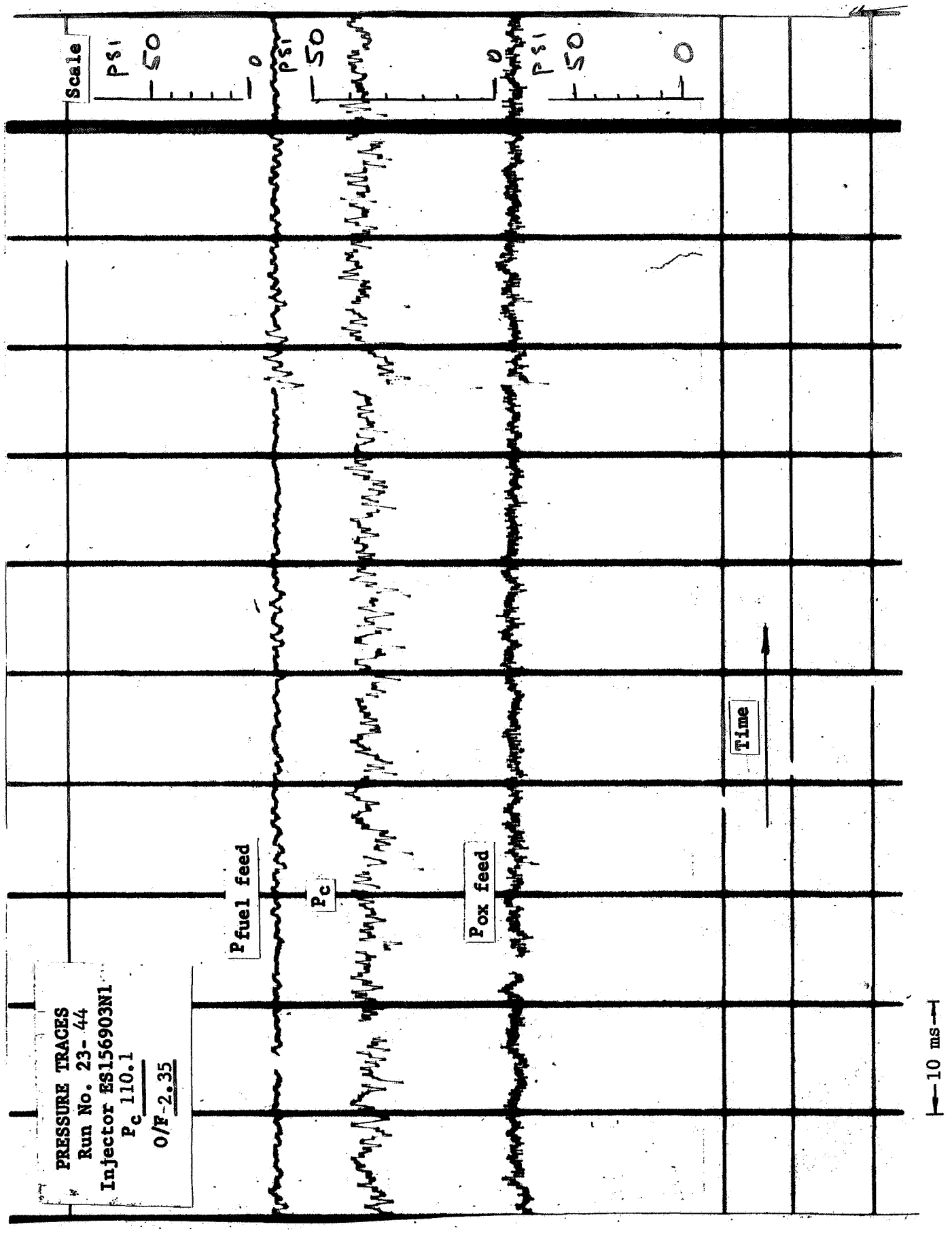

20-409

Figure 2-43

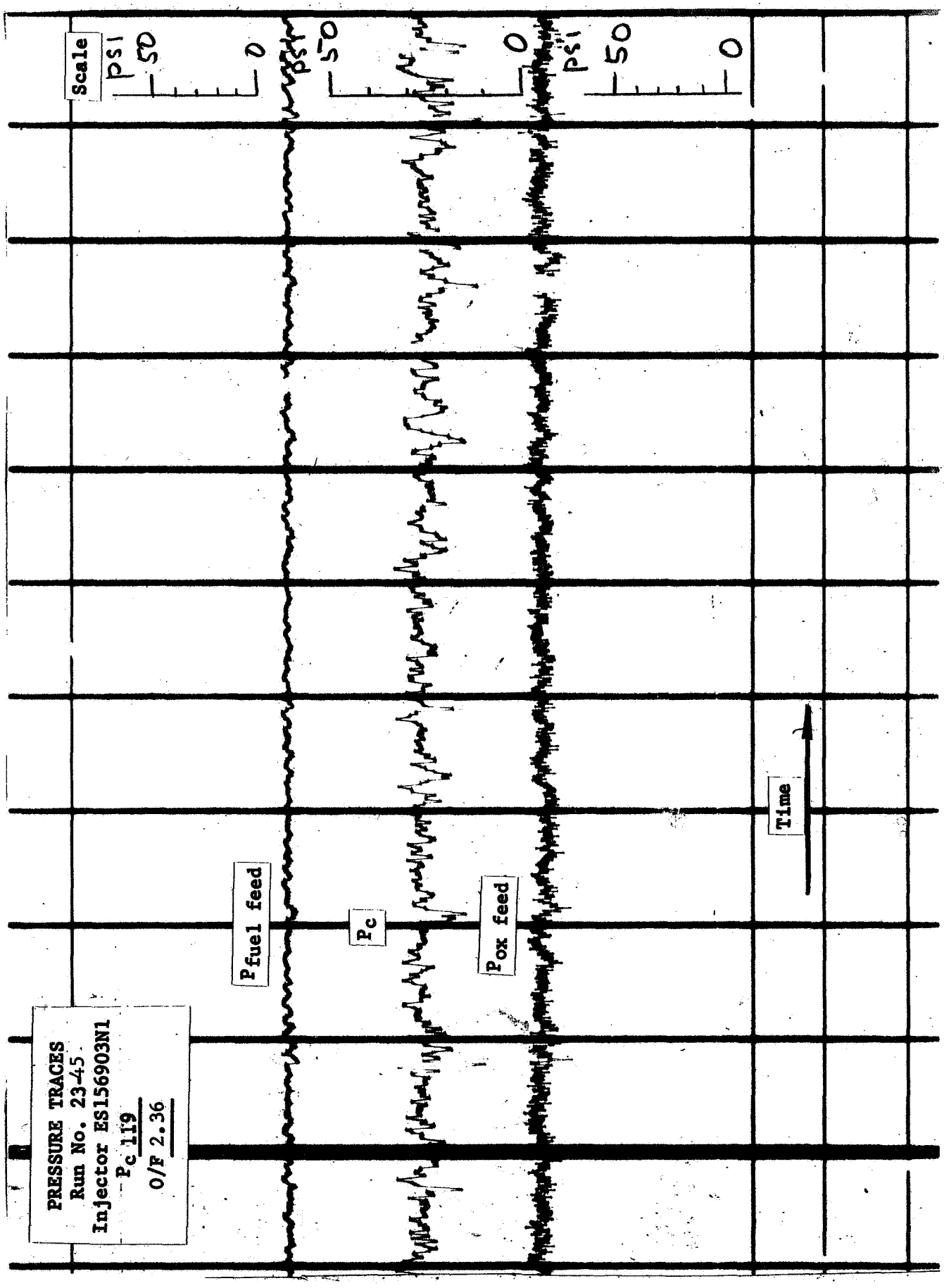

20-031

Figure 2-44

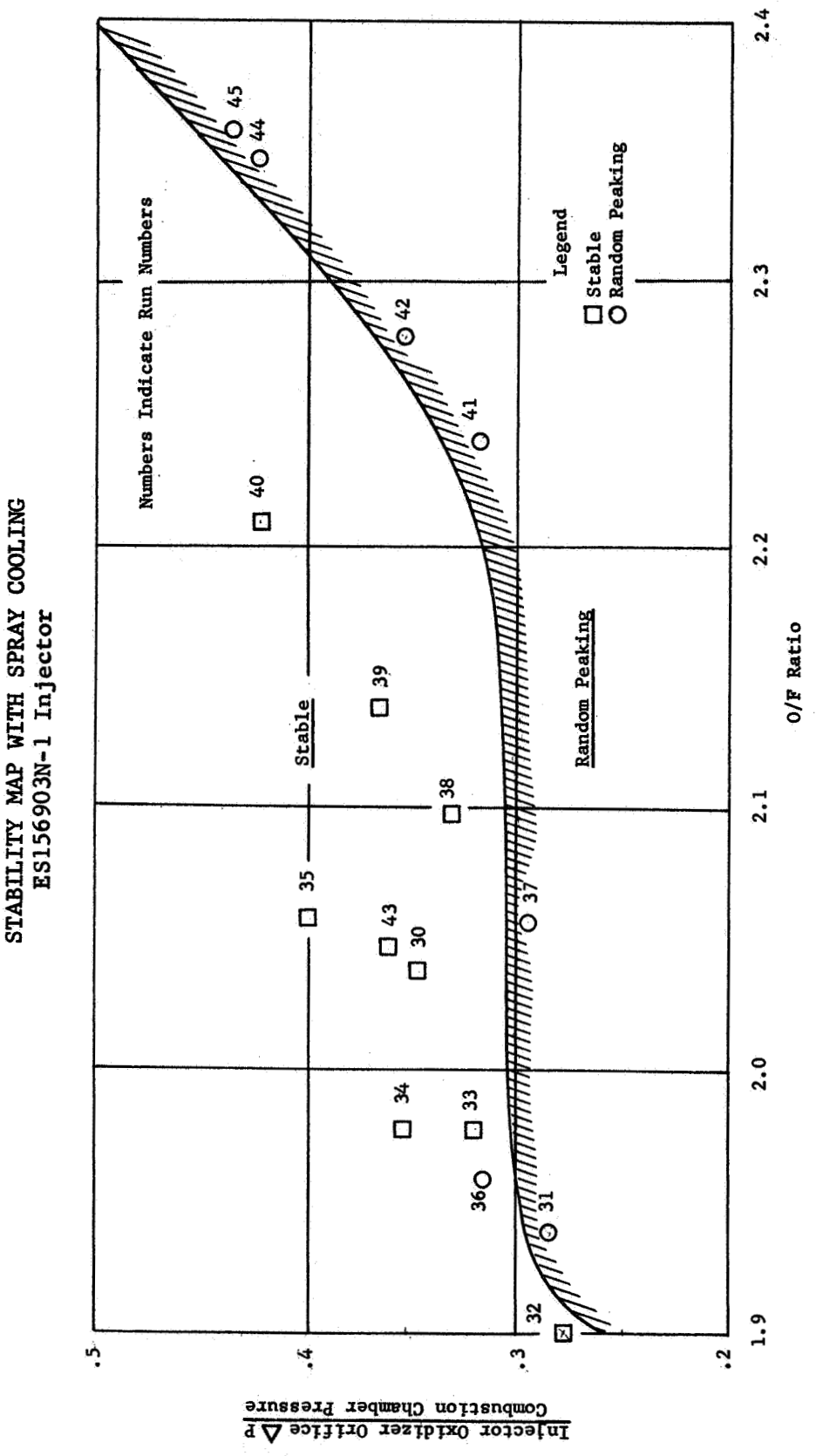
STABILITY MAP WITH SPRAY COOLING
ES156903N-1 Injector
Numbers Indicate Run Numbers
Legend
Stable
Random Peaking
Stable
Random Peaking
Injector Oxidizer Orifice ΔP / Combustion Chamber Pressure
O/F Ratio
.5
.4
.3
.2
1.9
2.0
2.1
2.2
2.3
2.4
45
44
42
41
40
39
38
35
43
30
37
34
33
36
31
32

Figure 2-45

B. WLR-23 Rig Engine Evaluation

This section describes the planned test program and the test results for the series of tests using the WLR-23 rig engine, serial number 1, build 1 during the period between May 18 and May 26, 1966.

Test Plan

The test objectives were (1) to acquire hot firing engine test data on the thermal and structural characteristics for comparison to analytical predictions, and (2) to accumulate engine test time to evaluate durability characteristics.

The planned test series was to be conducted in the following sequence:

Test No.	Duration	Purpose
1	10 sec	Check instrumentation
2	60 sec	Gather data for comparison with analytical predictions
3	120 sec	Same as test number 2 plus endurance
4	250 sec	Same as test number 2 plus endurance
5	500 sec	Same as test number 2 plus endurance

During the tests, the following parameters were to be monitored as a basis for unscheduled shut down of the engine:

Chamber Pressure - An abnormal reduction of chamber pressure would indicate excessive wear or erosion of the nozzle throat.

Cavity Pressure - An indication of cavity pressure above ambient would indicate chamber leakage.

Watchband Temperature - Temperature would be monitored to insure that it did not exceed predicted design values.

Watchband and Wedge Assembly Deflection - Wide variations from predicted values would be investigated before allowing a test to continue.

Visual Observation - Sparking or change in flame color would indicate that the chamber material was being consumed.

The instrumentation provided for the initial rig engine evaluation is summarized in TableIII. The schematic of the test stand system and installation and rig engine instrumentation, Figures 2-46 and 2-47, indicate the instrumentation locations and pertinent features.

Test Results

The rig engine configuration has been described in the first quarterly report. Figures 2-48 and 2-49 show the engine installed on the test stand while Figure 2-50 shows additional data on engine instrumentation.

In accordance with practice established during the WLR-21 engine program, a pressure check of the engine was made prior to each run. A schematic of the pressure test setup is shown in Figure 2-51. The engine throat was blocked off with a rubber stopper and approximately 100 psi pressure was applied through the injector. The pressure was then allowed to decay while being traced on Bristol recorders through normal P_c instrumentation. The slope of the curve indicates the tightness of the engine. The pressure decay curve prior to the initial firing is shown in Figure 2-52 along with curves for each subsequent test. Based on previous experience, the pre-test decay curve was completely satisfactory.

Run #23-46 - The initial test, planned for 10 seconds duration to check out instrumentation, was conducted in accordance with plan. The performance, shown in TableIV, indicated satisfactory performance and normal operating conditions.

Examination of the instrumentation traces was made after the run. The only abnormal indication appeared to be deflection probe readings which were running a few thousandths higher than predicted. Since this instrumentation is repeatable only within a band of approximately 0.001 inches, these

readings were considered to be satisfactory at the time.

A pressure check of the engine was made after test and was considered satisfactory. A visual examination of the inside of the engine with a boroscope showed no abnormal conditions.

Run #23-47 - A 60 second duration test, planned to gather data for comparison with analytical predictions, was completed in accordance with plan. During the test, watchband temperature, chamber pressure, cavity pressure, and deflection probe readings were monitored. The chamber pressure appeared to be dropping at a rate somewhat in excess of the prediction. However, the cavity pressure remained at zero throughout the firing, indicating that the engine was pressure tight. The deflection probe readings rose considerably higher than predicted. However, it was decided during the test not to shut down but to continue for the planned duration to obtain usable data.

The engine performance is provided in Table IV. The deflection probe readings, plotted on Figure 2-53 , are substantially in excess of the predicted values. The watchband thermal history as shown in Figure 2-54 agrees essentially with the prediction. Chamber and cavity pressures as well as the temperatures of the swirl cup and deflection probe as a function of time are shown in Figures 2-55 and 2-56

The engine was examined after test with a boroscope and no discrepancies were found. In addition, the engine was pressure checked and the decay curve indicated the engine was pressure tight and satisfactory for further running.

Prior to further testing, the deflection probe data was converted to equivalent PG inner wall temperatures. The resultant temperature history is shown in Figure 2-57 compared with the analytical prediction. This shows that the engine was running substantially hotter than predicted and required adjustment of the spray cooling flows and/or configuration to reduce the temperature.

The higher temperatures presented two problem areas. First, the stresses in both the PG and the watchband were substantially increased due to the increase in temperature. This is because the temperature produces an increased expansion of the PG ring (formed by the wedge land) which results in increased

deflections of the watchband. It is estimated that the higher temperatures produced approximately 20-25% increase in PG land stress. In addition, the yield strength of the watchband material was exceeded causing a 0.006 inch radial permanent set in the watchband.

Run #23-48 - It was decided to use the rig engine rather than the copper chamber, to evaluate changes in spray cooling flow. Temperature would be determined by using probe deflection readings. The cooling flow would be adjusted by changing tank pressure settings. Twenty second firings were planned to limit the stresses in both the PG and the watchband to satisfactory levels.

An initial 20 second firing was made with oxidizer, fuel, and spray flows set to design point to check the deflection readings with those obtained during the previous run to insure that the slight watchband offset would not cause erroneous readings. The deflections obtained at 10 and 20 seconds for this run have been included on Figure 2-53. The results agree closely with the previous data. The run data is summarized in Table IV. The cavity pressure remained constant at 15 psia. All operating parameters appeared normal during the test.

Boroscope inspection after test indicated that there was a localized crushed area approximately an inch to two inches from the injector end of the chamber between adjacent wedges. A pressure check indicated that the engine could no longer hold pressure. It was then decided to remove the engine from the test stand for further inspection. Figure 2-58 indicates the appearance of the distressed area in the wedge assembly. Figure 2-59 shows the individual wedges while Figure 2-60 indicates typical minor crushing that occurred in some of the other wedges due to the overload condition.

The conclusions reached as a result of this series of tests are as follows.

- Overloading of the watchband and wedges caused by higher than predicted temperatures during Run 46 resulted in crushing of the PG material in the land area. The damage was not visible after the 60 second test. However, it was most likely present in the form of small cracks which had not yet

come to the surface. The following 20 second test resulted in further progression of the failure.

Adjustment of the spray cooled injector configuration is required to reduce the thermal history to the predicated design values. The copper engine correlation for the ACE engine design was done on the high fill time (ES 156732) injector. The current injector (ES 156903N1) is identical in swirl cup dimensions, injection velocities, flow rates, and injection pressure drops. However, there is a difference in upstream manifold size (reduced to provide satisfactory response and tail-off characteristics). This change has apparently had some effect on the spray cooling film. Further investigation is required on the copper chamber with the current injector to reduce the slope of the temperature curve.

TEST STAND SYSTEM AND INSTALLATION

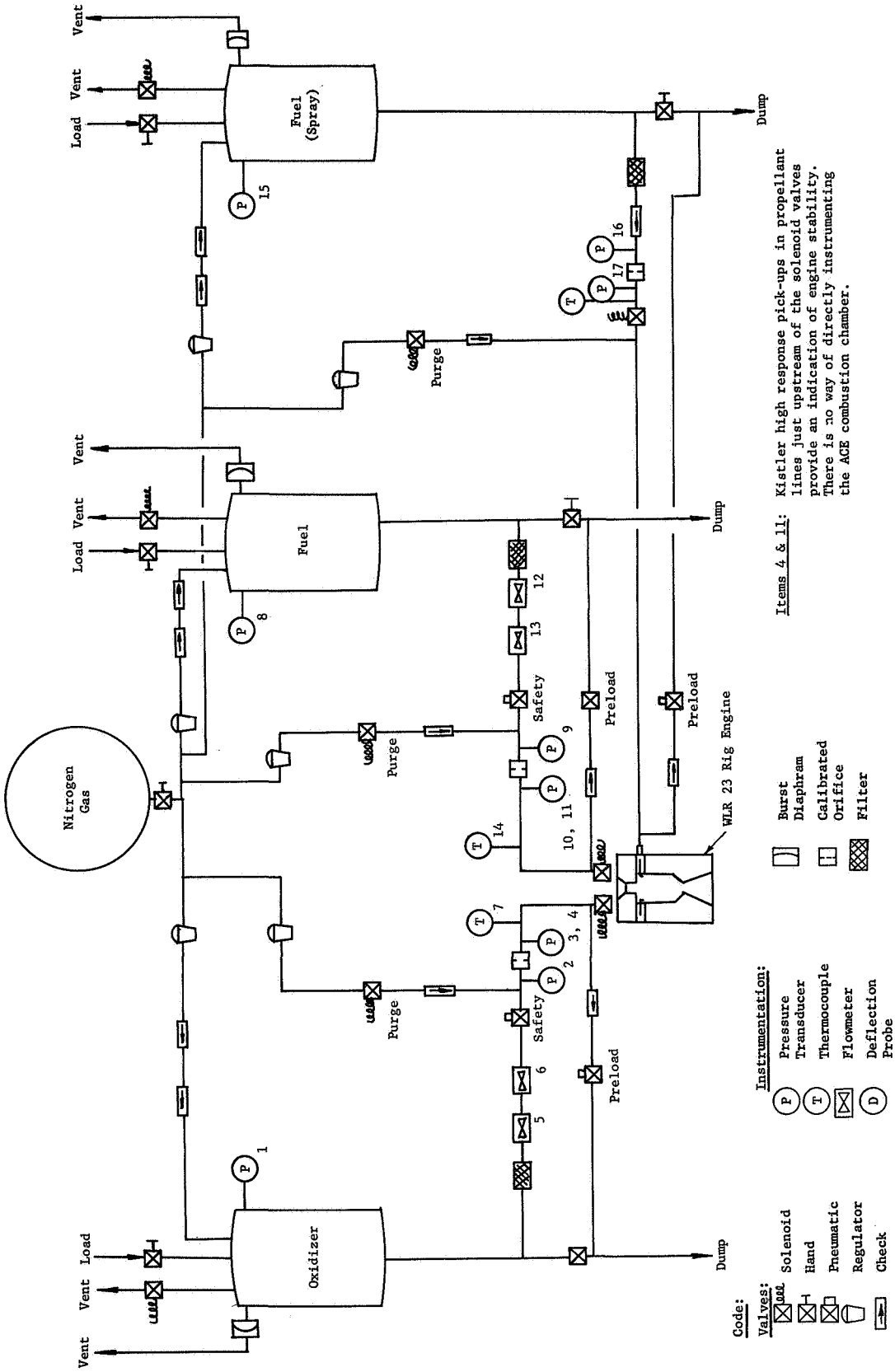

20-555

Figure 2-46

WLR-23 RIG ENGINE INSTRUMENTATION

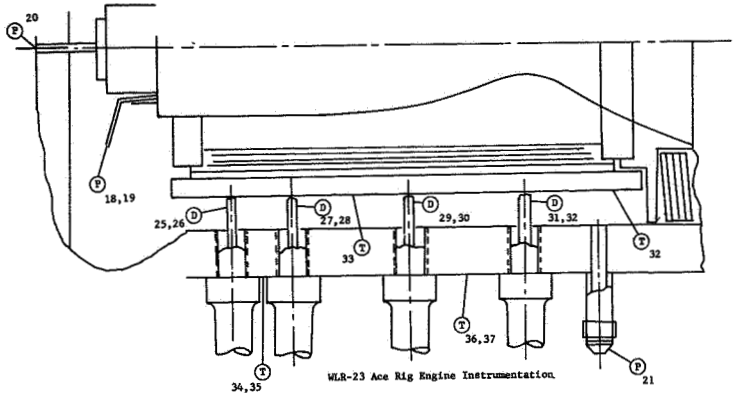

WLR-23 Ace Rig Engine Instrumentation

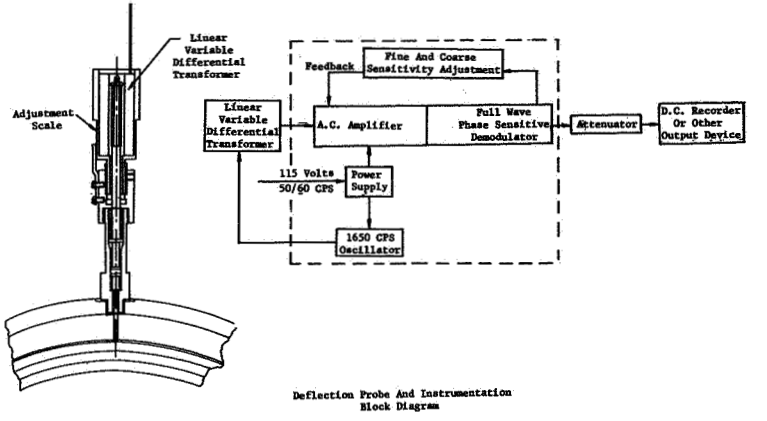

Deflection Probe And Instrumentation Block Diagram

Items 18 and 19 — Combustion chamber pressure is measured at the face of the swirl cup lip. Pressure passages cannot be provided directly in the ACE chamber. Earlier copper chamber test data is used to relate this value of chamber pressure to other chamber locations.

Item 21 — Pressure pick-up in the cavity between the outer diameter of the watchband and the rig housing inside diameter detect any possible chamber leakage.

Item 38 — Swirl cup temperatures are recorded to determine run and soak thermal histories for long duration tests.

Items 25 thru 31 — Positive measurement of the watchband and wedge assembly is obtained from eight probes mounted radially on the rig housing in four axial stations and located 180 degrees apart. Radial deflection of the watchband and wedge assembly is translated (through the probe rod) into an electrical signal via the linear variable differential transformer (LVDT). Polarity and amplitude of the electrical signal output from the demodulator varies with direction and displacement of the probe. Recorded values of deflection are corrected for thermal growth of the rig housing.

Figure 2-47

WLR-23 RIG ENGINE TEST STAND INSTALLATION

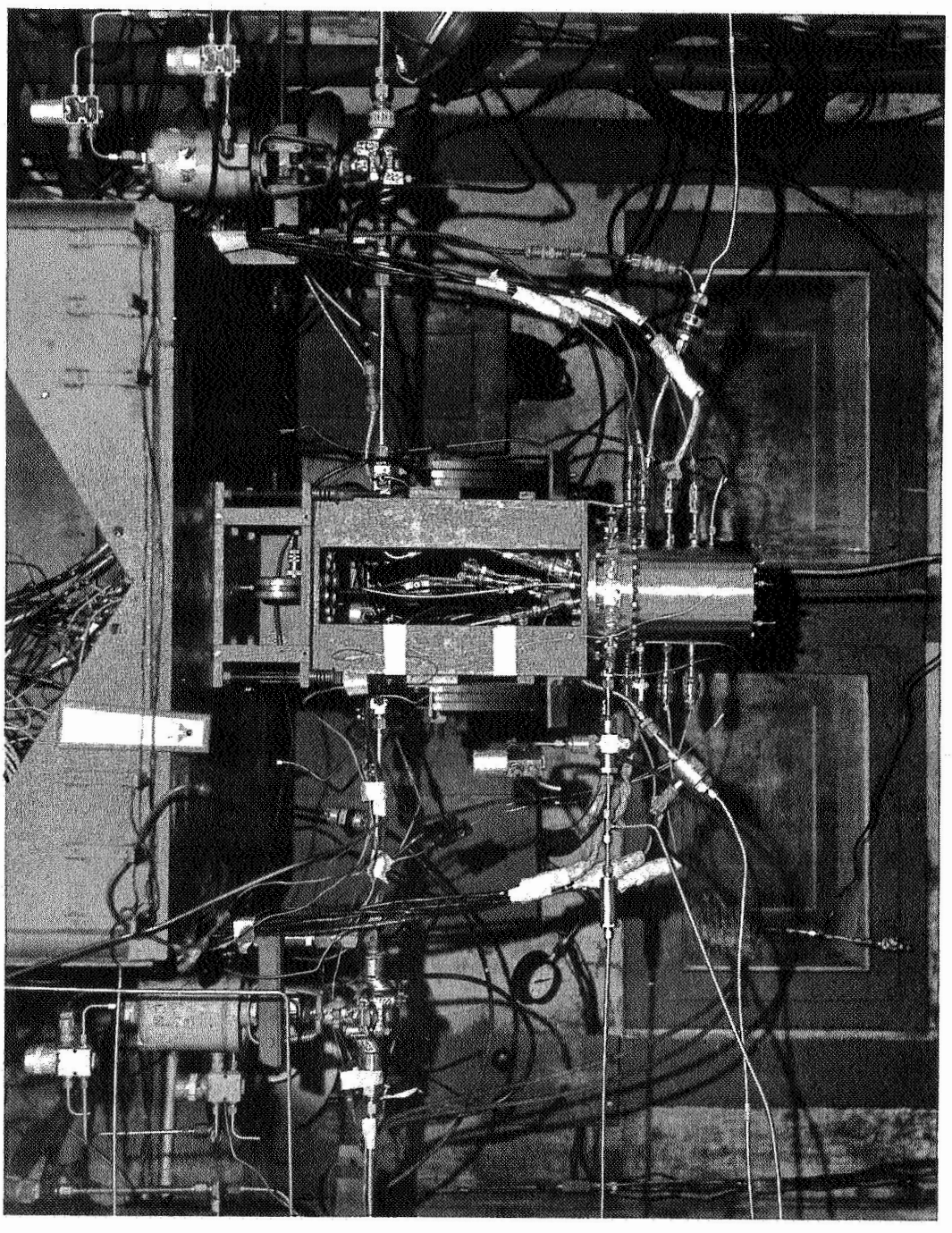

20-345

Figure 2-48

WLR-23 RIG ENGINE TEST STAND INSTALLATION

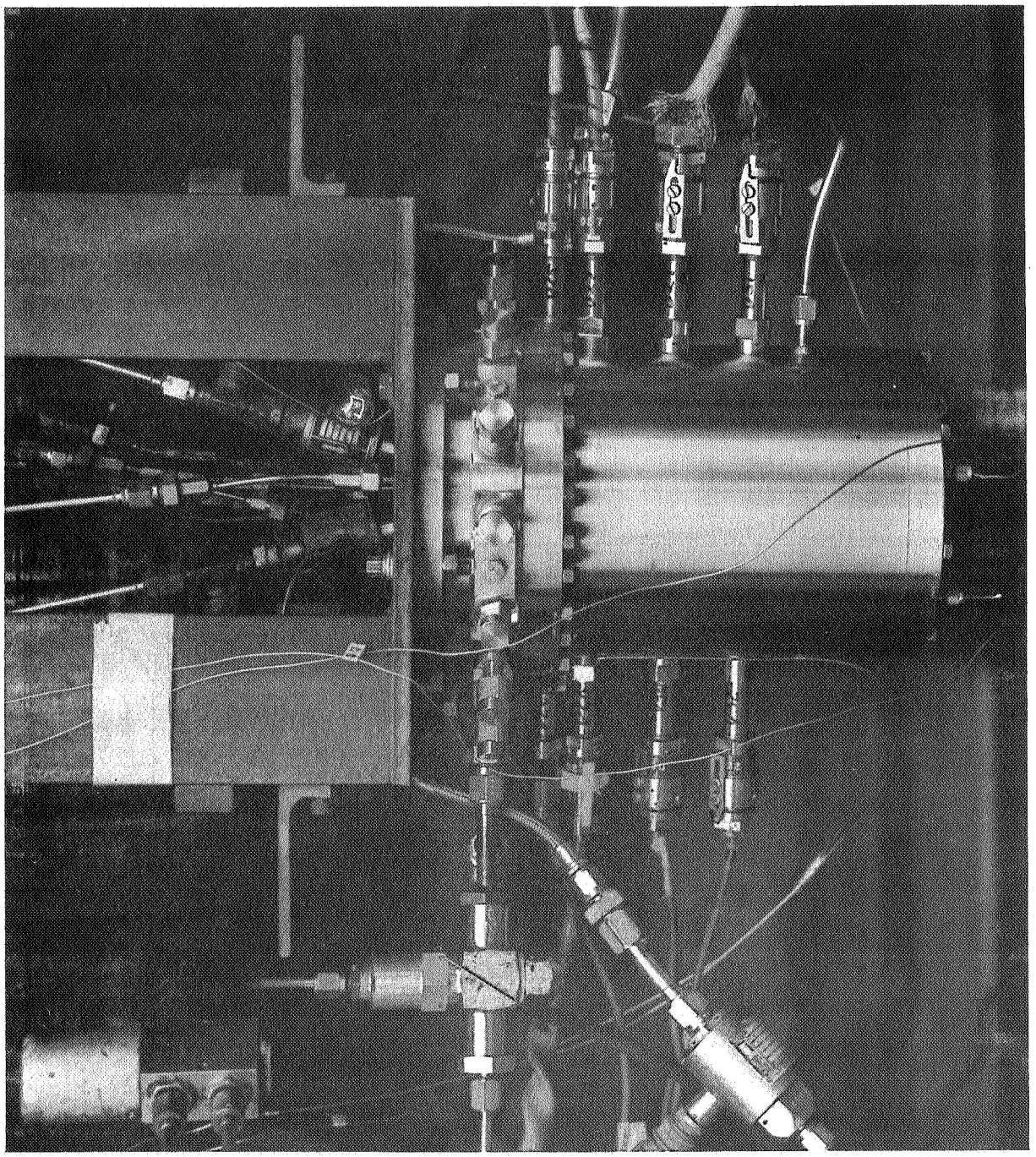

20-263

Figure 2-49

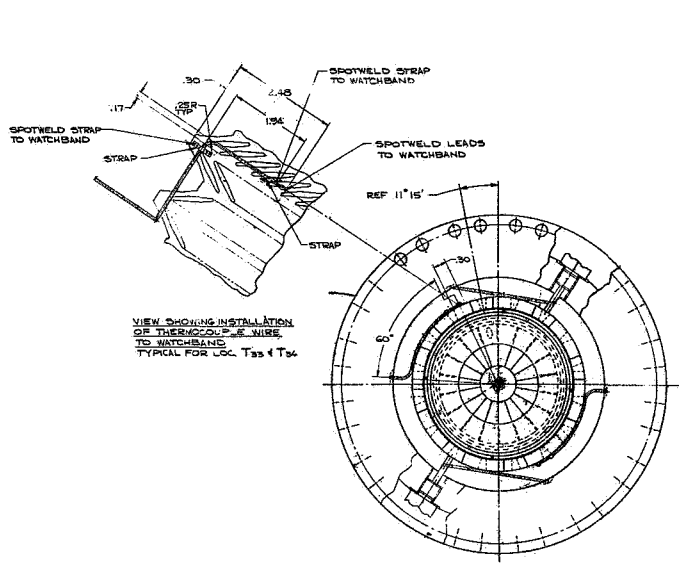

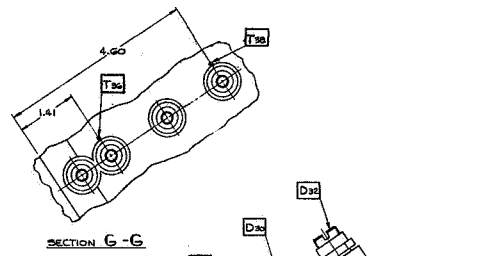

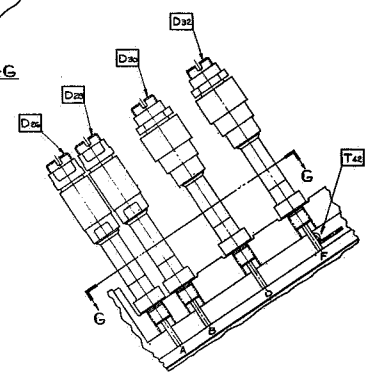

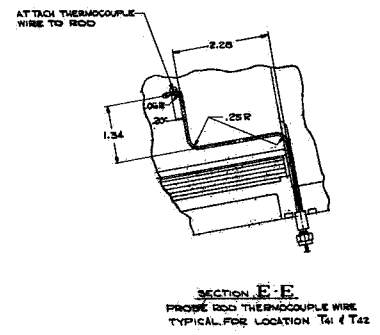

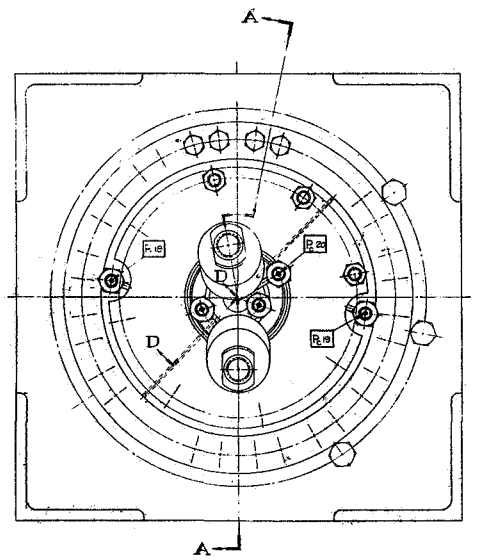

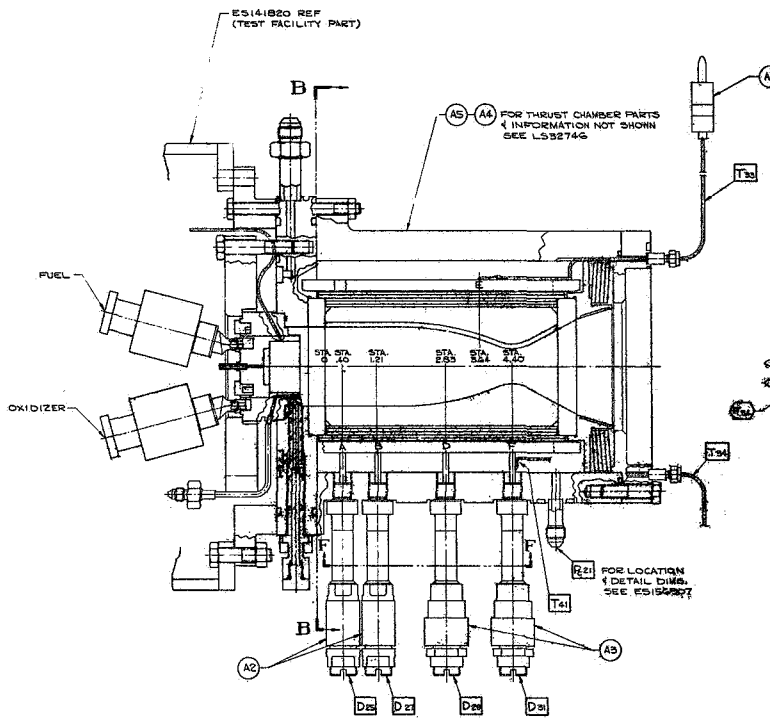

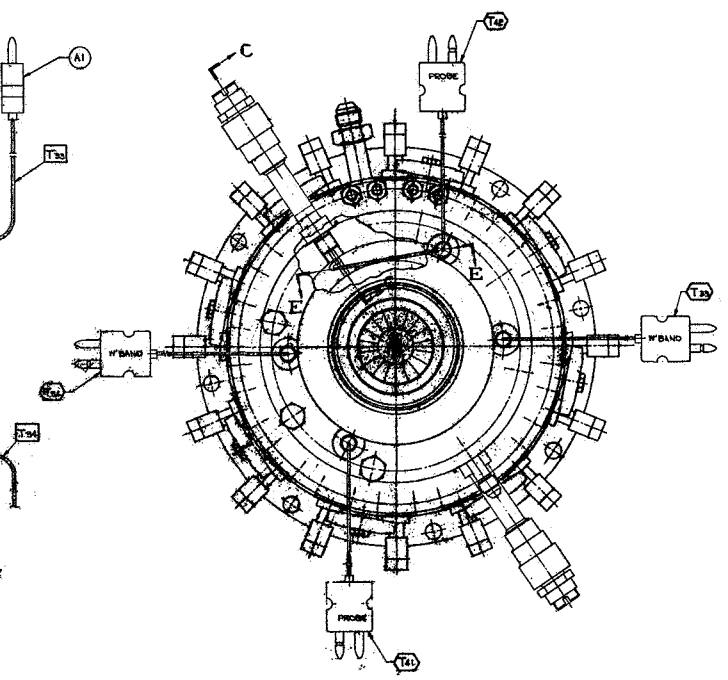

TEMPERATURE

T33	WATCHBAND - STA. 3.64
T34	WATCHBAND - STA. 3.64
T35	HOUSING - STA. 1.21
T36	HOUSING - STA. 1.21
T37	HOUSING - STA. 4.40
T38	HOUSING - STA. 4.40
T39	SWIRL CUP
T40	SWIRL CUP
T41	RADIAL PROBE ROD - STA. 4.40
T42	RADIAL PROBE ROD - STA. 4.40

PRESSURE

R18	CHAMBER - SWIRL CUP LIP
R19	CHAMBER - SWIRL CUP LIP
R20	SWIRL CUP
R21	CHAMBER CAVITY

DEFLECTION

D25	RADIAL PROBE - STA. .40
D26	RADIAL PROBE - STA. .40
D27	RADIAL PROBE - STA. 1.21
D28	RADIAL PROBE - STA. 1.21
D29	RADIAL PROBE - STA. 2.83
D30	RADIAL PROBE - STA. 2.83
D31	RADIAL PROBE - STA. 4.40
D32	RADIAL PROBE - STA. 4.40

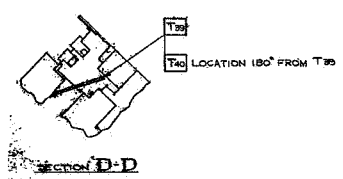

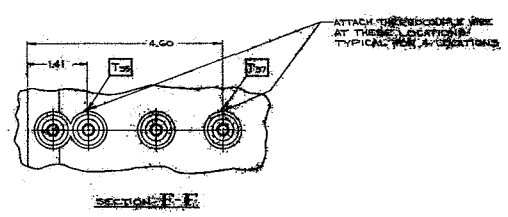

Figure 2-50

PRESSURE DECAY TEST SCHEMATIC

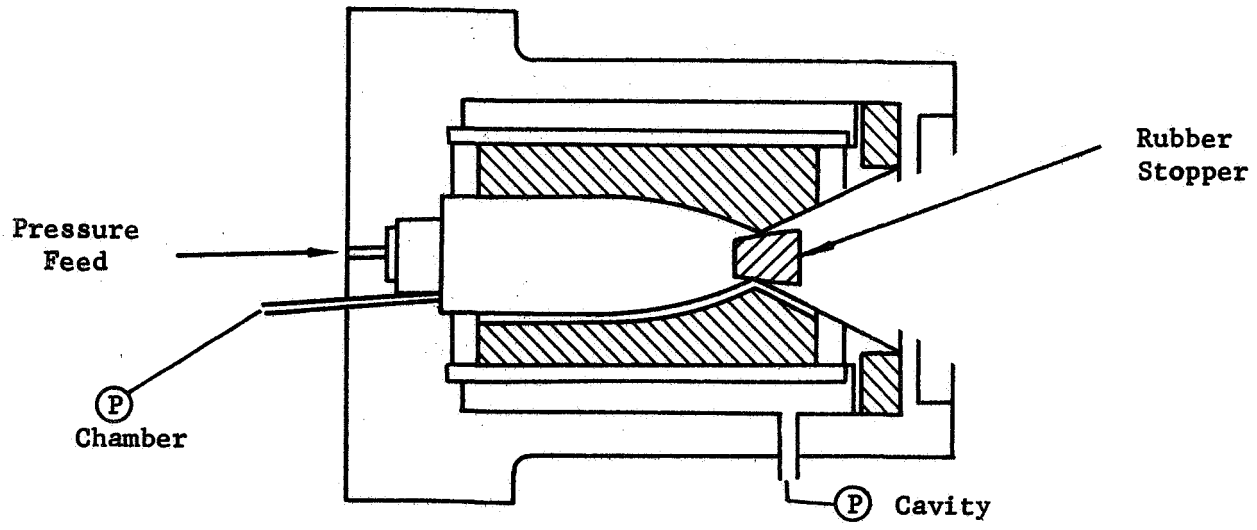

20-280

Figure 2-51

PRESSURE DECAY CURVES
WLR-23 Rig Engine
S/N 1 Build No. 1

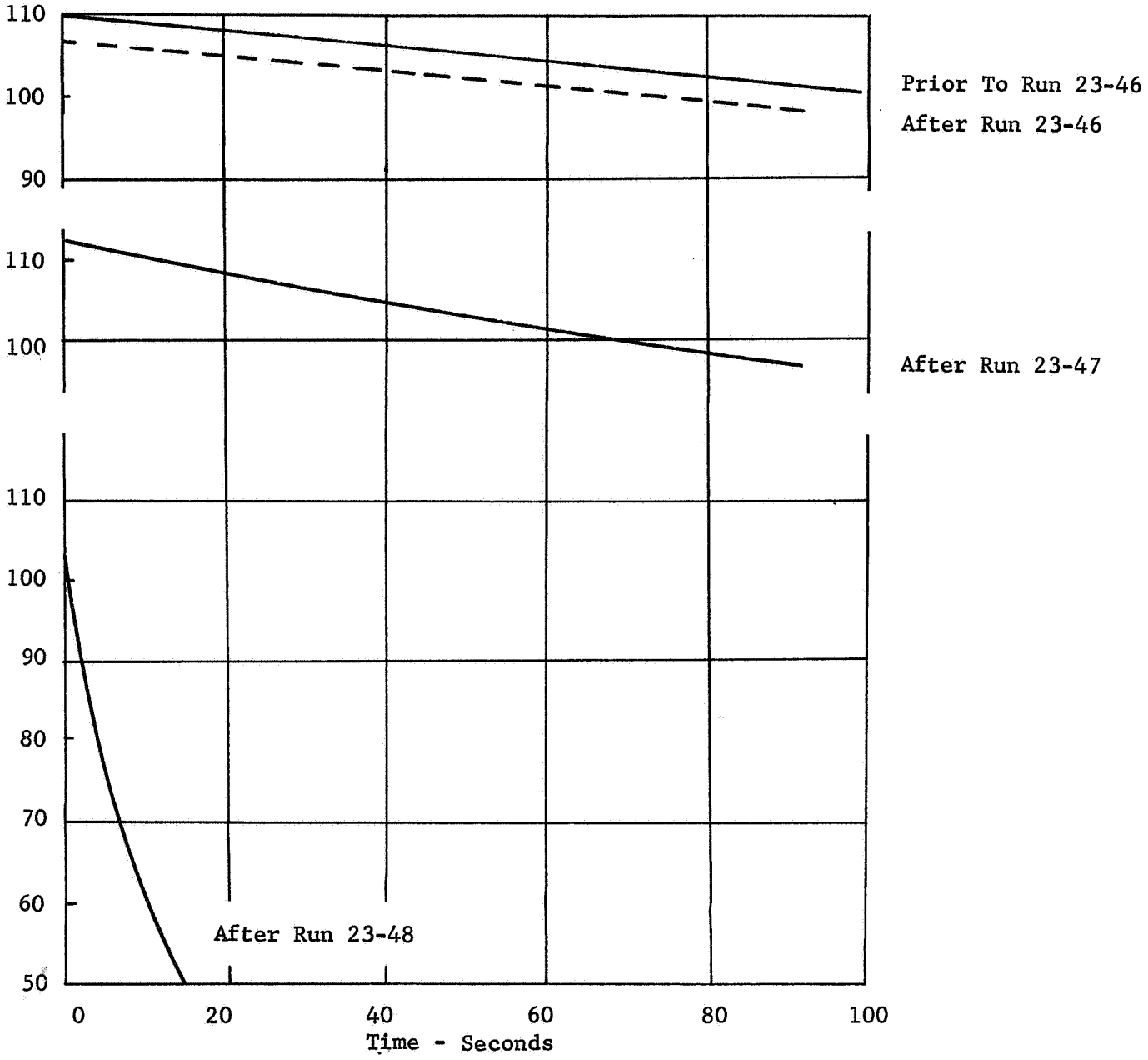

20-272

Figure 2-52

PROBE DEFLECTION DATA
WLR-23 Rig Engine
S/N 1 Build No. 1
Run No. 23-47

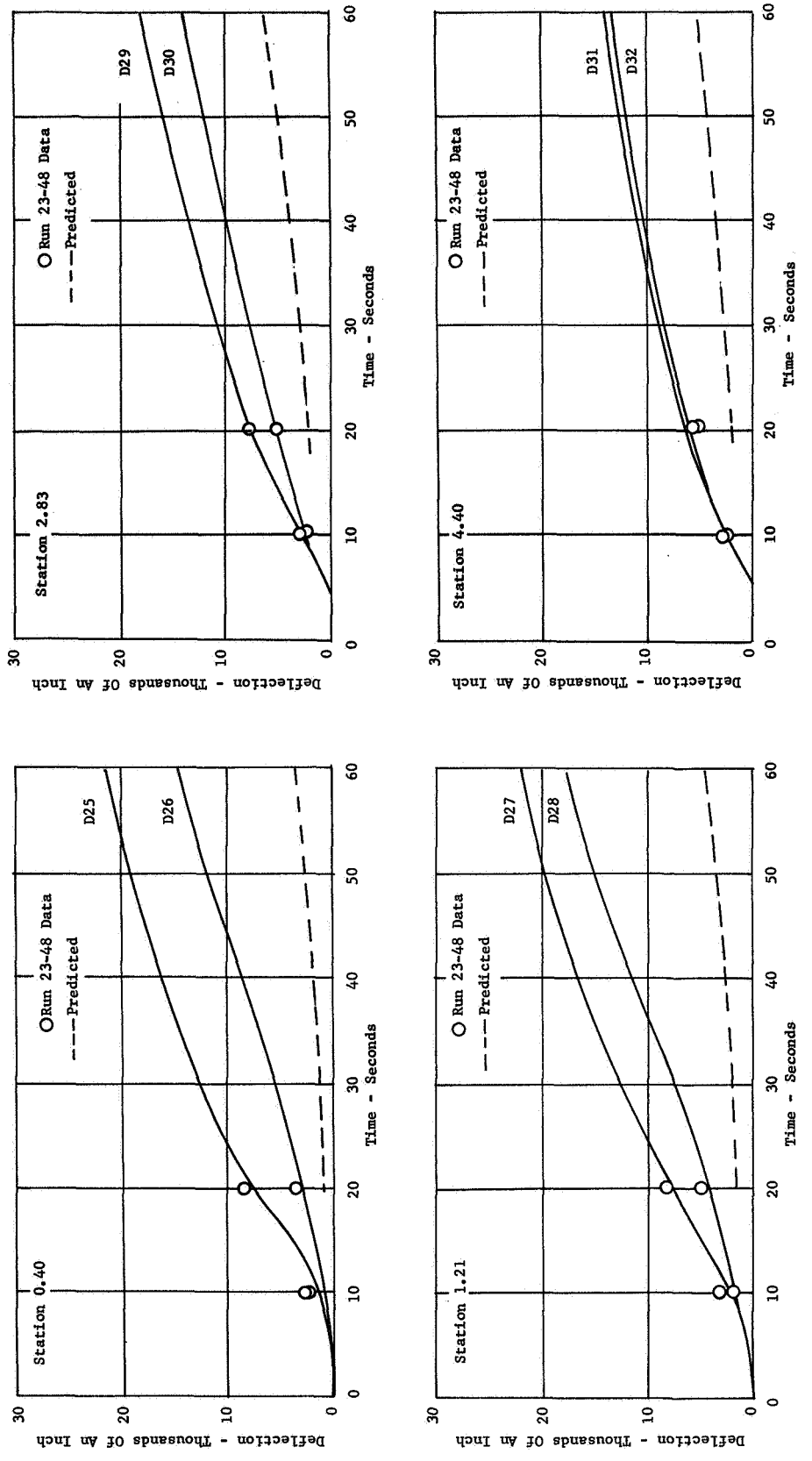

Figure 2-53

WATCHBAND TEMPERATURE
WLR-23 Rig Engine
S/N 1 Build No. 1
Run No. 23-47

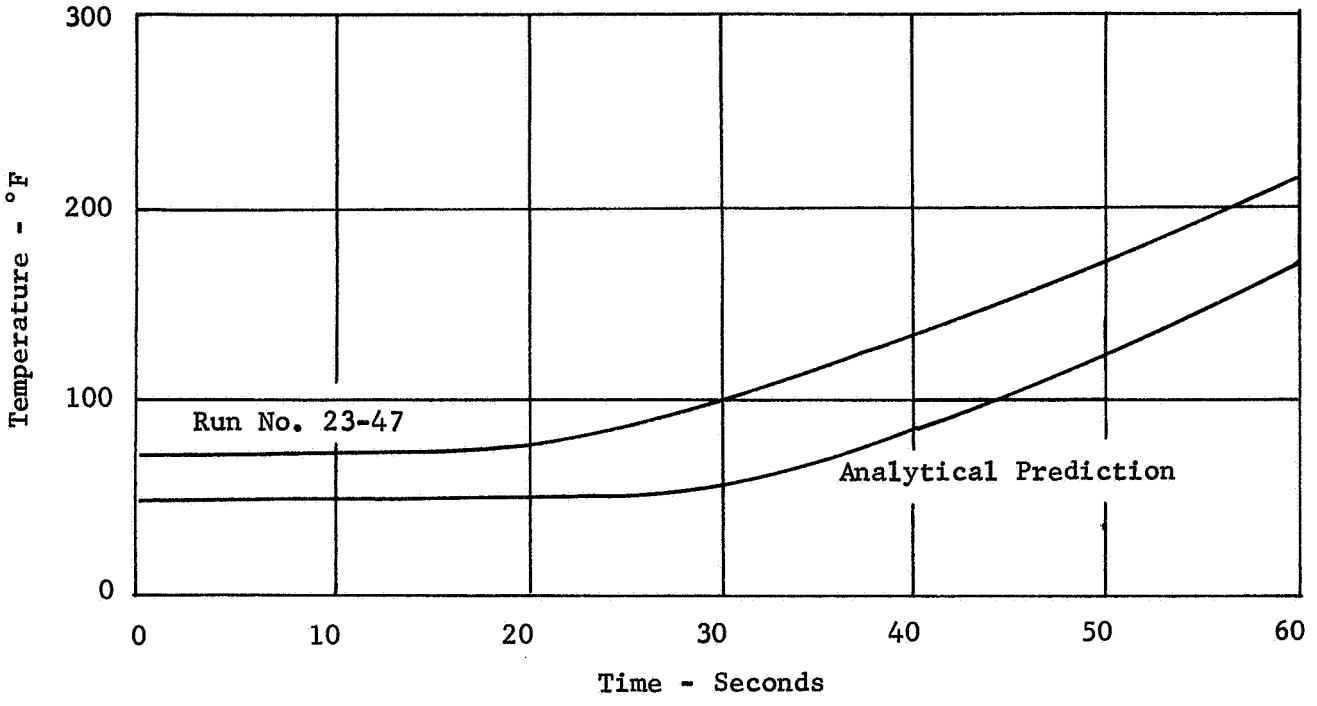

20-281

Figure 2-54

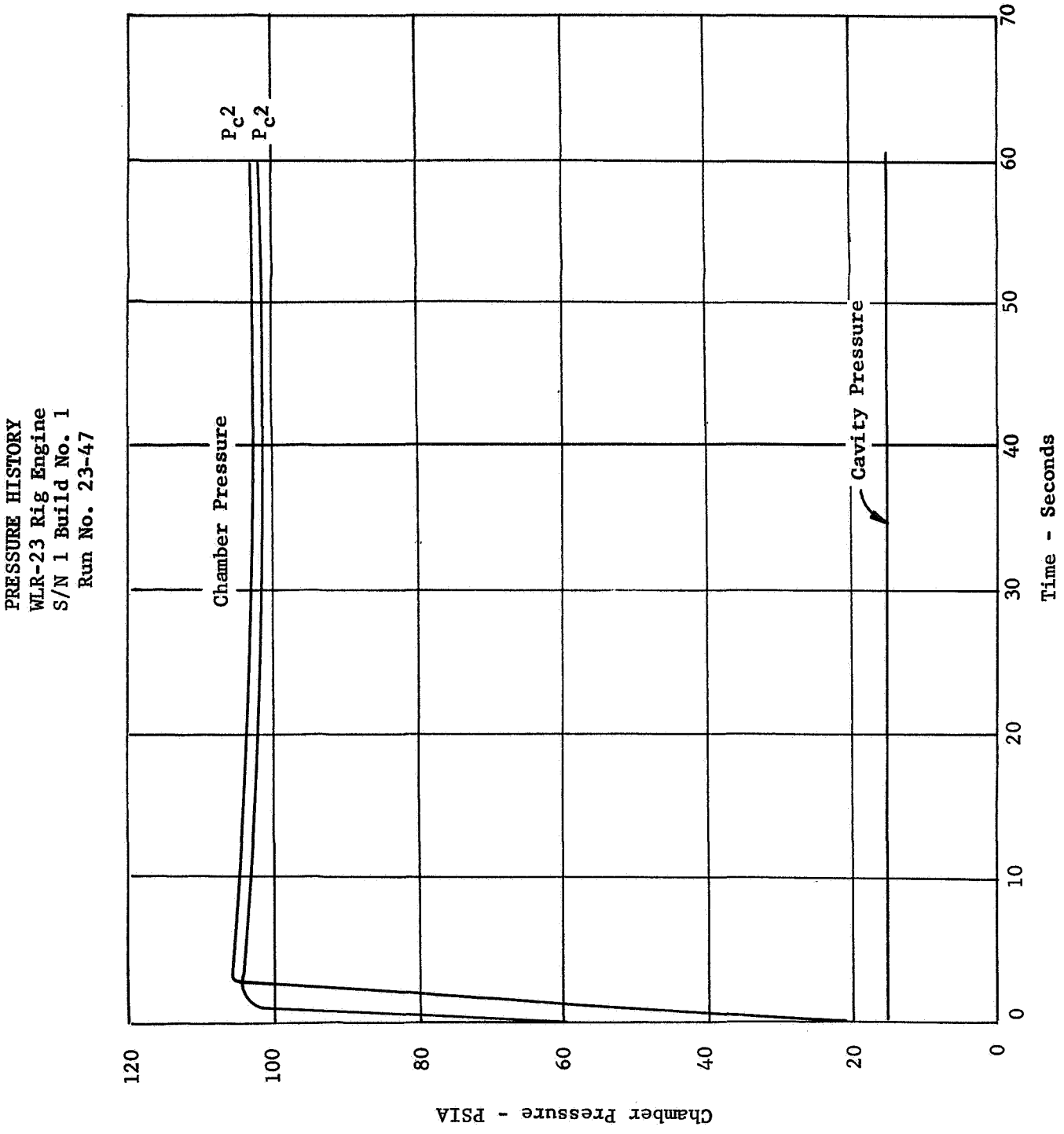
PRESSURE HISTORY
WLR-23 Rig Engine
S/N 1 Build No. 1
Run No. 23-47
Chamber Pressure
P_c2
P_c2
Cavity Pressure
Chamber Pressure - PSIA
Time - Seconds
120
100
80
60
40
20
0
0
10
20
30
40
50
60
70

Figure 2-55

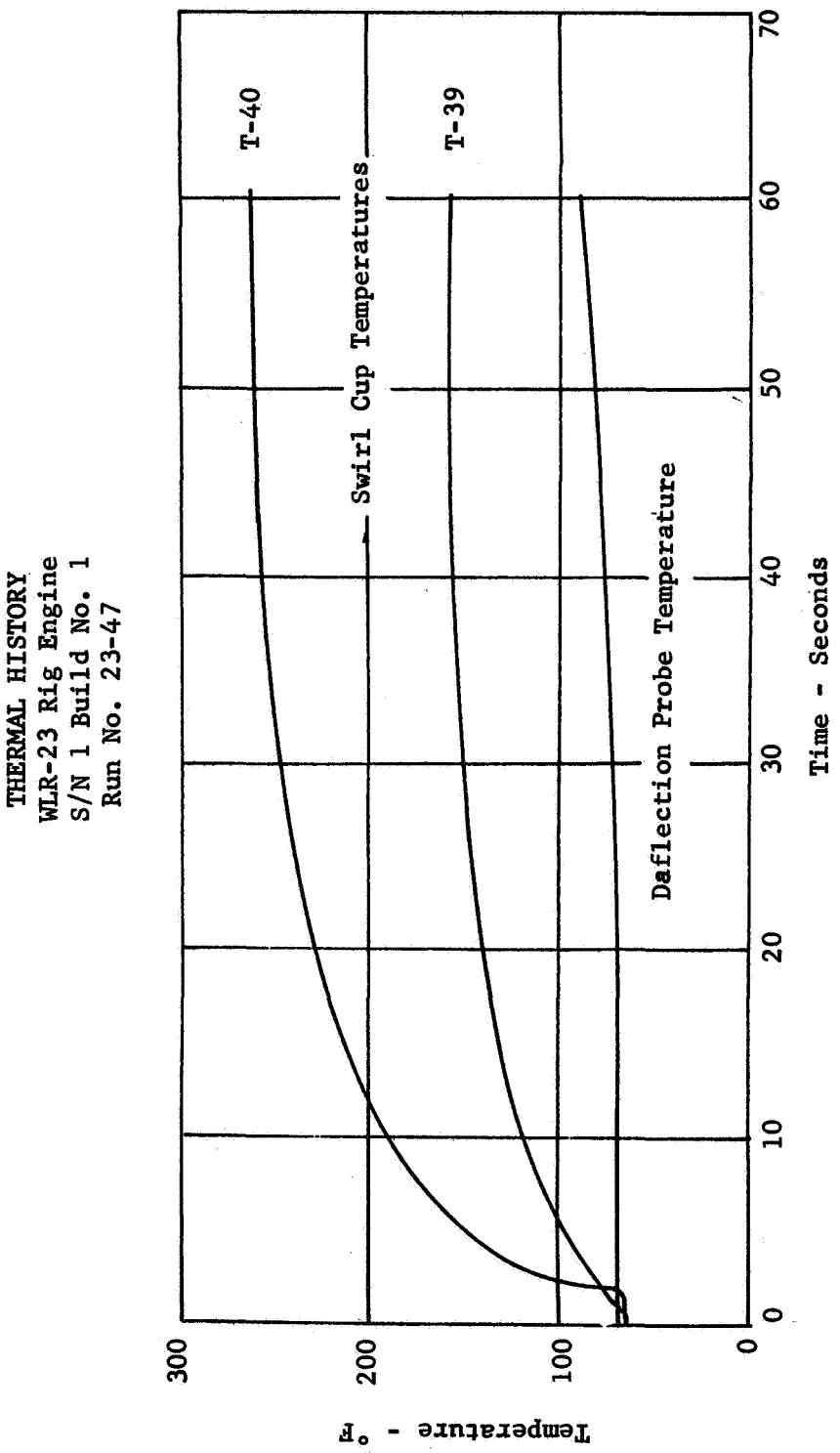

20-262

Figure 2-56

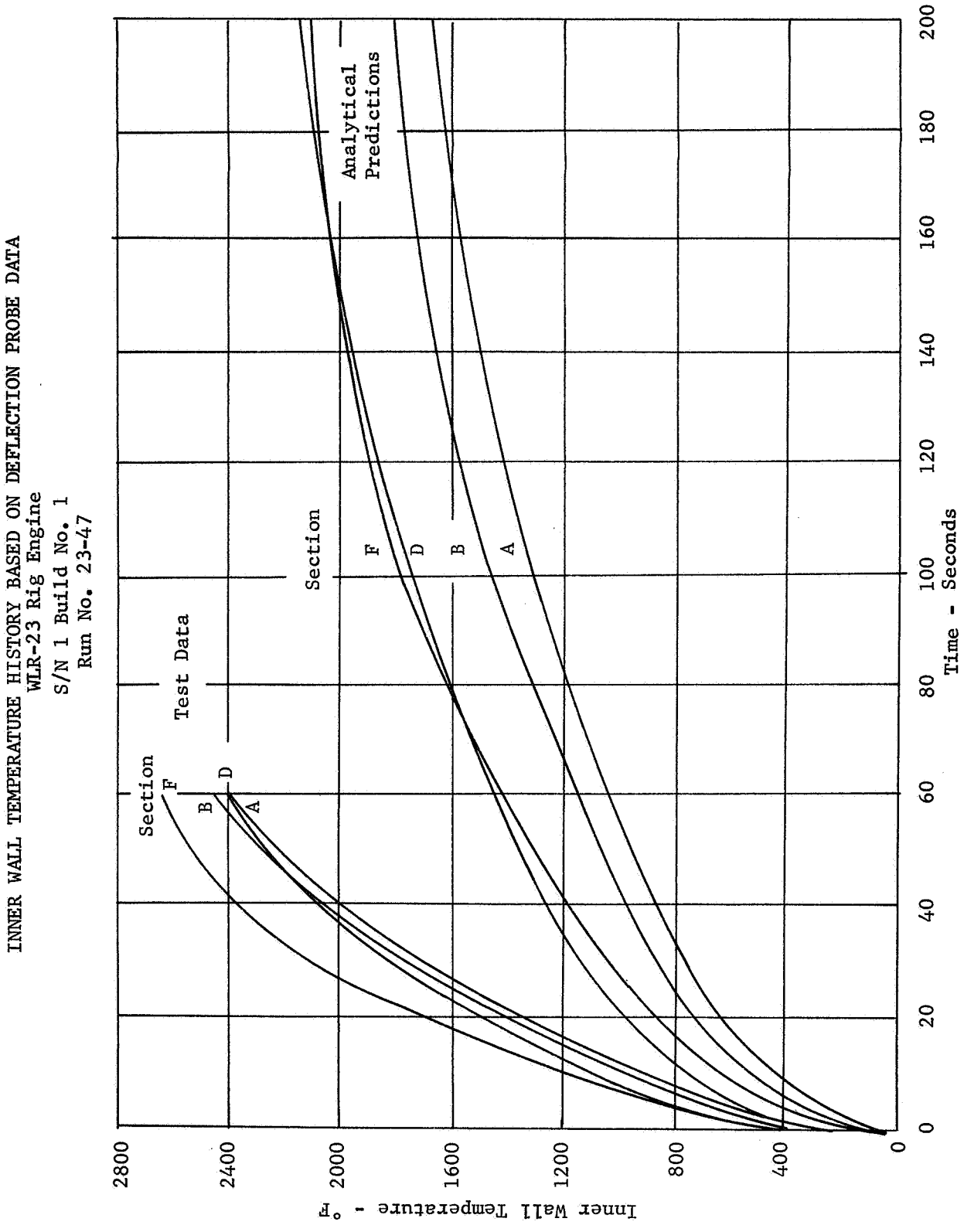
INNER WALL TEMPERATURE HISTORY BASED ON DEFLECTION PROBE DATA
WLR-23 Rig Engine
S/N 1 Build No. 1
Run No. 23-47
Inner Wall Temperature - °F
Time - Seconds
Analytical Predictions
Test Data
Section
F
D
B
A
0
400
800
1200
1600
2000
2400
2800
0
20
40
60
80
100
120
140
160
180
200

Figure 2-57

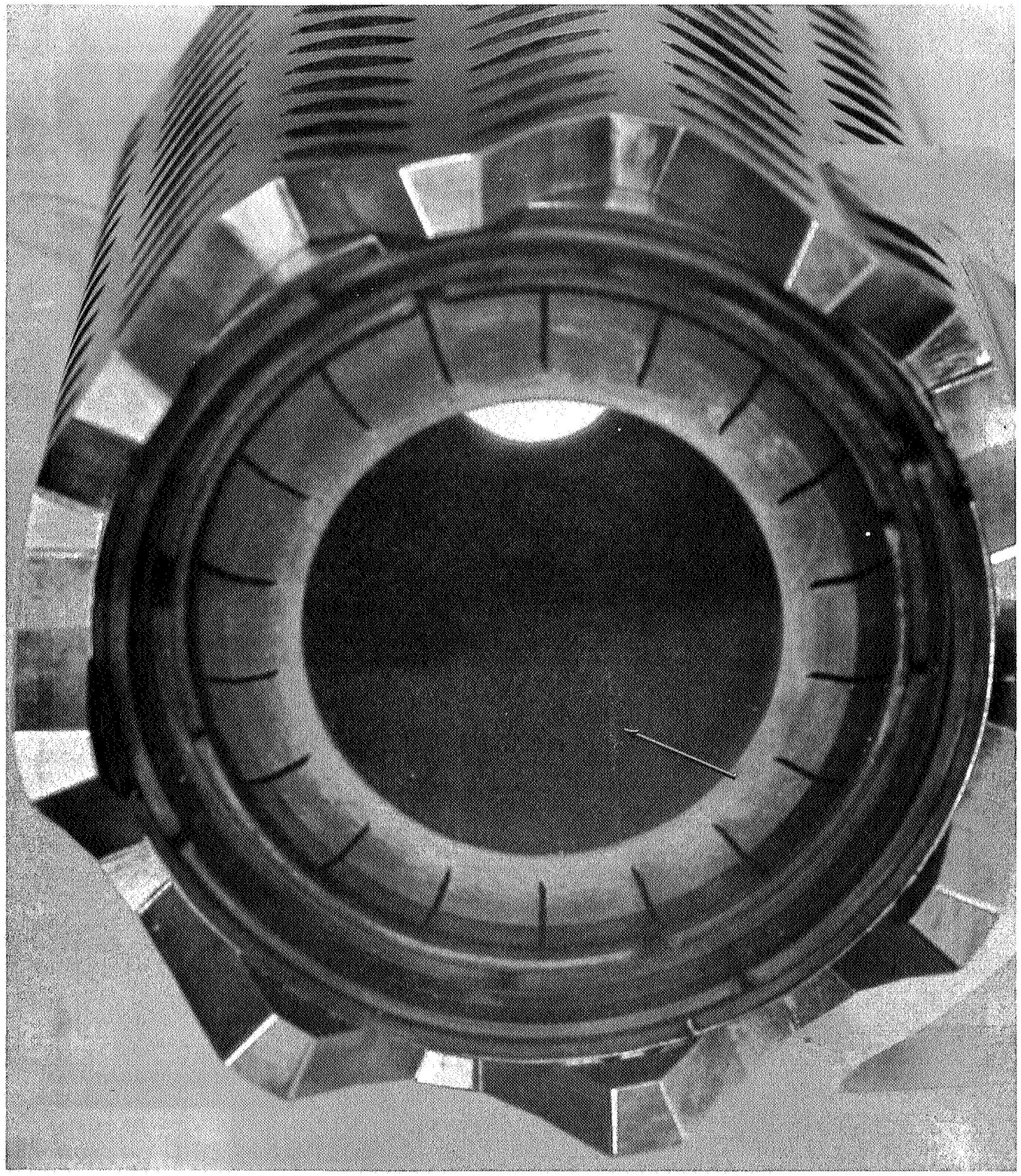

20-249

Figure 2-58

MINOR CRUSHING OF WEDGES

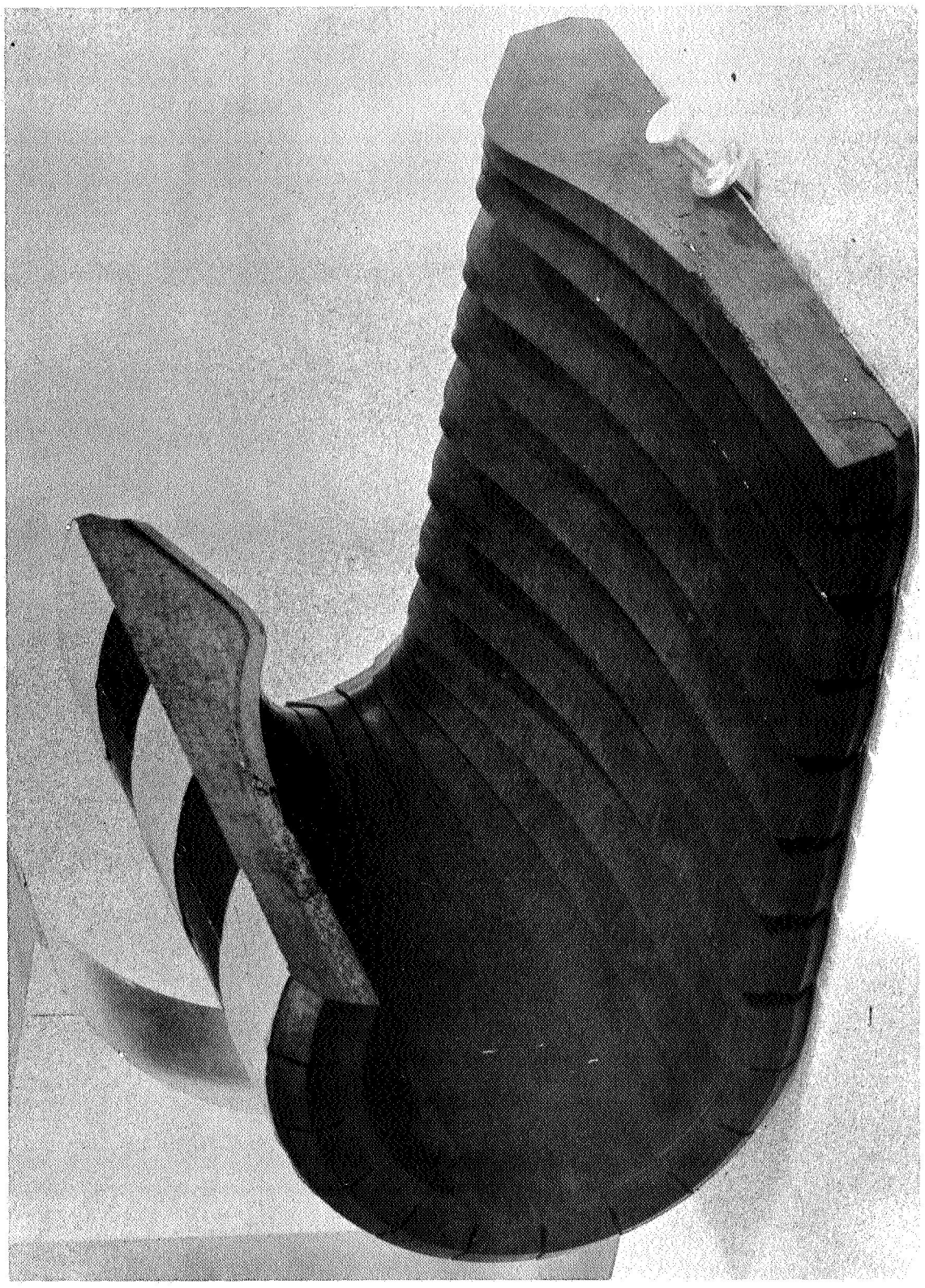

20-259

Figure 2-59

CLOSE-UP OF WEDGE LAND

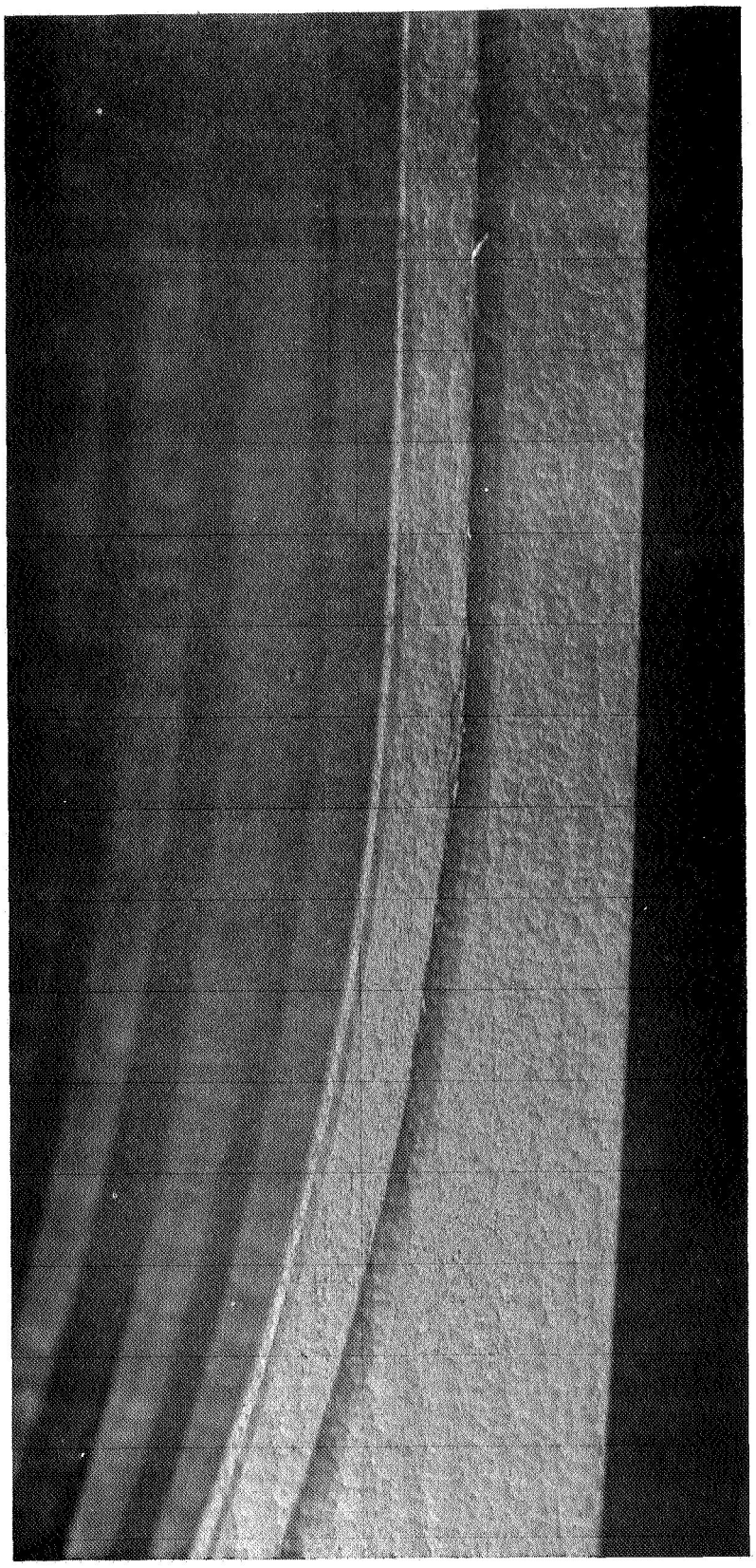

20-254

Figure 2-60

C. Copper Chamber Spray Cooling Evaluation

A program was initiated using the copper chamber to evaluate the effect of spray cooling changes on the temperature history and establish the thermal characteristics of the ES156903N1 injector without spray cooling.

Table V lists pertinent parameters for the runs accomplished to date. A comparison of the time-temperature histories for the spray cooled runs is given in Figure 2-61 . It indicates that a spray flow rate of between 0.054 to 0.060 lb/sec may be sufficient to achieve an acceptable temperature history. Run 23-1 and the analytical correlation upon which the rig engine design was based are shown for comparison.

Further exploration is required and some compromises may be necessary in overall O/F ratio and total flow rates to achieve the desired temperature history design objectives. Increasing the spray flow rate lowers the fuel flow in the swirl cup. Thus swirl cup O/F ratio is increased toward the stability limits established during the injector development program. The added spray flow through a fixed orifice size would cause the pressure drop to increase by a square function. Increased orifice size is thus required to prevent such a pressure penalty with the integral injector.

Four dry runs were also made to determine whether a difference exists between this injector and the high fill time injector used to provide data for the original design. Figure 2-62 shows the time-temperature histories. The original design data is provided for comparison.

It appears that the change in inlet manifolding caused some subtle change in combustion characteristics resulting in a higher heat loading of the chamber.

In summary, spray cooling evaluations to date indicate a substantial increase in flow is required to achieve satisfactory temperature levels with the existing injector. Further testing is required to establish a new design point with increased spray pintle orifice size and within the stability limitiations of the injector.

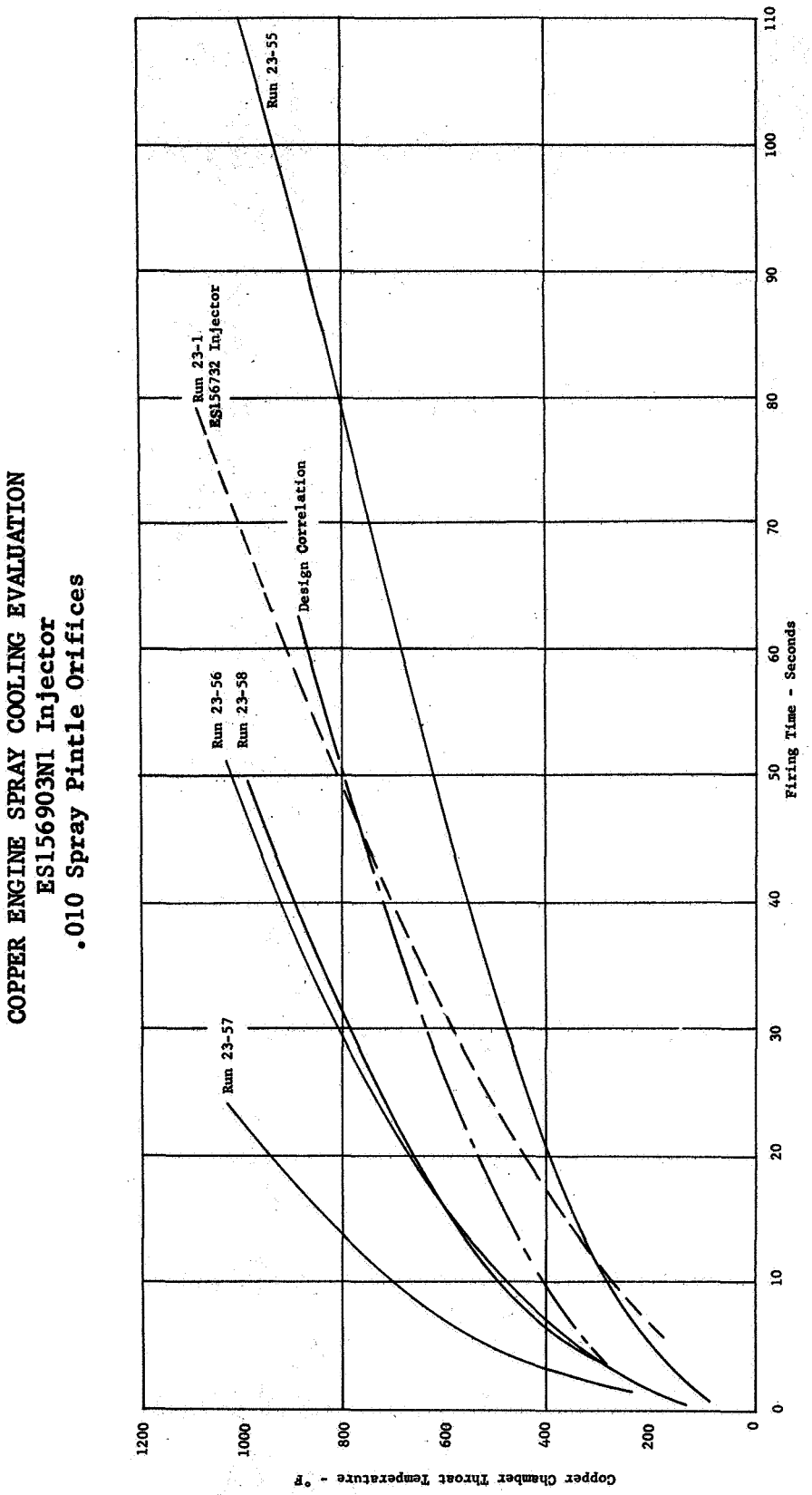
COPPER ENGINE SPRAY COOLING EVALUATION
ES156903N1 Injector
.010 Spray Pintle Orifices
Copper Chamber Throat Temperature - °F
1200
1000
800
600
400
200
0
0
10
20
30
40
50
60
70
80
90
100
110
Firing Time - Seconds
Run 23-55
Run 23-1
ES156732 Injector
Design Correlation
Run 23-56
Run 23-58
Run 23-57

Figure 2-61

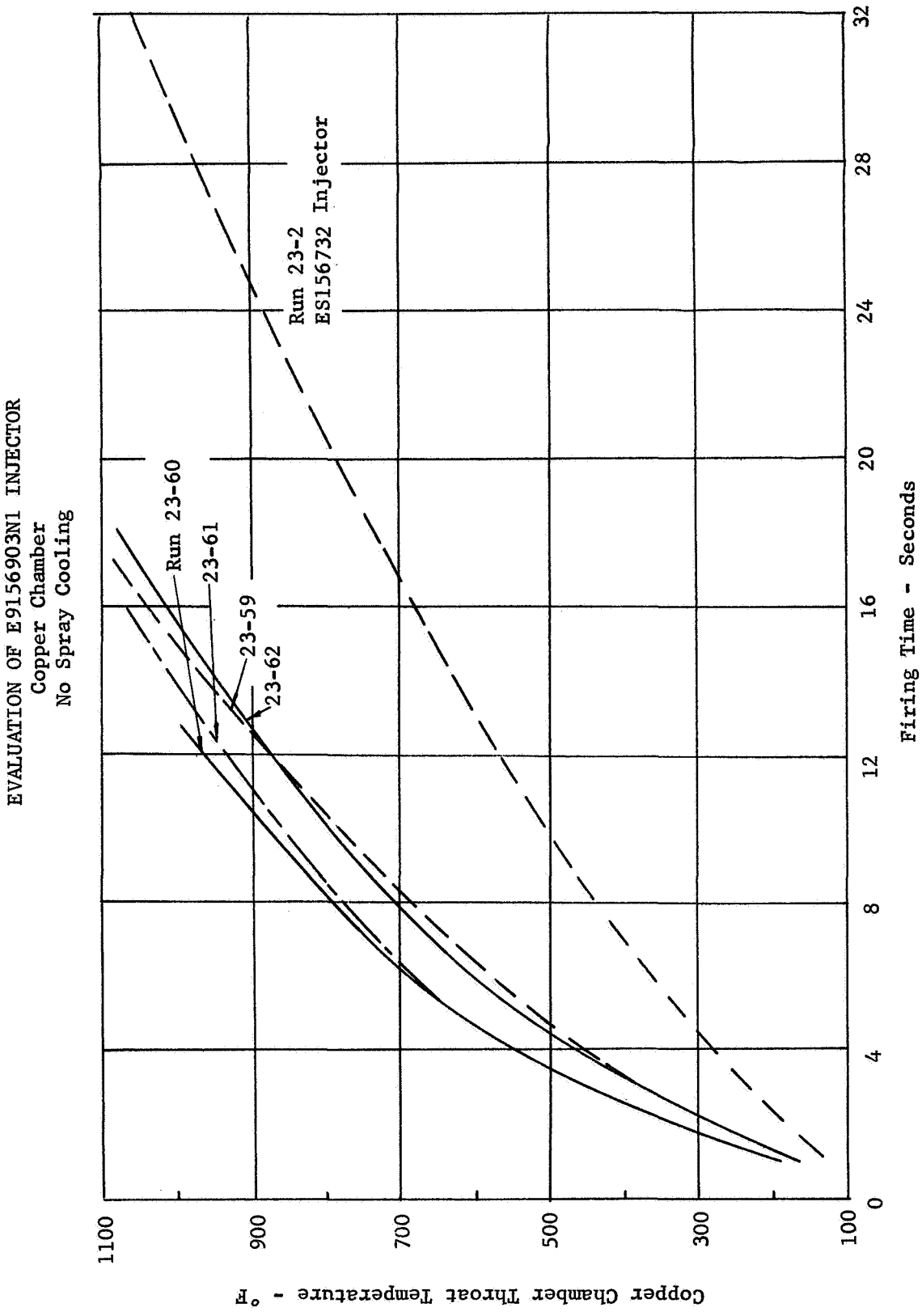
EVALUATION OF E9156903N1 INJECTOR
Copper Chamber
No Spray Cooling
Run 23-2
ES156732 Injector
Run 23-60
23-61
23-59
23-62
Copper Chamber Throat Temperature - °F
1100
900
700
500
300
100
0
4
8
12
16
20
24
28
32
Firing Time - Seconds

Figure 2-62

III DESIGN AND ANALYSIS

A. Watchband Stress Analysis Reivew

A review of the method of analysis of the watchband was made as part of the investigation of the watchband installation problem. The purpose of the review was to insure that all elements of loading which contribute to the total stress in the watchband were properly considered. It was recognized that both tensile and change-in-curvature stresses exist and add to those caused by bending. These were thought to be insignificant and therefore had not previously been included in the analysis.

A free body sketch of the hoop loading on a typical beam element in the watchband is shown in Figure 3-1a . This loading produces a bending stress about a radial axis through the beam and a tensile stress normal to the beam cross-section.

Figure 3-1b illustrates the change-in-curvature effect which develops a second bending stress in the beam as the watchband is stretched. In this case the bending axis is perpendicular to the radial axis as shown in Figure 3-1c.

Figure 3-1d shows the superimposed effect of all the stresses acting in the beam. Added together they give total watchband stress. The maximum stress occurs in the outer fiber in one corner of the beam at the supported ends.

The results of this study are summarized in graphical form on Figure 3-2 . Total watchband stresses are plotted against radial interference fit at assembly for t = 0, 50, 100 and 500 seconds of firing at Sections A, B, D and F in the engine. The wedge inner land stresses at the throat (Section F) are also shown. These compressive stresses indicate the degree of sealing that exists for a particualr watchband interference fit and firing time. Since the most critical seal along the wedge land is at the throat, these stresses are an important consideration in the engine design.

Figure 3-3 compares total watchband stress and bending stresses due to the hoop load against firing time for 0.025 inches radial interference fit at

assembly. Figure 3-4shows total watchband stress versus firing time for a 0.023 inches radial interference fit at assembly.

In the first Quarterly Report the radial watchband interference fit was established at 0.025 inches based on the results of the tensile specimen pull test. This fit assured a tight inner land seal at the throat throughout a 500 second test. Superimposing the effects of tension and change-in-curvature on the bending stresses in the watchband results in a higher total stress. (See Figures 3-2 and 3-3).

By reducing the radial interference at assembly to between .022 - .023 inches, the throat sealing load is maintained and the watchband stresses are lowered (See Figure 3-4) to values considered satisfactory.

Although the calculated watchband stress exceeds the yield strength of the material at Sections B and D, the stress results almost completely from beam bending and is a maximum only at the outer surfaces. The local nature of the maximum stress condition minimizes its effect on the overall structure and the ductility of the material allows a sufficient load redistribution before the watchband function is diminished. A comparision of the critical stresses in Section D with the tested material properties of Rene' 41 bears out this conclusion.

Time, sec	100	500
0.2% Yield, PSI	131,000	103,000
Ultimate Tensile Strength, PSI	180,000	125,000
Temperature °F	400	1400
Total Watchband Stress, PSI	137,800	110,800

The slight overstress at both time intervals is well below the ultimate strength and therefore within the range of ductility.

By reducing the radial interference fit from 0.025 inches to 0.023 inches the following objectives were thus obtained:

- Lower overall watchband stresses.
- Greater safety regarding sensitivity to material properties.
- The requirements for a 500 second run are met.

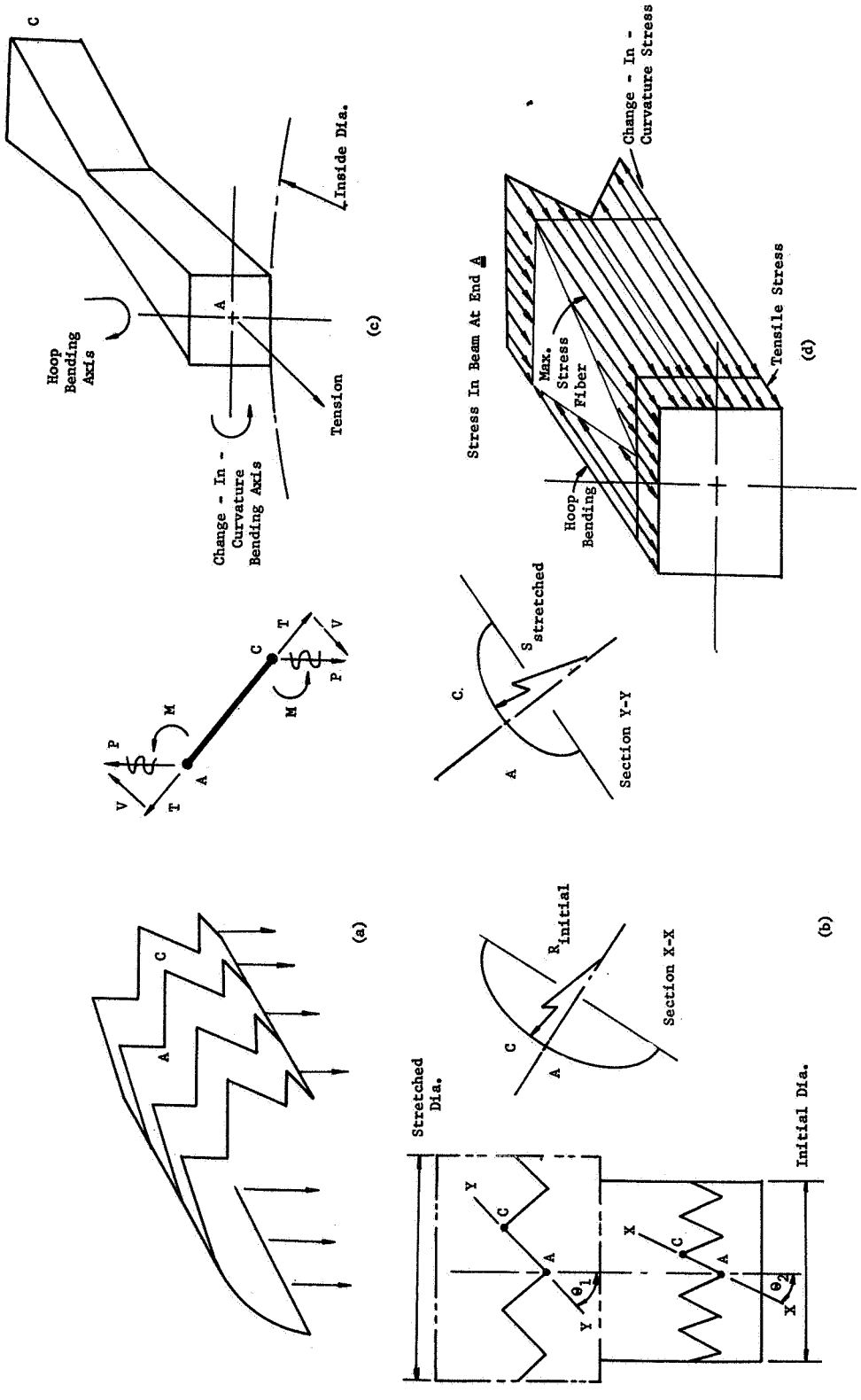
WATCHBAND STRESS CHARACTERIZATION
C
A
(a)
Stretched Dia.
Initial Dia.
Y
X
θ_1
θ_2
(b)
$R_{initial}$
Section X-X
Stress In Beam At End A
Change - In - Curvature Stress
Max. Stress Fiber
Tensile Stress
Hoop Bending
(d)
$S_{stretched}$
Section Y-Y
P
V
T
M
(c)
Inside Dia.
Hoop Bending Axis
Tension
Change - In - Curvature Bending Axis

Figure 3-1

TOTAL WATCHBAND STRESS VS FIRING TIME

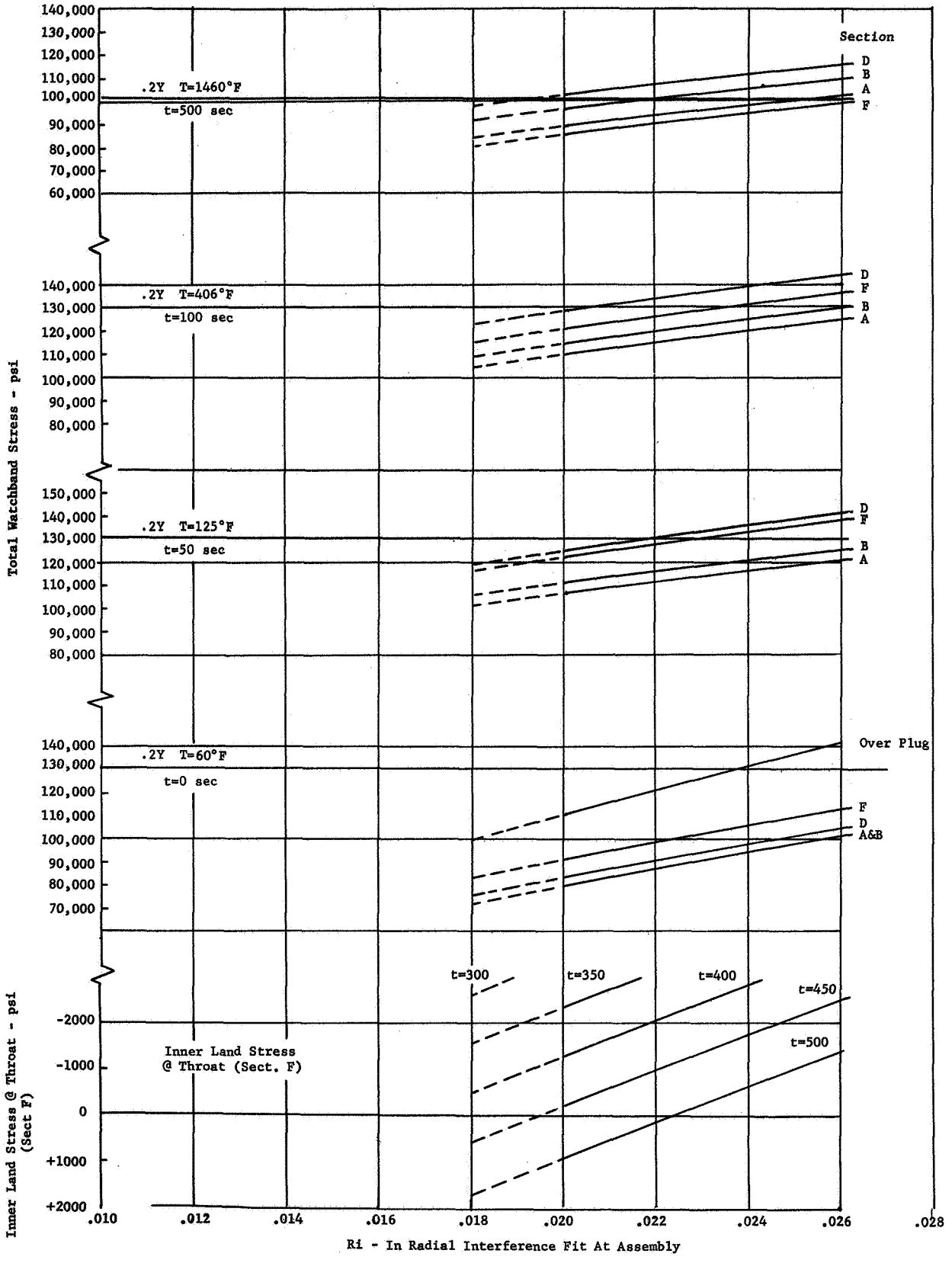

20-342

Figure 3-2

WATCHBAND STRESS VS. TIME
(Total Stress & Hoop Bending)
.025 Radial Interference

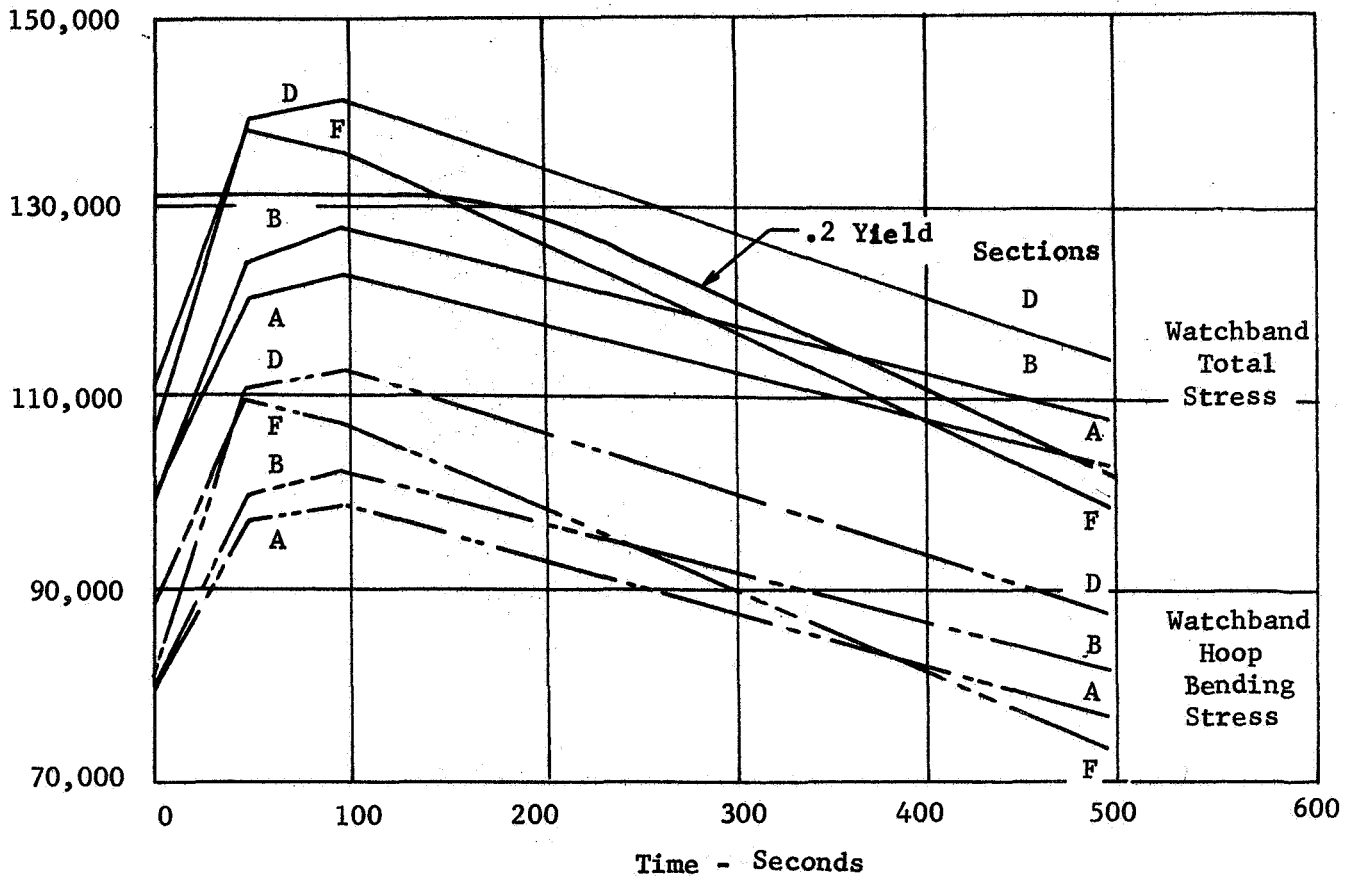

Figure 3-3

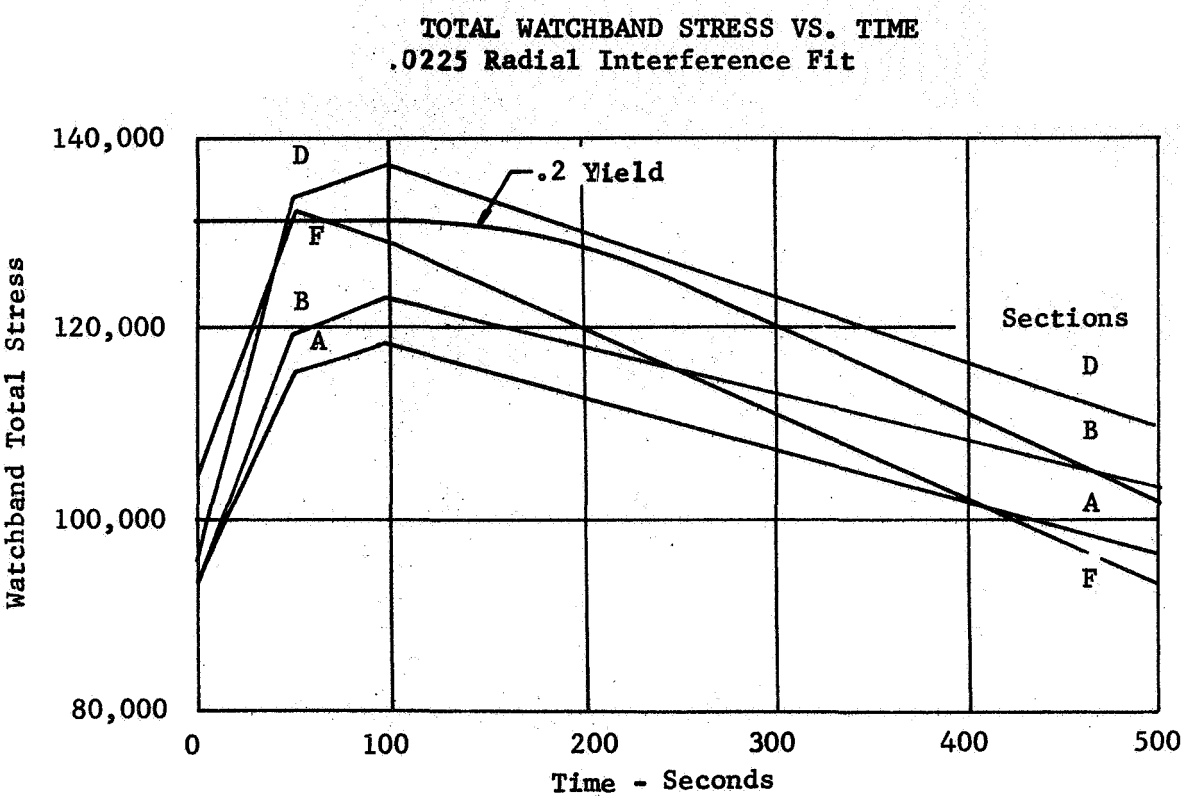

20-305

Figure 3-4

B. WLR-23 Rig Engine Data Analysis

After the first series of WLR-23 rig engine tests an analytical study was made to determine the cause of the machanical problems. The deflection probe data (Figure 3-5) was used to analytically derive via an iterative method the temperature at the inner wall of the wedge chamber. Normally this data is adjusted to correct for temperatures of the rig housing and deflection probe rod. However, the temperature rise at these locations, Figure 3-6, was not enough to affect the deflection probe readings within the first four decimal places and no temperature correction was made.

Figure 3-7 shows the inner wall temperature history (based on the deflection probe data) vs time compared with the analytical predictions. It can readily be seen that the engine ran substantially hotter than predicted.

Figure 3-8 shows the watchband stresses calculated based on the derived engine temperature history. The high engine temperatures resulted in increased watchband deflections and stress levels. The stresses are over the ultimate tensile capability of the material based on the assumption that the material is elastic and that it conforms to Hookes Law. Above the proportional limit, however, the overstressed areas deform plastically and the load is redistributed. Thus, the actual stresses in the watchband beam are much lower than if the material remained perfectly elastic.

The highly stressed region on the watchband beam is locallized at the surface. Therefore, the volume of material affected is small and the overall strength of the watchband is not appreciably affected. Inspection of the watchband showed no damage other than a 0.006 inch radial set. This value approximates calculated values based on the watchband test specimen data. No cracking or fracturing of the material took place and the watchband is satisfactory for use for the next series of tests. It will, however, be reground to eliminate out of roundness and a slight taper that resulted from the initial tests.

The higher watchband deflections caused by the increased inner wall temperature in turn provided added restraining forces on the PG wedge land. These forces were calculated and are plotted in Figure 3-9. The average

land stress is about 30% higher than predicted which resulted in crushing of the lands.

In summary, the mechanical problems associated with the initial series of engine tests are the result of the engine running substantially hotter than predicted. Both the abnormally high watchband stresses that caused permanent deformation of the watchband, and the increased wedge land stresses that resulted in crushing of the land can be eliminated by reducing the engine operating temperature regime. The initial design temperature predictions were made on the basis of using the high fill time injector (ES156732). The current injector being used (ES156903N1) was copied directly from the original except for a reduction in upstream manifolding to improve response requirements. Subsequent test of this injector indicated no change in stability characteristics. However, there apparently is a substantially higher heat load on the engine due to the use of this injector. It appears that added spray cooling development is required to reduce the temperature to satisfactory levels.

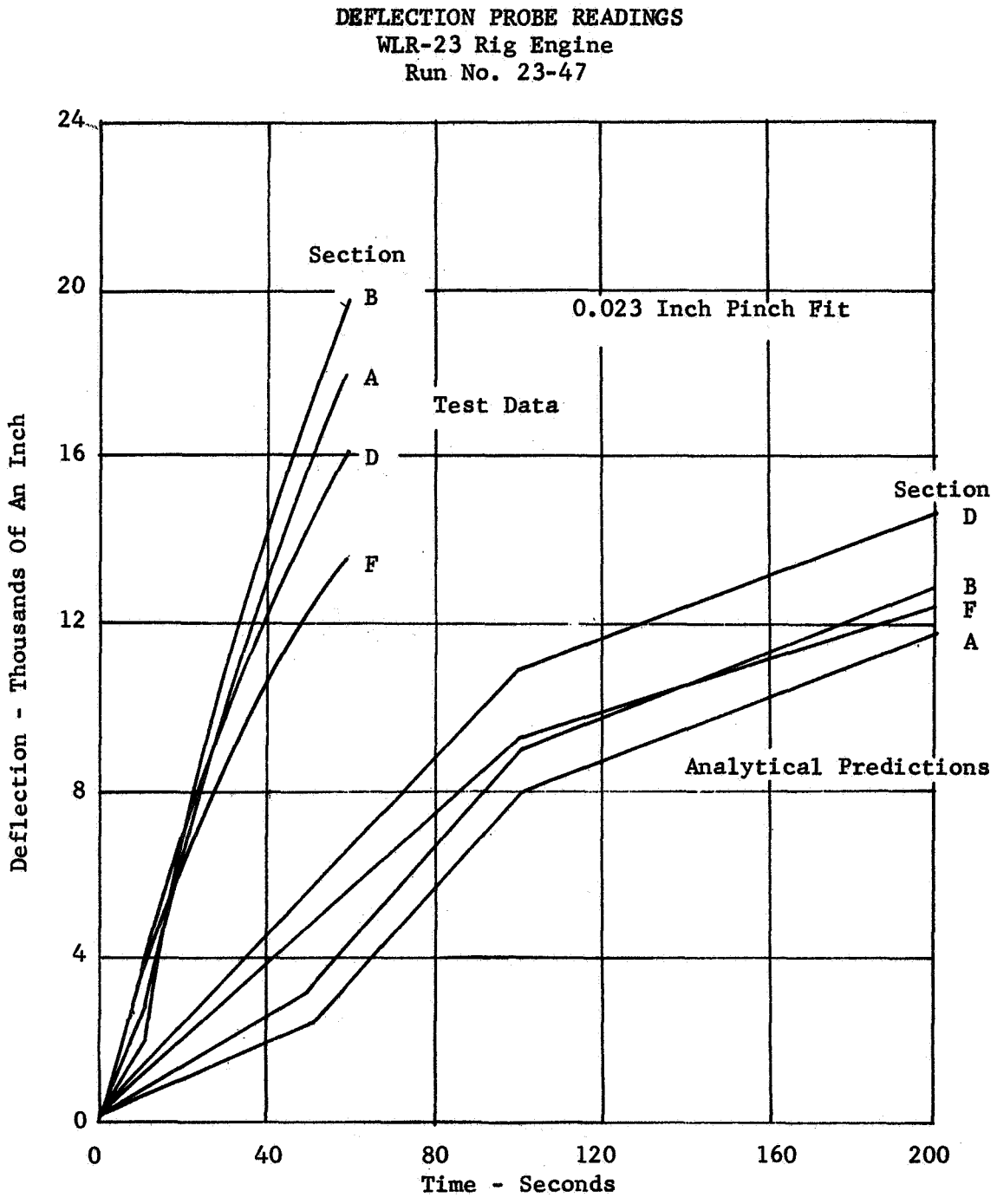
DEFLECTION PROBE READINGS
WLR-23 Rig Engine
Run No. 23-47
Deflection - Thousands Of An Inch
Time - Seconds
0
4
8
12
16
20
24
0
40
80
120
160
200
Section
B
A
D
F
0.023 Inch Pinch Fit
Test Data
Section
D
B
F
A
Analytical Predictions

Figure 3-5

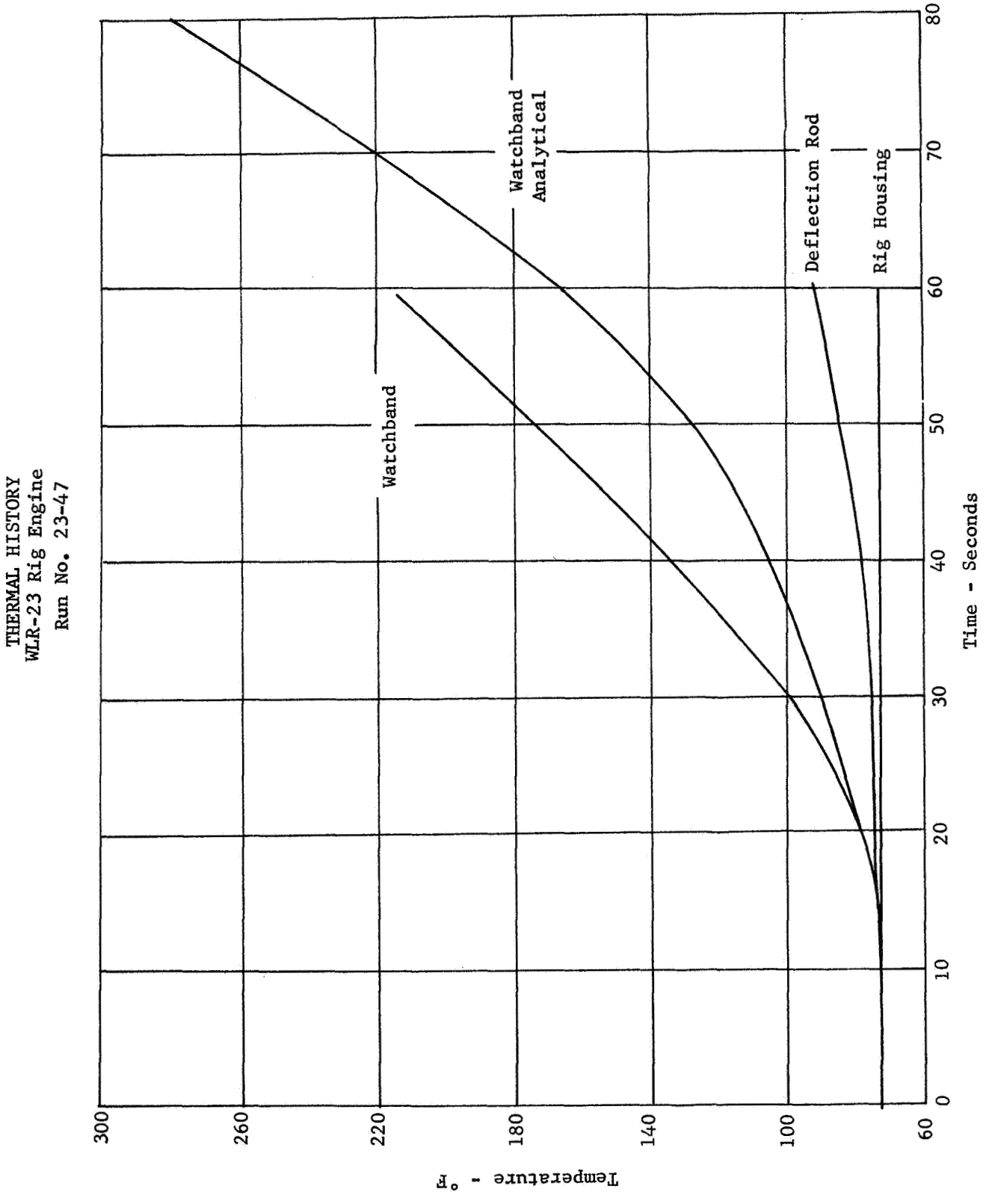

20-286

Figure 3-6

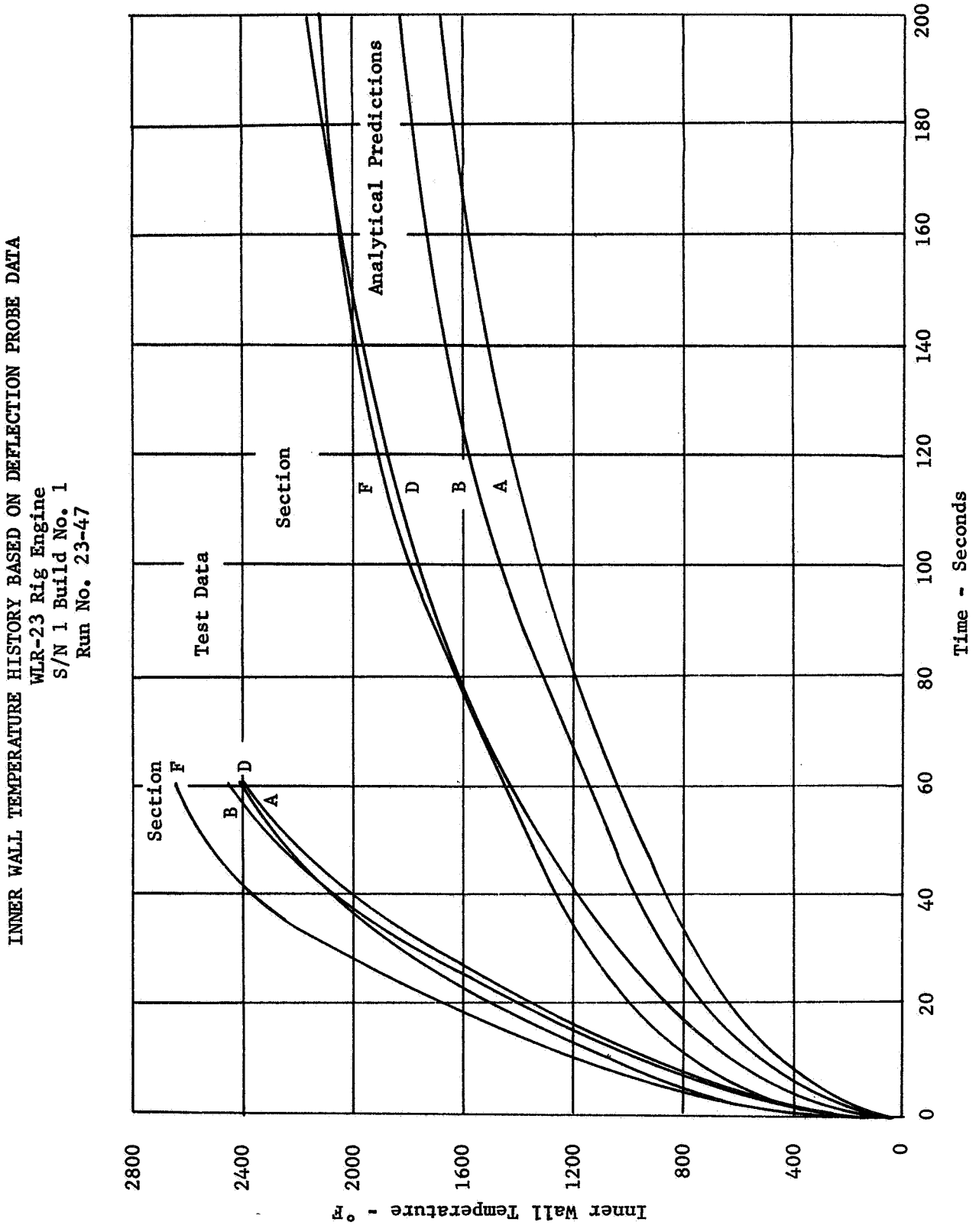
INNER WALL TEMPERATURE HISTORY BASED ON DEFLECTION PROBE DATA
WLR-23 Rig Engine
S/N 1 Build No. 1
Run No. 23-47
Inner Wall Temperature - °F
2800
2400
2000
1600
1200
800
400
0
Time - Seconds
0
20
40
60
80
100
120
140
160
180
200
Analytical Predictions
Test Data
Section
F
D
B
A
Section
F
D
B
A

Figure 3-7

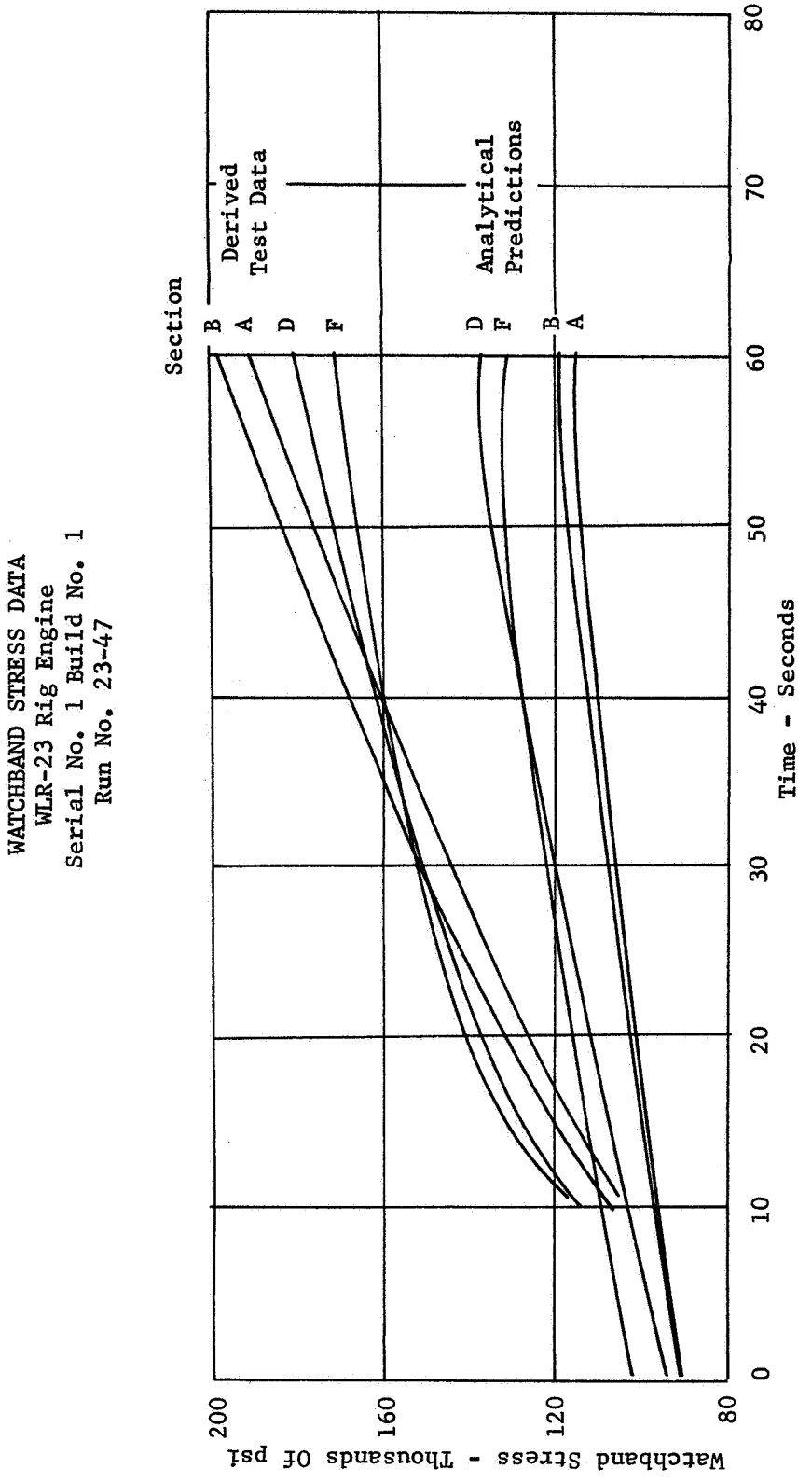
WATCHBAND STRESS DATA
WLR-23 Rig Engine
Serial No. 1 Build No. 1
Run No. 23-47
Section
B
A
D
F
Derived
Test Data
Analytical
Predictions
D
F
B
A
Watchband Stress - Thousands Of psi
200
160
120
80
0
10
20
30
40
50
60
70
80
Time - Seconds

Figure 3-8

WEDGE LAND STRESS DATA
WLR-23 Rig Engine
Serial No. 1 Build No. 1
Run No. 23-47

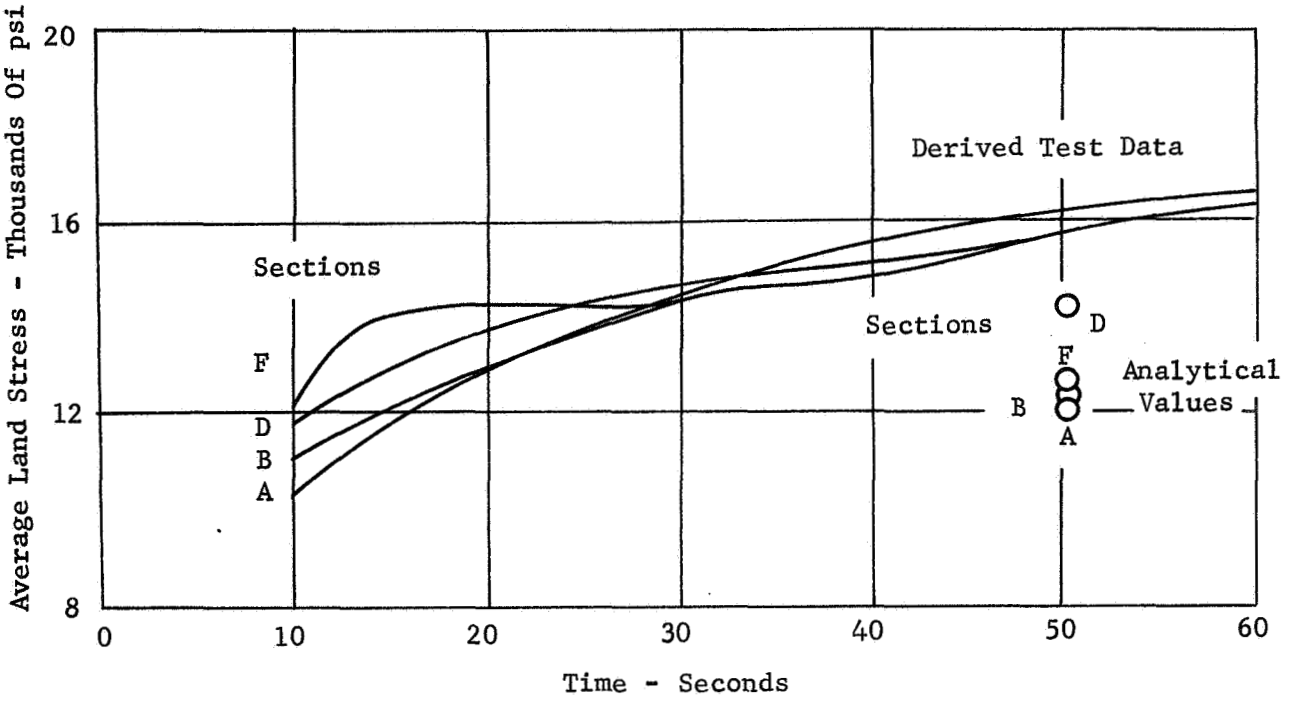

20-277

Figure 3-9

C. Flight Engine Preliminary Design

Design work has started on the Flight Engine Configuration, Figure 3-10 The most significant change in going from the rig engine to the flight design is the relocation of the axial loading belleville springs. The springs have been moved to the injector end to allow for the exit cone attachment at the aft end. These Rene' 41 springs are sized for both load and thermal compensation requirements.

The one piece housing has integral flanges, one for the injector and another for the aft closure and exit cone mount. Material selection will be based on thermal and structural requirements. The aft closure ring retains the thrust chamber assembly and loads the belleville springs.

The injector, shown in Figure 3-11 features an integral sixteen orifice spray ring with internal fuel connections. The internal spray ring replaces 16 individual rig engine pintles. This injector will be used with a Moog bipropellant valve which requires a flush sealing surface at the inlet side. A small adapter pad used with the valve provides attaching holes and brings the injector-valve assembly within the required four inch diameter envelope. Purge fittings and pressure taps are provided in the adapter pad.

The injector configuration shown in Figure 3-11 will be used for rig engine tests and later reworked for the flight engine as shown in Figure 3-12 The extra diametral stock in the rig configuration provides space for an extra chamber pressure tap, a spray manifold pressure tap, and a variable orifice screw for regulating spray manifold flow.

Tentative design data for the fuel spray ring is given below:

$\dot{W}$, Spray Flow	- lb/sec	0.0256
ΔP, Spray Orifice	- psi	28
Diameter, Spray Orifice	- in	0.010
C_D, Spray Orifice		0.75
Actual Velocity, Spray Orifice	- ft/sec	51.6

A thermal model is being constructed for the flight engine heat transfer analysis. The new model differs from the rig version due to the additional nodal points for the relocated belleville springs, the flight housing and aft closure ring. No changes are needed in the thrust chamber assembly. The thermal model will include the calculated film coefficients and latest data derived from the rig engine tests.

PRELIMINARY FLIGHT ASSEMBLY

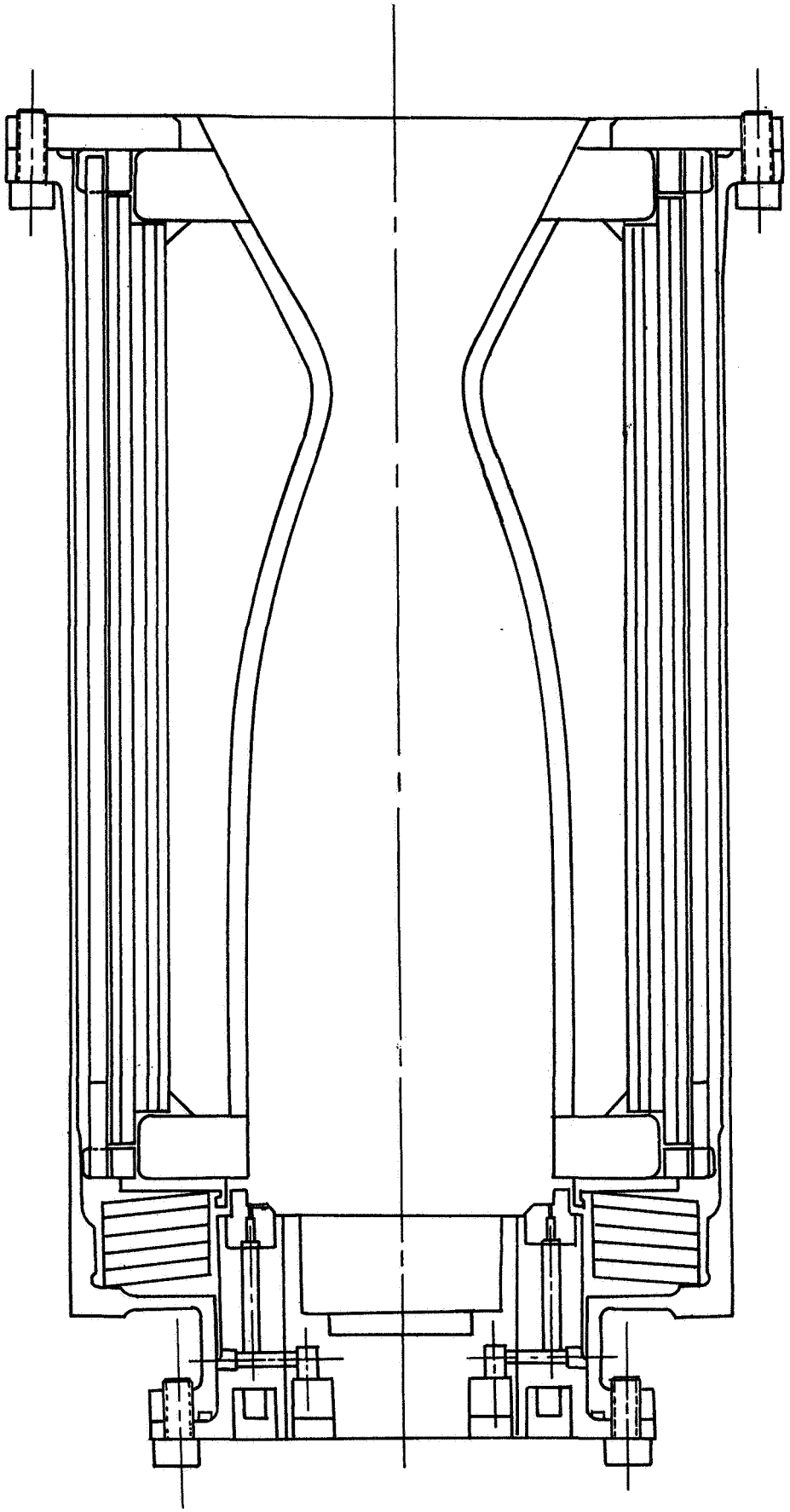

20-564

Figure 3-10

INJECTOR ASSEMBLY
16 Port Swirl Cup - Single Plane
With Integral Spray

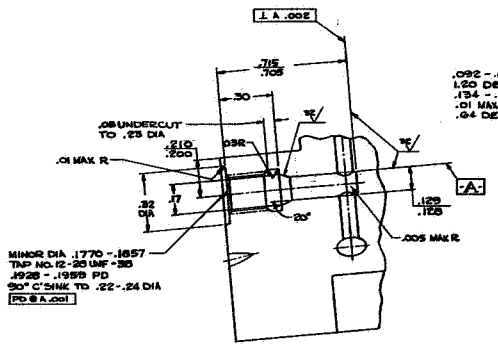

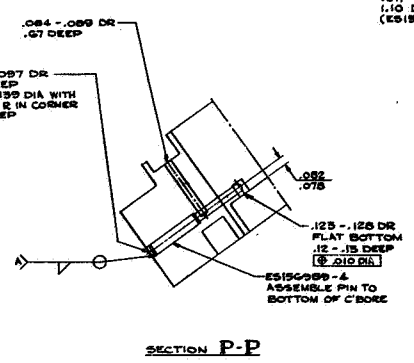

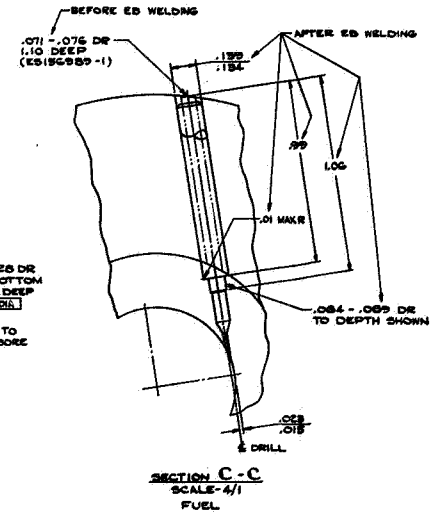

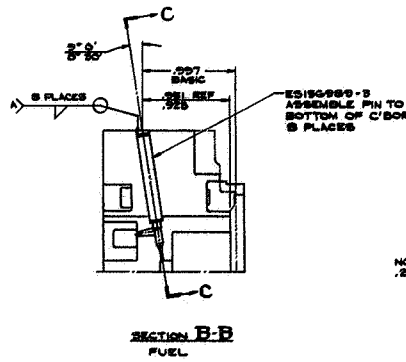

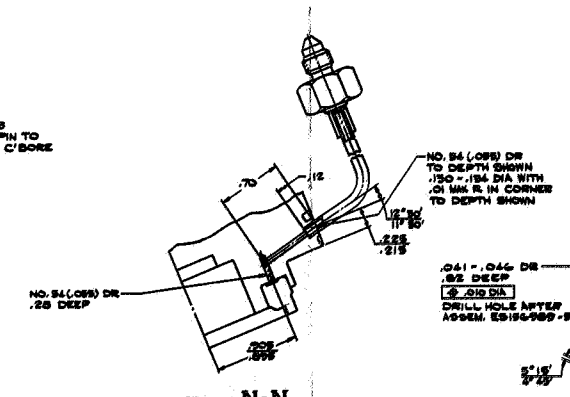

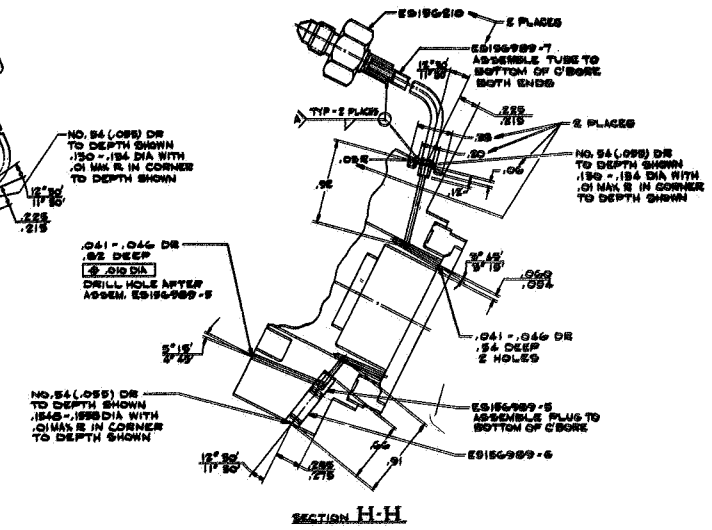

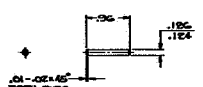

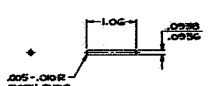

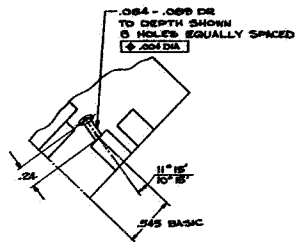

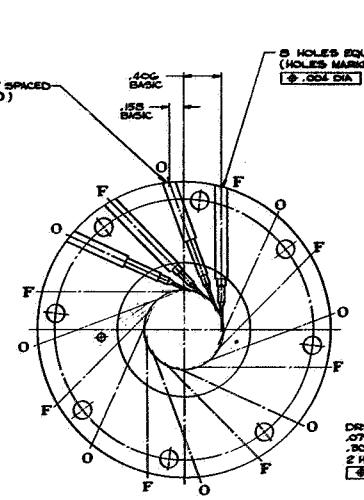

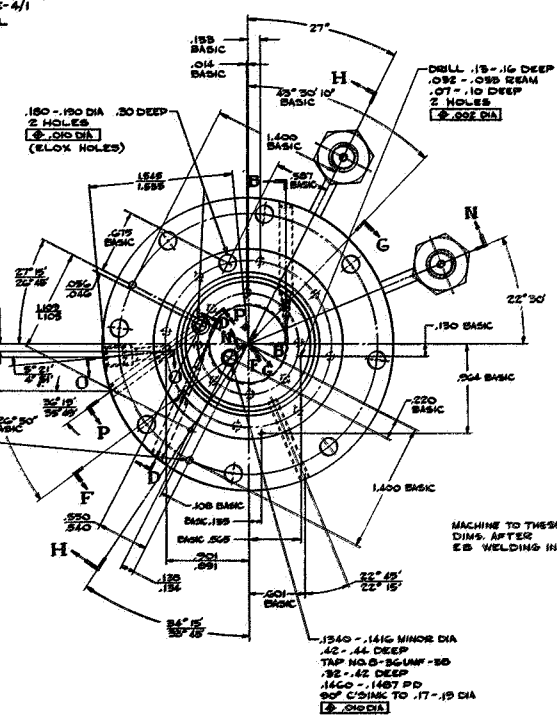

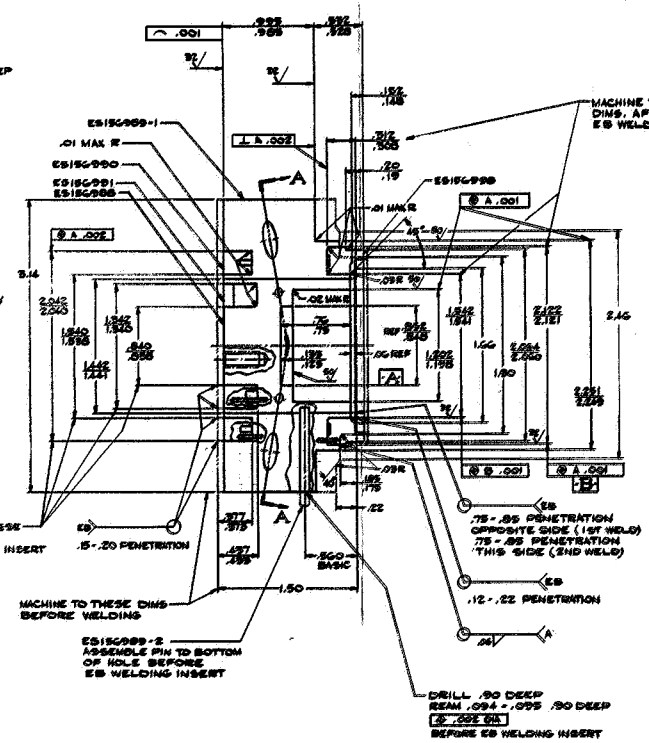

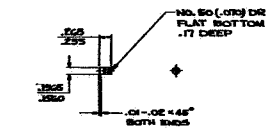

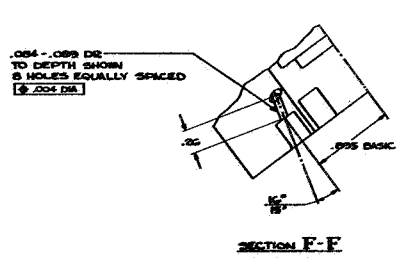

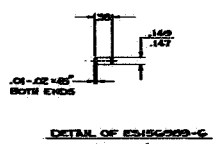

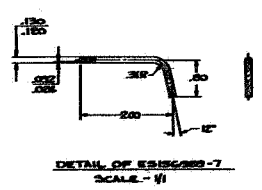

Figure 3-11

FLIGHT INJECTOR ASSEMBLY
16 Port Swirl Cup - Single Plane With Integral Spray (Rework)

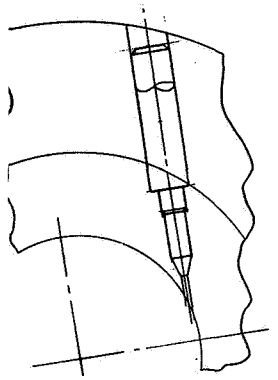

SECTION C-C (REF.)
SCALE - 4/1

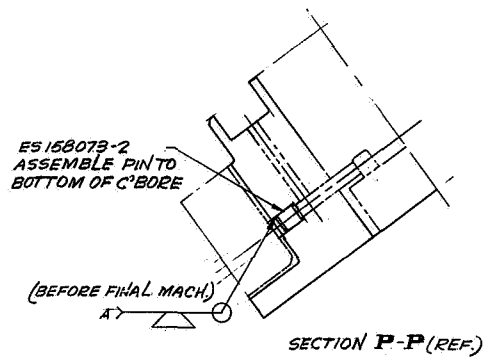

SECTION P-P (REF.)

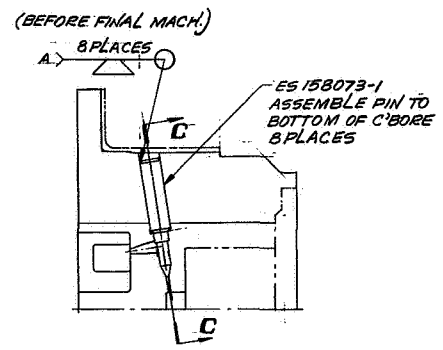

SECTION B-B (REF.)

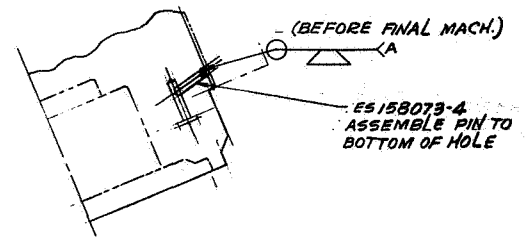

SECTION N-N (REF.)

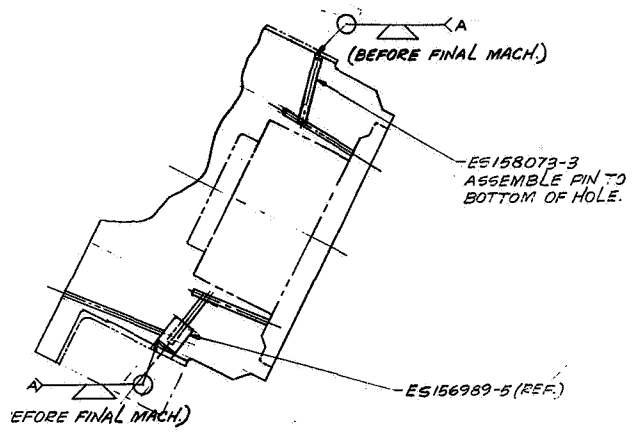

SECTION H-H (REF.)

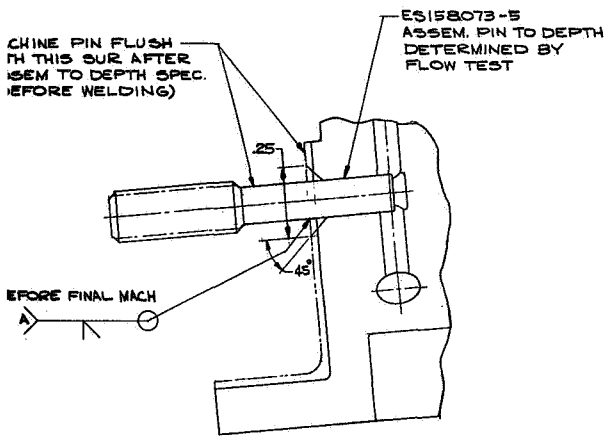

SECTION O-O
SCALE - 4/1

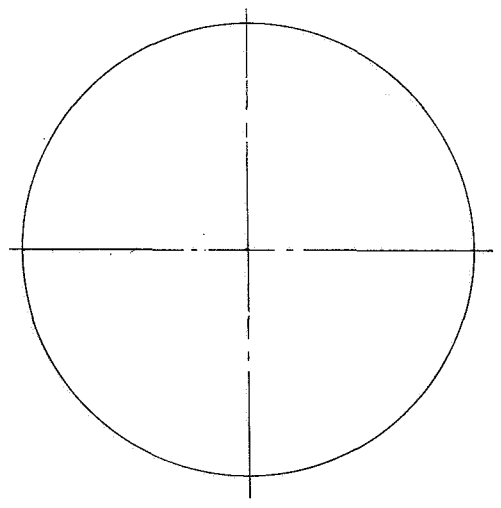

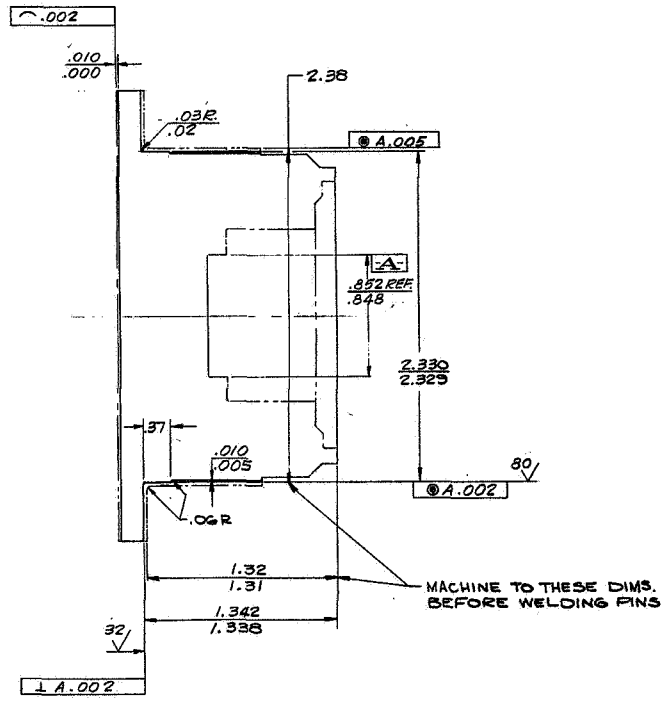

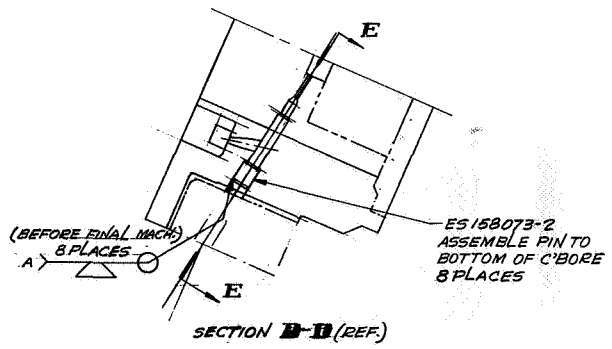

SECTION B-B (REF.)

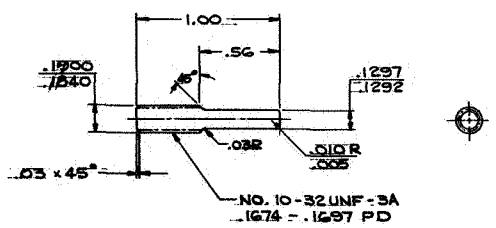

DETAIL OF ES158073-5

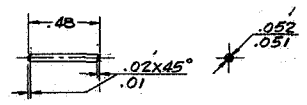

DETAIL OF ES158073-3

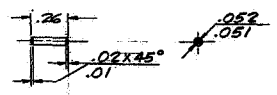

DETAIL OF ES158073-4

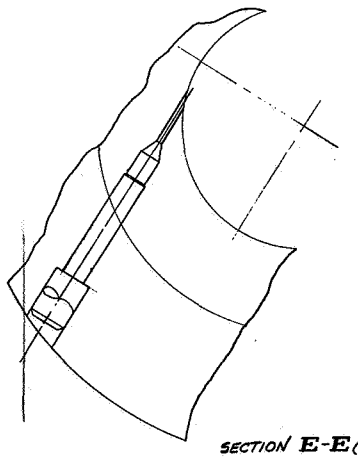

SECTION E-E (REF.)

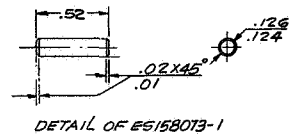

DETAIL OF ES158073-1

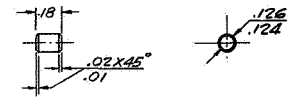

DETAIL OF ES158073-2

Figure 3-12

IV. PLANNED FUTURE ACTIVITY

Activity planned for the third quarter of the program is outlined below.

1) Spray Cooling Evaluation

Evaluation of changes to the spray cooling/injector configuration will continue into the third quarter in order to provide an arrangement that will result in satisfactory chamber temperatures. Completion of this effort is targeted for late June 1966.

2) Rig Engine Evaluation Testing

The second series of rig engine evaluation tests will be initiated when item (1) above is complete. This series of tests is scheduled for completion by early July 1966.

3) Flight Configuration Design

Design studies of the flight configuration engine will continue into the third quarter. The second series of rig engine tests should provide sufficient data to finalize the flight engine design.

4) Fabrication of the Flight Engine

Fabrication of detail parts required for the flight engine will be initiated early in August 1966. Completion of the first engine for test is scheduled for the start of the fourth quarter.

5) Development of Integral Spray Injector

The development and test of this item is being held pending the outcome of item (1) above. Initiation of test activity on this injector is currently scheduled for mid-July 1966.

INJECTOR PERFORMANCE DATA

ES156903N-2 16 PORT INJECTOR

LOW ORIFICE Δ P DESIGN

RUN NO.	23	-3	-4
Oxidizer System			
Feed Pressure	psig	189	188
Flow	lb/sec	.208	.210
Fuel System			
Feed Pressure	psig	163	150
Flow	lb/sec	.112	.102
Spray System			
O/F Ratio		1.86	2.06
Pc	psia	98.8	94.8
P swirl cup	psia	107	103
Psc/Pc		1.08	1.07
At	in^2	.544	.544
C*	ft/sec	5400	5320
C^*_η	%	95.2	94.8
Stability			
Oscillation	cps	1200	1200
Amplitude	psi	18	20
Amplitude as % of Pc $\pm$		9.1	10.5
Remarks		Random Peaks & Incipient Chugging Type Instability	Random Peaks & Incipient Chugging Type Instability

Table I

INJECTOR PERFORMANCE DATA

ES156903N-1 16 Port Injector

		WITHOUT SPRAY COOLING																									WITH SPRAY COOLING									
RUN NO. 23		5	6	7	8	9	10	11	12	13	14	15	16	17	18	19	20	21	22	23	24	25	26	27	28	29	30	31	32	33	34	35	36	37	38	39	40	41	42	43	44	45
OXIDIZER SYSTEM																																									
Feed Press	psig	188	137	163	230	264	144	170	191	230	274	135	168	195	231	265	120	162	188	223	257	135	157	180	220	135	194	122	142	168	197	226	119	142	169	202	233	148	175	199	210	241
Flow	lb/sec	.212	.175	.192	.236	.258	.186	.204	.218	.245	.272	.174	.202	.219	.242	.264	.170	.193	.209	.237	.260	.174	.192	.210	.234	.173	.206	.157	.170	.192	.210	.2305	.155	.174	.196	.219	.240	.181	.201	.214	.225	.245
FUEL SYSTEM																																									
Feed Press	psig	186	137	165	212	237	126	150	161	195	225	125	153	180	200	241	135	156	182	203	237	136	158	182	210	140	183	121	143	166	191	215	119	140	161	186	210	134	155	190	180	202
Flow	lb/sec	.104	.090	.098	.115	.122	.082	.091	.092	.106	.116	.084	.094	.104	.112	.124	.090	.096	.106	.113	.123	.109	.097	.105	.114	.092	.101	.081	.090	.097	.106	.112	.079	.085	.094	.102	.109	.081	.088	.104	.096	.104
SPRAY SYTEM																																									
Tank P	psig	-	-	-	-	-	-	-	-	-	-	-	-	-	-	-	-	-	-	-	-	-	-	-	-	-	485	310	391	459	538	722	279	362	429	504	613	340	405	537	473	474
Orifice USP	psig	-	-	-	-	-	-	-	-	-	-	-	-	-	-	-	-	-	-	-	-	-	-	-	-	-	465	298	381	448	527	714	268	352	418	495	602	328	392	527	463	463
Orifice DSP	psig	-	-	-	-	-	-	-	-	-	-	-	-	-	-	-	-	-	-	-	-	-	-	-	-	-	115	82	96	112	126	148	765	95	109	122	141	91	104	128	119	135
P	psi	-	-	-	-	-	-	-	-	-	-	-	-	-	-	-	-	-	-	-	-	-	-	-	-	-	350	216	285	336	401	566	192	257	309	373	461	237	288	399	344	328
Flow	lb/sec	-	-	-	-	-	-	-	-	-	-	-	-	-	-	-	-	-	-	-	-	-	-	-	-	-	.0243	.0193	.022	.0238	.026	.031	.0182	.021	.0229	.025	.028	.0201	.0221	.026	.0241	.0235
O/F Ratio$_{total}$		-	-	-	-	-	-	-	-	-	-	-	-	-	-	-	-	-	-	-	-	-	-	-	-	-	1.64	1.57	1.53	1.59	1.59	1.61	1.60	1.65	1.69	1.73	1.76	1.8	1.82	1.64	1.37	1.92
O/F Ratio$_{swirl\ cup}$		2.04	1.95	1.96	2.04	2.11	2.26	2.25	2.36	2.30	2.34	2.09	2.15	2.10	2.16	2.13	1.89	2.01	1.97	2.10	2.11	1.94	1.98	2.0	2.05	1.87	2.04	1.94	1.90	1.98	1.98	2.05	1.96	2.06	2.1	2.14	2.21	2.24	2.28	2.05	2.35	2.36
P_c	psia	98.2	80.6	89.8	109.1	120.5	80.5	88.8	93.03	106.9	118.6	79.2	90.6	99.8	110.2	130.6	80.5	89.4	98.5	108.3	118.9	81.2	89.1	98.4	108.4	80.6	105.1	79.9	89.03	99.03	109.0	120.2	78.7	87.6	98.5	109.6	119.6	89.0	99.0	108.9	110.1	119.0
P_{sc}	psia	105.3	87.1	96.5	116.7	126.9	86.9	95.9	100.7	115.1	128.5	85.3	97.3	107.1	117.9	128.7	86.7	96.3	105.3	116.3	127.1	86.1	96.9	107.1	117.9	88.3	112.1	85.3	94.7	105.1	115.1	125.9	90.1	93.5	104.7	116.5	126.7	94.9	105.1	115.3	116.7	126.5
P_{sc}/P_c		1.07	1.07	1.06	1.05	1.05	1.08	1.09	1.08	1.07	1.08	1.075	1.07	1.08	1.065	1.065	1.075	1.077	1.07	1.07	1.078	1.055	1.08	1.057	1.083	1.09	1065	1.07	1.06	1.06	1.05	1.05	1.14	1.07	1.06	1.06	1.06	1.07	1.06	1.06	1.06	1.06
A_t	in^2	.544	.544	.544	.544	.544	.544	.544	.544	.544	.544	.544	.544	.544	.544	.544	.544	.544	.544	.544	.544	.544	.544	.544	.544	.544	544	544	544	544	544	544	544	544	544	544	544	544	544	544	544	544
C*	ft/sec	5450	5350	5410	5450	5500	5270	5270	5270	5340	5360	5390	5360	5420	5450	5450	5420	5410	5470	5425	5450	5380	5400	5470	5460	5350	5580	5430	5540	5540	5580	5640	5460	5490	5520	5550	5560	5550	5570	5640	5675	5580
C^*_η	%	96.7	94.7	95.8	96.8	97.7	94.8	95.0	95.6	96.4	96.8	96.2	96.1	96.5	97.4	97.0	95.7	96.2	96.8	96.6	97.0	95.2	95.8	97.9	97.2	94.5	98	95.7	97.5	97.5	98.2	99.2	96.3	96.7	97.2	97.6	97.8	97.5	98	97.9	98	98.5
STABILITY																																									
Oscillation	cps	1100	1100	1100	1000	1100	1100	1100	1300	1300	1100	1100	1200	1100	1300	1300	1100	1200	1000	1000	1200	1000	1000	1000	1200	1100	1700	1500	1300	1600	1600	1700	1400	1400	1400	1600	1900	1500	1600	1600	1600	1600
Amplitude	psi	9	10	9	9	10	10	9	10	8.	10	10	10	10	9	10	10	10	10	10	10	10	10	10	10	10	10	11	9	12	11	11	11	11	9	11	11	9	9	11	10	10
%Amp. Osc.	±	4.5	6.0	5.0	4.0	4.0	6.0	5.0	5.5	3.5	4.0	6.3	5.5	5.0	4.1	4.2	6.3	5.6	5.1	4.6	4.2	6.2	5.6	5.0	4.6	6.2	4.3	6.9	5.0	6.0	5.0*	4.5	7.0	6.8	4.6	5.0	4.6	5.0	4.6	5.0	4.0	4.0
Random Peaking Freq.	cps	-	-	-	-	-	10	25	40		2	5	8	-	-	-	-	-	-	-	-	-	-	-	-	-	-	-	20	10	-	-	20	20	-	-	-	100	80	-	60	40
Random Peaking Amp	psi	-	-	-	-	-	25-40	15-25	40-50		30	20	15	-	-	-	-	-	-	-	-	-	-	-	-	-	-	-	22	1.4	-	-	25	20	-	-	-	15-40	15-40	-	22	15-40

Table II

WLR-23 RIG ENGINE INSTRUMENTATION

Serial Number 1, Build 1

Item	Parameter	Qty.	Instrument Type	Readout	Design Values	Calibration Range	Accuracy
1	Oxidizer Tank Press.	1	Wianko	Bristol	300 psia*	0-750 psi	± 1%
2	Oxidizer Line Orifice-Upstream Press.	1	Wianko	Bristol	280 psia*	0-750 psi	± 1%
3	Oxidizer Line Orifice-Downstream Press (Eng. Feed)	1	Wianko	Bristol	185 psia*	0-750 psi	± 1%
4	Oxidizer Line Orifice-Downstream Press (Eng. Feed)	1	Kistler	CEC	AC only	0-100 psi	± 5%
5	Oxidizer Flow	1	Potter	Bristol & CEC	0.204 lb/sec	0.14-0.9 lb/sec	± 0.5%
6	Oxidizer Flow	1	Ramapo	Bristol	0.204 lb/sec	0.07-0.2 lb/sec	± 0.5%
7	Oxidizer Temp.	1	Chromel-Alumel	Bristol	---	0-200°F	± 0.5%
8	Fuel Tank Press.	1	Wianko	Bristol	265 psia*	0-750 psi	± 1%
9	Fuel Line Orifice-Upstream Press.	1	Wianko	Bristol	250 psia*	0-750 psi	± 1%
10	Fuel Line Orifice-Downstream Press (Eng. Feed)	1	Wianko	Bristol	195 psia*	0-750 psi	± 1%
11	Fuel Line Orifice-Downstream Press (Eng. Feed)	1	Kistler	CEC	AC only	0-100 psi	± 5%
12	Fuel Flow	1	Potter	Bristol & CEC	.102 lb/sec	0 09-0.60 lb/sec	± 0.5%
13	Fuel Flow	1	Ramapo	Bristol	.102 lb/sec	0.05-0.16 lb/sec	± 0.5%
14	Fuel Temp.	1	Chromel-Alumel	Bristol	---	0-200°F	± 0.5%
15	Fuel Spray Tank Press.	1	Wianko	Bristol	635 psia	0-1000 psi	± 1%
16	Fuel Spray Line Orifice-Upstream Press.	1	Wianko	Bristol	630 psia	0-1000 psi	± 1%
17	Fuel Spray Line Orifice-Downstream Press.	1	Wianko	Bristol	165 psia	0-750 psi	± 1%
18,19	Chamber Press. (Swirl cup lip)	2	Wianko	Bristol	100 psia	0-200 psi	± 1%
20	Swirl Cup Press.	1	Wianko	Bristol	105 psia	0-200 psi	± 1%
21	Chamber Cavity Press.	1	Wianko	Bristol	15 psia	0-200 psi	± 1%
22	Thrust	1	Strain Gage	Bristol	60 lb.	0-100 lb.	± 1%
23	Oxidizer Solenoid Valve Current	1	---	CEC	For Events Only	Not Applicable	--
24	Fuel Solenoid Valve Current	1	---	CEC	For Events Only	Not Applicable	--
25,26	Chamber Radial Deflection-Station 0.40 Injector End	2	Linear Transformer	Bristol	0.025 inch	0-.050 inch	± 2%
27,28	Chamber Radial Deflection Station 1.21 Mid-Chamber	2	Linear Transformer	Bristol	0.025 inch	0-.050 inch	± 2%
29,30	Chamber Radial Deflection Station 2.83 Nozzle Ent.	2	Linear Transformer	Bristol	0.025 inch	0-.050 inch	± 2%
31,32	Chamber Radial Deflection Station 4.40 Nozzle Throat	2	Linear Transformer	Bristol	0.025 inch	0-.050 inch	± 2%
33,34	Watchband Temp.	2	Chromel-Alumel	Bristol	1500°F**	0-2000°F	± 0.5%
35,36	Housing Temp-Chamber	2	Chromel-Alumel	Bristol	200°F**	0-500°F	± 0.5%
37,38	Housing Temp-Nozzle Throat	2	Chromel-Alumel	Bristol	200°F**	0-500°F	± 0.5%
39	Swirl Cup Temp.	1	Chromel-Alumel	Bristol	1000°F**	0-1000°F	± 0.5%

Notes: * Estimated values based on previous test stand component pressure drops.

** During soak period

Table III

PERFORMANCE DATA

N_2O_4 System	Run Number 23-46	23-47	23-48
Tank Pressure - psig	307	307	308
Engine Feed Pressure - psig	188	188	192
Flow Rate - lbs/sec	0.212	0.214	0.215
MMH System			
Tank Pressure - psig	242	240	242
Engine Feed Pressure - psig	182	182	184
Flow Rate - lbs/sec	0.101	0.102	0.102
MMH Spray Cooling System			
Tank Pressure - psig	481	482	482
*Orifice Upstream Pressure - psig	474	477	472
*Orifice Downstream Pressure - psig	116	122	120
Flow Rate - lbs/sec	0.025	0.025	0.025
Total Propellant Weight Flow - lbs/sec	0.338	0.341	0.342
Oxidizer/Fuel Ratio	1.68	1.68	1.69
Chamber Pressure - psia	105	105	105
Swirl Cup Pressure - psia	112	112	112
C*	5480	5435	5420
C* Efficiency ** - %	96.2	95.4	95.1

Notes: * Calibrated fuel spray line orifice
** Uncorrected for heat loss to the chamber

Table IV

SPRAY COOLING EVALUATION WITH COPPER CHAMBER

ES156903N1 Injector

Run No. 23-		55	56	57	58	59	60	61	62
Chamber Pressure	psia	105	105	104	105	101	101	101	101
Swirl Cup Pressure	psia	111	111	110	111	108	108	108	108
Oxidizer Flow	lb/sec	0.192	0.192	0.196	0.192	0.211	0.213	0.228	0.228
Fuel Flow	lb/sec	0.095	0.096	0.098	0.087	0.106	0.104	0.095	0.095
Spray Flow	lb/sec	0.060	0.044	0.028	0.054	-	-	-	-
Total Flow	lb/sec	0.347	0.332	0.322	0.333	0.317	0.317	0.323	0.323
$O/F_{\text{Swirl Cup}}$	-	2.02	2.0	2.0	2.2	1.99	2.06	2.4	2.4
O/F_{Total}	-	1.24	1.37	1.56	1.36	1.99	2.06	2.4	2.4
C*	ft/sec	5260	5490	5640	5460	5570	5580	5460	5460
C^*_{η}	%	93.2	96.3	99.0	97.0	97.5	98.5	98.0	98.0

Table V